INVESTIGATION OF PARABOLIC REFLECTOR ANTENNAS AS SINGLE- AND MULTI-PHASE CENTRE VIRTUAL ANTENNAS

By

Zahra Allahgholi Pour

A Thesis submitted to the Faculty of Graduate Studies of

The University of Manitoba

in partial fulfilment of the requirements of the degree of

DOCTOR OF PHILOSOPHY

Department of Electrical and Computer Engineering
The University of Manitoba
Winnipeg, Manitoba, Canada

Copyright © September 2011 by Zahra Allahgholi Pour

Abstract

In this thesis, the concept of multi-phase centre virtual antenna is thoroughly investigated when a dual-mode primary feed is placed at the focal point of an offset reflector antenna. The virtual antenna requires that the antenna have multiple phase centre locations with identical radiation patterns. It is shown that different polarizations and mode content factors of a dual-mode circular waveguide can displace the phase centre location of an offset reflector antenna without changing its radiation patterns in any direction. This novel idea has promising applications in modern satellite, remote sensing, global positioning systems, and radars with moving platform. The concept is well matched for the modern Displaced Phase Centre Antenna technique, in which a simple signal processing technique is employed to electronically displace the phase centre locations. To avoid mechanically rotating the primary feed, a novel dual-mode feed is also proposed and implemented. It is capable of generating two perpendicular polarized TE_{11} modes with a fixed aligned TE_{21} mode. The antenna such developed has a potential application as a transceiver in ground moving target indicator radars. All numerical results are successfully validated by fabricating and testing a prototype antenna in practice.

As known, an offset reflector fed by a conventional linear polarized feed suffers from high cross polarization level. This property is also investigated for single-phase centre antenna applications along with sidelobe level and aperture efficiencies. A simplified feed model is proposed utilizing the TE_{11} and TE_{21} type modes to reduce the cross polarization at both asymmetry and inter-cardinal planes. It is shown that an

asymmetric dominant TE_{11} mode with the presence of the TE_{21} mode is sufficient in order to reduce the unwanted cross polarization. The results of this investigation are used to design practical dual-mode feeds using simple circular waveguide geometries. To complete the study, the effects of linear and quadratic phase errors associated with the optimized primary feed are also investigated on the cross polarization of the offset reflector antennas. In particular, the phase errors resulting in separate phase centre locations of each mode produce broadside-shape cross polarized patterns instead of boresight-null ones.

Acknowledgements

I would like to express my most sincere appreciation and gratitude to my academic and research advisor, Professor L. Shafai for his wise advice and invaluable guidance throughout my research. This work would not have been possible without his priceless support and encouragement. In a word, it has been an honor for me to do my graduate studies under his direct supervision on antennas.

I would also like to thank the members of my examining committee, Dr. V. Okhmatovski and Dr. S. Lui from the University of Manitoba and Dr. S. K. Chaudhuri from University of Waterloo. Moreover, I especially want to thank Mr. B. Tabachnick for his technical support during my studies and especially his help and willingness to do the laborious antenna measurements over the last two years, Mr. A. Symmons for fabricating the antennas with complex geometries, and Ms. S. Girardin for her extensive help, whenever it was needed, during my studies at the University of Manitoba.

Finally, I would like to thank my beloved family for their endless love and support. I would like to specially thank my husband, Ali, who has always encouraged me. In particular, I enjoyed fruitful discussion with him on the radar part.

Table of Contents

List of Tables

List of Figures

Chapter 1

Introduction

1.1 Preface

Reflector antennas have been the focus of many studies investigating various applications such as satellite communications, radiotelescopes, radars, and remote sensing systems [1-2]. They are classified as high gain antennas, as well as the simplest and yet most practical type of antennas. A reflector antenna comprises of a primary feed, to radiate electromagnetic waves, and a curved reflecting surface to collimate these waves over a larger secondary aperture [3]. The radiation pattern of the composite antenna, the reflector and the feed, is described as a secondary pattern in contrast to the primary pattern of the feed system. With the view of applying geometrical optics, a parabolic reflecting surface will focus a beam of parallel incoming rays to a point which is known as the focal point. Similarly, the reflected rays from a parabolic surface, illuminated by a point source placed at the focal point, will radiate as a parallel beam [4]. Simply, it transforms a spherical wave, produced by a point source, into a plane wave. Therefore, it will provide a uniform phase distribution over its aperture, which is a fundamental design requirement for aperture antennas [5].

In certain applications, such as global positioning systems (GPS), virtual array antennas, remote sensing, radar and military applications, it is important to know the phase centre location of the antenna. In particular, in radar applications with moving platforms [6], the well-known Displaced Phase Center Antenna (DPCA) processing technique [7] is employed to reduce the platform motion noise and scanning modulation

noise. The main focus of this thesis is to develop a novel multi-phase centre antenna within a single hardware as a virtual array antenna. This is done by employing a dual-mode feed as a primary feed in offset reflector antennas. The effects of feed polarization and the mode content factor on the phase centre displacement of an offset reflector antenna are thoroughly investigated to develop a multi-phase centre virtual antenna providing different phase centre locations in two orthogonal directions, which can be easily extended to any direction. Since offset reflector antennas generate a high cross polarization level in the plane of asymmetry, this property is also studied in detail as a single-phase centre antenna application using the same dual-mode feed but with a proper inter-mode phase shift. A cross polarization reduction technique is presented based on a simplified feed model representing tapered dual-mode circular waveguide antennas as a primary feed in offset reflector antennas. Finally, three novel dual-mode feed antennas are designed, fabricated and tested to validate the numerical calculations for both single- and multi-phase centre antennas.

1.2 Literature Review

Paraboloidal reflectors, which are formed by rotating the parabola around their axis, are the most widely used large aperture ground-based antennas. When fed efficiently from the focal point of the main reflectors, which are called as prime focus reflector antennas, they produce a high gain pencil-beam with low sidelobes and good cross polarization discrimination characteristics [4]. The symmetrically cut paraboloids have the major drawback that the feed must be located at the focal point, resulting in a front-fed structure. In this case, the feed, which is usually a horn antenna operating at its

dominant mode, introduces a considerable blockage on the reflector illumination aperture. Other than the feed, the supporting struts will also block the effective illumination surface of the reflector, especially in multi-beam antennas having a relatively large feed array. This, in turn, leads to a decrease in the gain and an increase in the sidelobe levels and cross polarizations, and an increase in the mutual coupling between the feeds via the reflector and struts [8].

The above-mentioned defects can be eliminated by the offset reflector antenna, which is a portion of a paraboloid. The feed is still located at the focal point, but its axis must be tilted toward the center of the offset reflector. Hence, the blockage will be decreased or cancelled due to the asymmetrical geometry of the reflector antenna, which is a major advantage [4]. Another advantage of the offset structure is that the reaction of the reflector to the feed is of a very low order. Because there is no direct reflection back into the feed, excellent isolation between the reflector and the feed is achieved. Furthermore, the offset geometry provides structural advantages that may be easily deployed after launching in spacecraft antenna applications. Mechanically, the choice of supporting struts and means of thermal control will be more relaxed in the offset geometry than in the symmetric reflector. Finally, an offset reflector can accommodate larger focal length to diameter ratios while maintaining a reasonable structural rigidity and a larger feed array in comparison to its symmetric counterpart [2].

The major drawback of an offset reflector antenna is that it generates the crosspolarized radiation in the plane of asymmetry when illuminated by a conventional linearly-polarized feed. As for the circular polarization case, the two orthogonal linear crosspolar components may result in a copolar component with a squinted beam [9].

Recently, an antenna with low cross polarization was required in frequency-reuse applications, such as modern satellite communication systems. Two orthogonally linear or opposite circularly polarized signals were used for each frequency band. This idea enhances the communication channel bandwidth. The orthogonality can be between either two perpendicular linear polarizations or left-hand and right-hand circular polarizations. In either case, any crosspolar response may create crosstalk between separate channels [3]. To minimize the interaction between the signals, the crosspolar component should be of a very low order of approximately -40dB [8].

Rudge and Adatia [10] showed that, the cross polarization of offset reflectors can be cancelled by a proper feed design. A tri-mode conical horn as the feed was employed to minimize the cross polarization. Jacobson [8] proposed two ways to reduce or eliminate the undesired cross polarization in the offset reflector antenna. His focus was on improving feed design with the development of a dual-mode rectangular horn and a linear array of small aperture round waveguide feeds with their axes parallel to the optical axis of the offset reflector.

In [11] the computational study on the radiation properties of offset prime-focus-reflector antennas was reported. The emphasis was placed on reducing sidelobes and cross polarization without sacrificing the gain. It was shown that, these parameters can be minimized by tilting the primary feed without sacrificing the antenna gain.

In addition to minimum crosspolar components, the high gain is necessary in radar antenna applications. To maximize the gain of the composite reflector-feed antenna, uniform amplitude and phase distributions over the aperture plane are required. In accordance to these requirements, the phase centre of the feed must coincide with a focal

point of the reflecting surface [5]. Moreover, knowledge of the phase centre location of the antenna is of great importance in various applications, such as global positioning system (GPS) and virtual array antennas [12]. Carter [13] studied the phase centre location of microwave antennas particularly paraboloidal reflector antennas. He showed that the phase centre location of the reflector antenna is a function of its feed and geometrical parameters of the dish. In particular, the phase centre is located at the center of the aperture plane when it is illuminated by a prime-focus point source feed having an axially symmetric pattern based on the aperture theory. He also showed that the phase centre would be different if the phase calculations were based on current distribution over the reflector.

It is clear that if one displaces the antenna phase centre, the apparent location of the antenna will move. This leads to a virtual antenna. The virtual array antenna can be thought of as an antenna having multiple identical beams, with multiple displaced phase centre locations. Such a property is desirable in many applications such as remote sensing and ground moving target indicator (GMTI) radars, to allow multiple antenna representations. GMTI radars are extensively used to detect and track the moving targets on the ground. The main challenge in such radars is to sufficiently suppress the clutter from targets. The clutter signals come from different unwanted reflection sources such as terrain, sea, atmosphere, high radar cross-section objects, and most importantly moving platforms [6]. One of the techniques to reduce the platform motion noise and scanning modulation noise is the displaced phase center antenna processing technique [7]. The main idea is to make the antenna appear stationary in space. Traditionally, the above-mentioned technique exploits multi–aperture antennas which provide displaced phase

center locations. This will, in turn, increase the hardware and complexity of the antenna systems. Authors in [14] showed that the phase centre location of symmetric and offset reflectors could be changed by using a dual-mode circular waveguide as a feed. These modes were the fundamental TE_{11} mode and the higher order TM_{01} mode of a circular waveguide and were described in detail in [15]. The displacement of the phase centre was simply obtained by changing the excitation amplitude and phase ratios of these two modes. Another multiple phase center reflector antenna was introduced for GMTI radar applications in [16-17]. They used a different dual-mode feed horn employing the fundamental TE_{11} mode and a higher order TE_{21} mode. No polarization control was investigated in any of the above work. Also, the phase centre motion was achieved only in a single plane.

In this thesis, the impact of the feed polarization on the phase centre location of offset reflector antennas will be addressed. The feed is a dual-mode circular waveguide antenna operating at its fundamental TE_{11} mode and the higher order TE_{21} mode. It will be shown that the phase centre displacement can be controlled in two orthogonal directions by simply changing the excitation amplitude and phase of each mode, as well as employing different mode orientations. Thus, the phase centre location can be moved away from the physical center of the antenna in any direction with a proper mode alignment. This case can lead to the virtual antenna concept, and the antenna can be made to have more than one phase centre by sequentially altering its excitation. That is, it becomes equivalent to multiple antennas. This property can be manipulated for application in remote sensing and signal processing techniques. Since the antenna polarization is also controlled, the case of a fixed antenna phase centre, but with variable

polarization property is also studied. Thus, the effect of a dual-mode circular waveguide, as a feed for an offset reflector antenna, on the cross polarization will be investigated for single-phase centre applications. The simulations are carried out using the physical optics, geometrical optics, and geometrical theory of diffraction software TICRA's GRASP v.7 [18] for reflector antennas. The results are also verified based on the aperture distribution method using MATLAB. To prove the concept in practice, a novel dual-mode waveguide antenna is designed and fabricated to move the phase centre in two orthogonal directions for multi-phase centre antenna applications. As for the single-phase centre antenna case, an analytic model for the primary feed of offset reflector antennas is presented that facilitates a more general investigation of the cross polarization reduction in both asymmetric and inter-cardinal planes. It includes both first and second order azimuthal modes, primarily the TE_{11} and TE_{21} type modes, and allows selection of symmetric and asymmetrical patterns, with different field tapers in the principal planes. It will be shown that the asymmetrical aperture distribution of the fundamental mode in the presence of the higher TE_{21} mode is sufficient to reduce the cross polarization of offset reflector antenna even for small focal length to diameter ratios. Finally, the results of this investigation are used to design practical dual mode feeds using simple circular waveguide geometry. Their performance on an offset reflector antenna is then investigated and shown that the reflector cross polarization is significantly reduced within a respectable frequency band. The feed designs are simulated using the finite-element based software HFSS v.12 [19]. In addition, the impact of the phase error associated with the primary feed is conceptually investigated on the cross polarization of offset reflector antennas.

1.3 Structure of the Thesis

This thesis contains six chapters. Chapter one covers introduction and literature review on the topic and describes its overall goals. Chapter two provides the background theory on offset reflector antennas as well as circular waveguide feeds. The proposed theory is also given in this chapter. Some properties of single-phase centre offset reflectors will be studied in chapter three. In particular, a simplified feed model will be presented and used to investigate the cross polarization reduction in offset reflector antennas. Then, practical feeds, which approximately fit the analytical model, are designed to verify the concept. In this chapter, the effect of phase errors on the cross polarization is also studied. Chapter four focuses on the multi-phase centre antennas, which are capable of generating identical secondary patterns, while their phase centre locations are displaced along two orthogonal directions. To do so, the impact of the mode alignment of a primary dual-mode feed on the phase centre displacement is investigated and it is addressed in chapter four. The feed is a dual-mode circular waveguide operating at the TE_{11} and TE_{21} type modes. Four cases of different mode alignments are studied. It is shown that by controlling the mode content factor, and more importantly, the polarization of each mode, the phase centre location can be displaced in any direction for any polarization. In practice, such a control is feasible by a proper signal processing technique to electronically change the effective source of antenna radiation. In chapter five, a practical dual-mode feed is proposed that its mode alignments and mode power ratios can be individually controlled. A prototype antenna is fabricated and tested. It is then used to illuminate an offset reflector antenna to verify the multi-phase centre antenna

concept and the polarization control. The measurement results satisfactorily validate the numerical ones. Finally, the conclusion and future work are described in chapter six.

Chapter 2

Background Theory

2.1 Introduction

The waveguide horn antenna has been used as a primary feed for reflector and lens antennas for many years. It is easy to excite, yet convenient to build in practice. Because of its simplicity, it is commonly employed as an antenna element in phase array applications as well. A simple waveguide antenna consists of a hollow metallic pipe with an arbitrary cross section shape, such as a rectangle, or a circle. It is excited from one end and radiates from the other open end into space. In this thesis, the emphasis is placed on the circular waveguide horn antenna application as a primary feed in paraboloid reflector antennas, particularly in an offset reflector structure. In this type of antenna, which is a portion of a paraboloid, the primary feed is located at the focal point tilted toward the center of the offset reflector. The offset geometry antenna has a profound advantage over its symmetric-cut counterpart. That is, the blockage of the feed and the supporting struts on the reflector illumination aperture can be cancelled. This will, in turn, increase the gain and decrease the sidelobe level of the secondary pattern in the far field region. However, the asymmetrical structure of the reflector itself either increases the undesired component orthogonal to the favored polarization when fed by a conventionally linear polarized feed, or squints the main beam when illuminated by a circular polarized feed. This problem can be alleviated by using a multimode waveguide feed, as a matched feed, with proper amplitude and phase ratios.

In this chapter, the offset reflector and the circular waveguide antennas, both known as aperture antennas, will be briefly reviewed. The offset reflector will be studied using the aperture field method. Following this study, the circular open-end waveguide will be explained for both transverse electric (*TE*) and transverse magnetic (*TM*) modes.

2.2 Offset Reflector Antenna

Parabolic reflector antennas are widely used to achieve high gain antenna in many applications such as radar, satellite communications, and radio astronomy. These antennas are well known as “pencil-beam” [20] antennas due to their relatively large aperture area. These focusing reflectors convert a spherical wave into a plane wave when illuminated by a point source feed located at their focal point. The resulting aperture field will be in phase because all rays travel the same distance when they arrive at the focal point [21], as illustrated in Fig. 2.1. Consequently, the system is potentially able to operate over a broad-band frequency range.

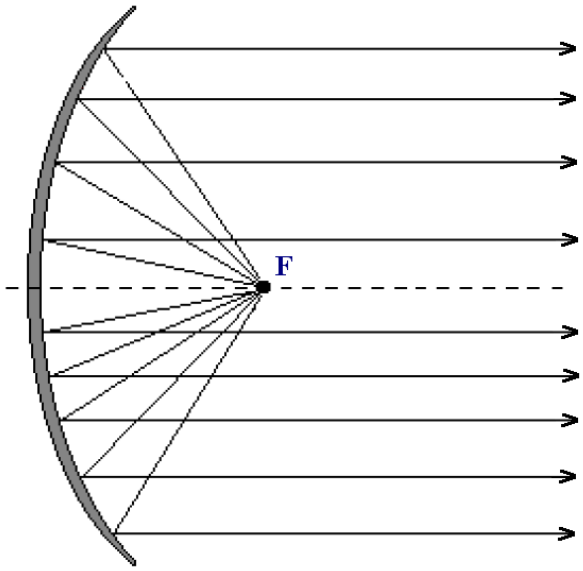

Fig. 2.1. The reflected rays of a parabolic reflector.

In practice, the primary feed is not a point source and has finite physical dimensions, which partly shadows the effective illumination aperture of a symmetric reflector. To eliminate this deficiency of the symmetric configurations, offset-parabolic reflectors have been developed for single and dual reflector systems. As a result, both aperture blocking and the interaction between the feed and the reflector will be reduced. Moreover, higher aperture efficiency compared to that of a symmetrical reflector antenna can be obtained. In terms of the focal length to the diameter ratio, *F/D*, the offset reflector can accommodate larger *F/D* ratios while maintaining structurally rigidity. This option provides an opportunity for improved feed-pattern shaping and better suppression of crosspolarized radiation emanating from the feed [4]. Due to the asymmetrical geometry of the offset reflector, the analysis is more complicated, which may be a major drawback. However, in some applications, like spacecraft antennas, an offset structure can easily be implemented [2, 4].

2.2.1 Offset Geometry

The offset reflector is the result of an intersection of a paraboloid and an inclined circular cone with its apex located at the focal point. Figure 2.2 shows the geometry of an offset reflector antenna [22], in which F is the focal length of the parent parabola, θ_o is the offset angle representing the tilted angle of the above mentioned circular cone, θ^* is the half-angle subtended by the reflector rim, D is the diameter of the projected aperture of the offset reflector, and d_c is the offset clearance distance, which is the distance between the axis of the parent parabola and the lower edge of the reflector rim.

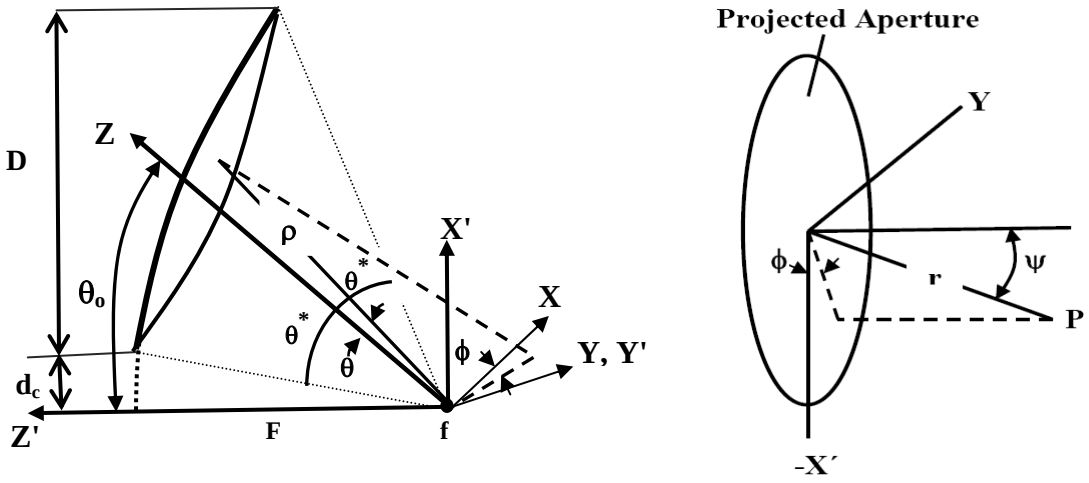

Fig. 2.2. The geometry of an offset reflector antenna.

In the above geometry, the coordinates of the parent parabola is expressed in terms of primed spherical (ρ', θ', ϕ') or Cartesian (X', Y', Z'), while the offset parabola has unprimed coordinates of (ρ, θ, ϕ) or (X,Y,Z). The required coordinate transformations, from the symmetric parabola to an offset reflector, are then simply obtained as:

$$\rho' = \rho \tag{2.1}$$

$$\cos\theta' = \cos\theta\cos\theta_o - \sin\theta\sin\theta_o\cos\phi \tag{2.2}$$

$$\sin\theta'\sin\phi' = \sin\theta\sin\phi \tag{2.3}$$

$$\sin\theta'\cos\phi' = \sin\theta\cos\theta_o\cos\phi + \cos\theta\sin\theta_o \tag{2.4}$$

$$\tan\phi' = \sin\theta\sin\phi / (\cos\theta\sin\theta_o + \sin\theta\cos\theta_o\cos\phi) \tag{2.5}$$

Using the above transformations, one can easily find the distance from the reflector focus to a point on the parabolic reflector surface, ρ, the diameter of the projected aperture of the offset reflector, D, and the offset clearance distance d_c as follows [2, 22-23]:

$$\rho = 2F / (1 + \cos\theta\cos\theta_o - \sin\theta\sin\theta_o\cos\phi) \quad (2.6)$$

$$D = 4F \sin(\theta^*) / (\cos\theta_o + \cos\theta^*) \quad (2.7)$$

$$d_c = 2F \tan((\theta_o - \theta^*)/2) \quad (2.8)$$

$$\tan\theta_o = 2F(D + 2d_c)/(4F^2 - d_c(D + d_c)) \quad (2.9)$$

$$\tan\theta^* = 2FD / (4F^2 + d_c(D + d_c)) \quad (2.10)$$

Also, the distance x'_0, or $D/2+d_c$, from the axis of the parent parabola to the center of the projected aperture is simply equal to:

$$x'_0 = 2F \sin(\theta_o) / (\cos\theta_o + \cos\theta^*) \quad (2.11)$$

Distances from the reflector focus in the plane of $Z'=0$ can be written as:

$$x' = \rho(\cos\theta_o \sin\theta\cos\phi + \sin\theta_o\cos\theta) \quad (2.12)$$

$$y' = \rho \sin\theta\sin\phi \quad (2.13)$$

The Jacobian surface element is also expressed by:

$$dx'dy' = \rho^2 \sin\theta' d\theta' d\phi' = \rho^2 \sin\theta\, d\theta\, d\phi \quad (2.14)$$

Finally, the normal unit vector to the parabolic surface, $\hat{a}_n$, is given by,

$$\hat{a}_n = -\sqrt{(\rho/4F)}\,[(\sin\theta\cos\phi - \sin\theta_o)\,\hat{a}_x + \sin\theta\sin\phi\,\hat{a}_y + (\cos\theta + \cos\theta_o)\,\hat{a}_z] \quad (2.15)$$

2.2.2 Analysis of an Offset Reflector Antenna

As already mentioned, the analysis of the offset reflector antenna is more complicated than that of the symmetrical one because of the asymmetrical geometry. There are two common techniques to analyze the offset reflector antenna [1-3]. The first one is the surface-current method, in which the geometrical optics approximation of the surface current density is integrated over the reflecting surface. The second method is the aperture field version of physical optics, in which the geometrical optics approximation of the aperture field is integrated over the projected aperture. The latter is explained here for a linearly polarized feed located at the focal point. The field with linear polarization is usually described by copolar and crosspolar components. Based on Ludwig's third definition [24], the copolar and crosspolar components of the electric field of an *x*-polarized wave are defined as:

$$E_{co}(\theta,\phi) = \cos\phi\, E_\theta - \sin\phi\, E_\phi \qquad (2.16)$$

$$E_{xpol}(\theta,\phi) = \sin\phi\, E_\theta + \cos\phi\, E_\phi \qquad (2.17)$$

Similarly, if the electric field is aligned along the *y*-direction, the above components are defined as:

$$E_{co}(\theta,\phi) = \sin\phi\, E_\theta + \cos\phi\, E_\phi \qquad (2.18)$$

$$E_{xpol}(\theta,\phi) = \cos\phi\, E_\theta - \sin\phi\, E_\phi \qquad (2.19)$$

In the same manner, the copolar and crosspolar of the secondary pattern can be obtained from the right-hand side of the above equations by substituting θ and ϕ with Θ and Φ, respectively, where Θ and Φ are the secondary coordinate system.

To find the tangential electric field in the aperture plane of the offset reflector antenna, it is assumed that the reflector is located at the far-field zone of the primary feed.

Moreover, the field outside the aperture is assumed zero, which requires a relatively large aperture dimension in comparison to the electrical wavelength. With these assumptions, the tangential electric field in the projected aperture plane can be obtained using physical-optics approximations. That is, the reflected field from the offset reflector, $\boldsymbol{E}_r$, is obtained from [5, 25]:

$$\boldsymbol{E}_r = 2(\boldsymbol{a}_n \,.\, \boldsymbol{E}_i)\, \boldsymbol{a}_n - \boldsymbol{E}_i \qquad (2.20)$$

where $\boldsymbol{E}_i$ and $\boldsymbol{a}_n$ are the incident electric field at the reflector and the surface unit normal, respectively. The incident field, which is the primary radiation pattern of the feed, can then be expressed as [2]:

$$\boldsymbol{E}_i = [A_\theta(\theta,\phi)\, \boldsymbol{a}_\theta + A_\phi(\theta,\phi)\, \boldsymbol{a}_\phi] \exp(-jk\rho)/\rho \qquad (2.21)$$

where A_θ and A_ϕ are the normalized components of the feed pattern described in the spherical coordinate and k is the propagation constant and equal to $2\pi/\lambda$. Now using Eqs. 2.15, 2.20, and 2.21, the Cartesian components of the offset reflector projected-aperture field distribution can be expressed as [2]:

$$\begin{bmatrix} E_{ay}(\theta,\phi) \\ E_{ax}(\theta,\phi) \end{bmatrix} = K \begin{bmatrix} -S_1 & S_2 \\ S_2 & S_1 \end{bmatrix} \begin{bmatrix} A_\theta(\theta,\phi) \\ A_\phi(\theta,\phi) \end{bmatrix} \qquad (2.22)$$

where S_1, S_2 and K are given by:

$$S_1 = (\cos\theta_0 + \cos\theta)\sin\phi \qquad (2.23)$$

$$S_2 = \sin\theta\,\sin\theta_0 - \cos\phi(1 + \cos\theta\,\cos\theta_0) \qquad (2.24)$$

$$K = \exp(-j2kF)/2F \qquad (2.25)$$

The normalized copolar and crosspolar secondary radiation patterns of an offset reflector, illuminated by a *y*-polarized primary feed, can then be written in terms of spatial Fourier

transforms of F_p and F_q, the copolar and crosspolar tangential electric field in the projected-aperture plane of the offset reflector, as follows [2]:

$$\begin{bmatrix} E_{con}(\Theta,\Phi) \\ E_{xpn}(\Theta,\Phi) \end{bmatrix} = \frac{1+\cos\Theta}{2F_p(0,0)} \begin{bmatrix} 1-t^2\cos 2\Phi & t^2\sin 2\Phi \\ t^2\sin 2\Phi & 1+t^2\sin 2\Phi \end{bmatrix} \begin{bmatrix} F_p(\Theta,\Phi) \\ F_q(\Theta,\Phi) \end{bmatrix} \qquad (2.26)$$

where Θ and Φ are the secondary far-field observation angles and $t = \tan\Theta/2$. The Fourier transforms are the transverse Cartesian components of the projected aperture field given by [2]:

$$F = \iint_{x'y} E_a(x',y)\exp\left(jkR'(x',y,\Theta,\Phi)\right)\,dx'dy \qquad (2.27)$$

where E_a is the tangential aperture field given by Eq. 2.22 and R' is expressed by:

$$R'(x',y,\Theta,\Phi) = (x_0' - x')\sin\Theta\cos\Phi + y\sin\Theta\sin\Phi \qquad (2.28)$$

x'_0, x', and y have been already given by Eq. 2.11-2.13. Some general cross polarization and sidelobe behaviors for the offset reflector antenna were addressed in [2]. It was shown that, the cross polarization increases as θ_o and θ^*, the offset angle and subtended half-angle respectively, increase.

As an example, the normalized secondary copolar and crosspolar patterns of an offset reflector with $D=20\lambda$, $d_c=\lambda$, $F/D=0.8$ are calculated employing the above method in MATLAB and shown in Fig. 2.3 in the asymmetry plane of $\phi=90^o$. The half-subtended and offset angles of this offset geometry are $\theta^*=31.48^o$ and $\theta_o=35.06^o$, respectively. For simplicity, the primary feed radiation pattern is chosen as $\cos\theta$ and has its principal

electric vector in the $\boldsymbol{a}_y$ direction. This feed model usually approximates a single mode circular waveguide antenna operating at its dominant mode [5]. As expected, the level of cross polarization is quite high in the asymmetry plane.

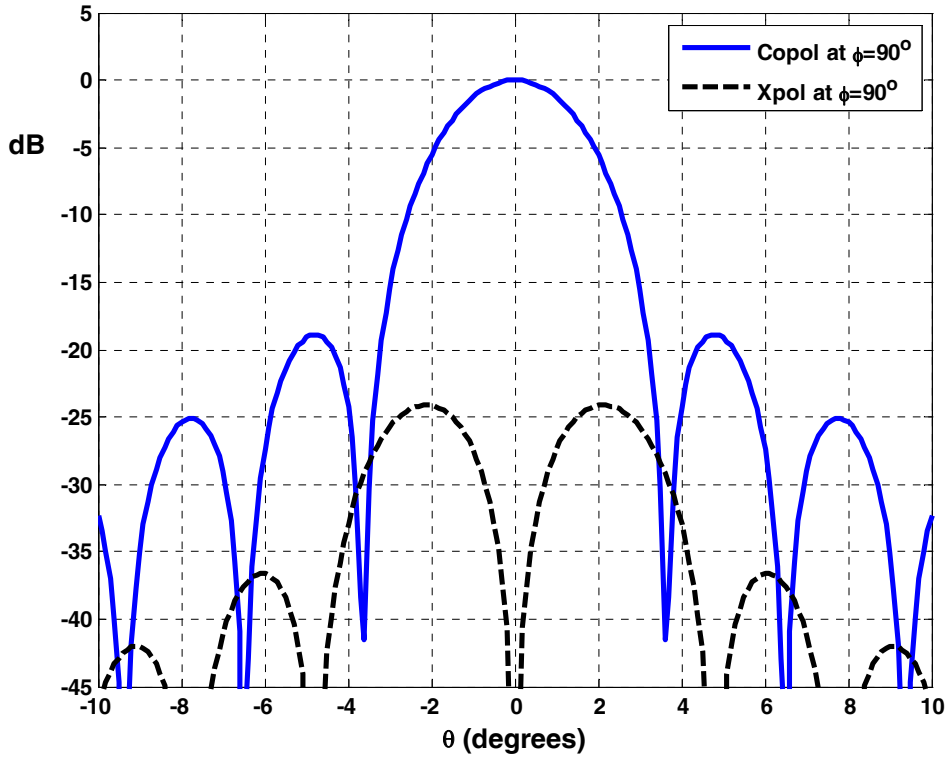

Fig. 2.3. The normalized secondary copolar and crosspolar patterns of an offset reflector with $D=20\lambda$, $d_c=\lambda$, $F/D=0.8$, $\theta^*=31.48^o$, and $\theta_o=35.06^o$, illuminated by a y-polarized $\cos\theta$ feed in the asymmetry plane ($\phi=90^o$).

In this thesis, the TICRA's GRASP v.7 [18] is also used to analyze the reflector geometry, which is based on the physical optics, geometrical optics, and geometrical theory of diffraction.

2.2.3 Gain of an Offset Reflector Antenna

The directivity is a measure of the directional properties of an antenna compared to those of an isotropic antenna which has equal radiation in all directions. Therefore, its directivity is unity. The directivity is defined as the ratio of the maximum power density in the main beam direction to the average radiated power density [4, 26]. The gain of an antenna has a similar definition, except the above ratio is calculated with respect to total input power. In this section, the gain factor of an offset reflector antenna is explained based on the aperture field method. It is assumed that the reflector is in the far-field region of the feed.

The gain factor of a reflector antenna is dominantly dependent on the feed radiation pattern. Let G_f be the gain function of the feed located at the focal point tilted toward the axis of the offset reflector antenna. The far-field of the offset reflector at $\theta=\phi=0^o$ can be expressed as [27]:

$$E(R,0,0)=\frac{\hat{e}_i\ j\omega\mu F}{\pi R}e^{-jk(R+2F)}\left[\sqrt{\frac{\varepsilon}{\mu}}\frac{P_T}{2\pi}\right]^{0.5}\sqrt{g_{nor}}\int_0^{2\pi}\int_0^{\theta^*}\frac{\sqrt{G_f(\theta,\phi)}\sin\theta\,d\theta\,d\phi}{1+\cos\theta\cos\theta_0-\sin\theta_0\sin\theta\cos\phi} \quad (2.29)$$

Where $\boldsymbol{e}_i$ is the unit vector of $\boldsymbol{a}_x$ or $\boldsymbol{a}_y$, P_T is the total radiated power, g_{nor} is the normalization factor of the feed which is usually normalized to 4π. The final gain of the offset reflector can be written as [27]:

$$G(0,0)=g_{nor}\frac{4f^2}{\lambda^2}\left|Integral\right|^2 \quad (2.30)$$

where |*Integral*| is the absolute value of the integral given in the right-hand side of Eq. 2.29.

2.2.4 Antenna Phase Centre

Knowledge of the phase centre location of an antenna is of great importance in many applications, such as the GPS, virtual arrays [12], and reflector antennas. Here, the phase centre is defined as the origin of a sphere that coincides with the phase front of the radiated field. For most antennas, such a spherical wave front does not exist over the entire space. However, it can be defined approximately over a finite angular range, normally around the main beam. From the far field point of view, the origin of this sphere is the source of radiation, and thus represents the antenna. For instance, in GPS applications, the phase centre is detected as the antenna location. Thus, displacing the antenna phase centre will move its apparent location. The virtual array antenna can have multiple identical beams, with multiple displaced phase centre locations. Such a property is desirable in remote sensing applications, to allow multiple antenna representations [14]. This concept is also addressed in [28-29] for the small gain antenna of dual-mode circular microstrip antenna. In reflector antennas, the feed phase centre must coincide with the reflector focal point, and any deviation will cause the reflector beam tilt [5]. However, for mechanical or other reasons, applications may exist where the antenna cannot be fully aligned with the target, or receiver. In such cases, the antenna beam may be scanned slightly to enable its full alignment. A possible means of the reflector beam scan is to move the feed phase centre laterally, away from its geometrical centre, located on the reflector focal point.

In this thesis, it will be shown that the phase centre location of an offset reflector antenna can be displaced by using a multimode circular waveguide as a feed. The higher order mode of TE_{21} is used along with the dominant mode to study the concept. The

effect of the polarization of each mode on the phase centre location will be also investigated resulting in virtual antennas with multi-phase centre locations for different polarizations.

2.3 Circular Horn Antenna

Horn antennas are classified as aperture antennas of medium gain. They have been used in diverse applications in communication systems, electromagnetic sensing, radio frequency heating, and antenna measurement, as well as feeds in lens and reflector antennas [30]. It is well known that a hollow conducting pipe radiates from its open end into a medium so as the acoustic wave does from a hollow tube [31]. This open end can then be flared to form a true horn introducing an extra phase term [32-33], which will be explained shortly. Horn antennas can have different aperture geometries, among which the circular one finds widespread attention in many applications due to its axial symmetry.

The pure-mode horn antennas contain a single mode and their radiation patterns are mostly specified by the transverse fields of the mode. Despite their simplicity, the applications of pure-mode horns, as the feeds in the reflector antenna, are limited to array elements. This is because they have poor electrical characteristics. In symmetric reflectors, to optimize the gain performance one needs to equalize the *E*- and *H*-plane patterns of the feed to provide a symmetric aperture-field distribution which, in turn, minimizes the feed and the reflector cross polarizations. More precisely, an optimum feed must provide symmetric field patterns for both the field amplitude and phase. The corrugated conical horn is an example of this optimum feed. In the design of this feed,

one can equalize the *E*- and *H*-plane amplitude patterns by a variation of the corrugated flange geometry and its separation distance form the open end of the waveguide [1]. Another example is the multimode horn which is used in this thesis. Dual-mode circular waveguides are used to reduce the cross polarization of offset reflectors, which will be addressed in chapter three. The required modes are TE_{11} and TE_{21} type modes in a dual-mode scenario. Furthermore, such dual-mode antennas are also employed to study the phase centre displacement of an offset reflector antenna in chapter four for multi-phase centre virtual antenna applications.

2.3.1 Analysis of Circular Horn Antenna

The first analysis of horn antennas, in the form of sectoral horn, was done by Barrow and Chu in 1939 [34]. However, the basic design procedure was introduced by Southworth and King [31, 35] in detail, during 1930s and 1940s for conical horn antennas. Since the foundation of radiation properties of circular horn antennas is identical to that of circular waveguide with equal aperture dimension, we start with the radiation from an open-end circular waveguide antenna.

The *TE* and *TM* modes in a multimode circular waveguide of radius "*a*" are described by following equations in terms of their axial component of the field [5],

TM modes: $$E_z = A_{mn} J_n(K_{mn} r) \cos(n\phi) \qquad (2.31)$$

TE modes: $$H_z = A_{mn} J_n(K_{mn} r) \cos(n\phi) \qquad (2.32)$$

The value of $K_{mn}a$ is given by the roots of either $J'_n(K_{mn}a)=0$ for *TE* modes or $J_n(K_{mn}a)=0$ for *TM* modes. Some eigenvalues (K_{mn}) for these modes are listed in Tables 2.1 and 2.2.

The lower cutoff wavelength for a particular *TE/TM* mode in circular waveguide is determined by the following equation:

$$\lambda_{c,mn}=2\pi a/K_{mn} \tag{2.33}$$

Table 2.1. Eigenvalues for TE_{mn} modes in circular waveguide

m	K_{m1}	K_{m2}	K_{m3}
0	3.832	7.016	10.174
1	1.841	5.331	8.536
2	3.054	6.706	9.970

Table 2.2. Eigenvalues for TM_{mn} modes in circular waveguide

m	K_{m1}	K_{m2}	K_{m3}
0	2.405	5.520	8.654
1	3.832	7.016	10.174
2	5.135	8.417	11.620

The far field radiation components of an open-ended circular waveguide are expressed by the following equations assuming a small reflection coefficient for the aperture [5]:

***TE_{mn}* mode:**

$$E_\theta = j^{m+1}\frac{m\omega\mu e^{-jkR}}{2R}\left[1+\frac{\beta_{mn}}{k}\cos\theta\right]\frac{J_m(K_{mn}a)J_m(k\,a\,\sin\theta)}{\sin\theta}\sin m\phi \tag{2.34}$$

$$E_\phi = j^{m+1}\frac{ka\omega\mu e^{-jkR}}{2R}\left[\frac{\beta_{mn}}{k}+\cos\theta\right]\frac{J_m(K_{mn}a)J'_m(k\,a\,\sin\theta)}{1-\left(\dfrac{k\,a\,\sin\theta}{K_{mn}a}\right)^2}\cos m\phi \tag{2.35}$$

***TM_{mn}* mode:**

$$E_\theta = -j^{m+1}\frac{ka\,K_{mn}e^{-jkR}}{2R\,\sin\theta}\left[\frac{\beta_{mn}}{k}+\cos\theta\right]\frac{J_m(k\,a\,\sin\theta)J'_m(K_{mn}a)}{1-\left(\dfrac{K_{mn}a}{k\,a\,\sin\theta}\right)^2}\cos m\phi \tag{2.36}$$

$$E_\phi = 0 \tag{2.37}$$

As mentioned earlier, the effect of flaring a circular waveguide to form a horn brings the spherical phase cap, which can be modeled using the quadratic phase factor *s* given by [1]:

$$s \approx \frac{a^2}{2\lambda L} \approx \frac{a\theta}{2\lambda} \tag{2.38}$$

where a is the radius of the horn, L is the axial length, and θ is the semi-flare angle as shown in Fig. 2.4.

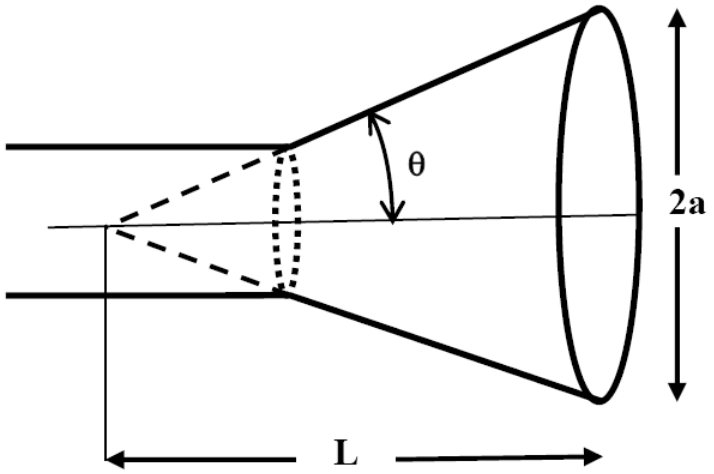

Fig. 2.4. Geometry of conical horn antenna.

The phase factor *s* can then be used to compute the radiation patterns of a conical horn as below [1]:

$$E(\theta,\phi) = C \int_0^{2\pi} \int_0^{a} E_a(r',\phi') e^{jkr' \sin\theta \cos(\phi-\phi')} \; e^{-j2\pi s} \, r' dr' d\phi' \tag{2.39}$$

where C is a constant factor and E_a is the aperture electric field due to a circular waveguide in the cylindrical coordinates.

The corresponding aperture distribution of the dominant mode, TE_{11}, and the higher order TE_{21} mode are shown in Fig. 2.5, which will be used to study different mode alignments in chapter four for virtual array antennas.

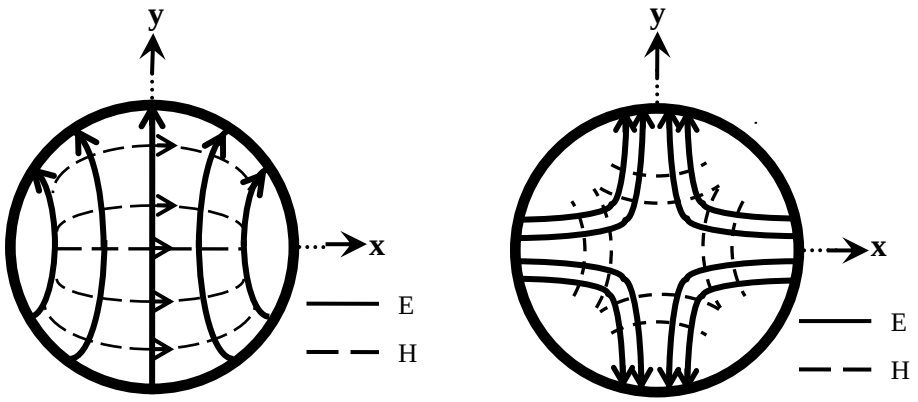

(a) (b)

Fig.2.5. Aperture distribution of the *y*-polarized (a) TE_{11} mode (b) TE_{21} mode.

2.3.2 Multi-mode Circular Horn Antenna

Multimode horns are used to make the pattern symmetric, similar to the corrugated horns, which are required in symmetrical-cut reflectors. The applications of multi-mode horns are not limited to feeds in symmetric reflectors as the higher order modes can be appropriately combined to illuminate an offset reflector antenna to cancel or decrease the cross polarization level, as reported in [8-10].

There are two broad classes of multi-mode horns: “tracking horns” and “shaped-pattern horns”. The basic excitation mechanism of higher order modes is usually either a sharp change in the cross-section dimensions of the horn or the insertion of discontinuity in the form of dielectric or conductor, like a ring or pin. Tracking horns are designed to provide information from the horn terminals which enable a target to be tracked. Shaped-pattern horns can be subdivided into three types [1]:

a) Horns designed to reduce the cross polarization and improve the pattern symmetry. The best example is the Potter horn [36], which is a conical horn

operating at TM_{11} and TE_{11} modes to cancel the crosspolar component of the TE_{11} and hence improve the pattern symmetry.

b) Horn designed to alter the shape of the basic Gaussian copolar pattern to provide a higher illumination efficiency of the reflector antenna.

c) Matched-feed horns designed to use a combination of modes to match the focal region fields of a reflector antenna, thereby improving the radiation performance of the reflector antenna. An example is the use of TE_{11}, TE_{21}, and TM_{11} modes to cancel the cross polarization in linearly polarized offset reflector antennas.

We have used a dualmode circular waveguide antenna operating at the dominant mode, TE_{11}, and higher order TE_{21} mode to reduce the cross polarization level and displace the phase centre location of an offset reflector antenna. A circular waveguide antenna at its fundamental mode generates a broadside radiation pattern, while it has a null at broadside as goes to the higher order modes. The far field radiation patterns of these modes are given below.

***TE_{11}* mode:**

$$E_\theta = -\frac{\omega\mu e^{-jkR}}{2R}\left[1+\frac{\beta_{11}}{k}\cos\theta\right]\frac{J_1(K_{11}a)J_1(k\,a\,\sin\theta)}{\sin\theta}\sin\phi \qquad (2.40)$$

$$E_\phi = -\frac{ka\omega\mu e^{-jkR}}{2R}\left[\frac{\beta_{11}}{k}+\cos\theta\right]\frac{J_1(K_{11}a)J'_1(k\,a\,\sin\theta)}{1-\left(\frac{k\,a\,\sin\theta}{K_{11}a}\right)^2}\cos\phi \qquad (2.41)$$

***TE_{21}* mode:**

$$E_\theta = -j\frac{\omega\mu e^{-jkR}}{R}\left[1+\frac{\beta_{21}}{k}\cos\theta\right]\frac{J_2(K_{21}a)J_2(k\,a\,\sin\theta)}{\sin\theta}\sin 2\phi \qquad (2.42)$$

$$E_\phi = -j\frac{ka\omega\mu e^{-jkR}}{2R}\left[\frac{\beta_{21}}{k}+\cos\theta\right]\frac{J_2(K_{21}a)J'_2(k\,a\,\sin\theta)}{1-\left(\frac{k\,a\,\sin\theta}{K_{21}a}\right)^2}\cos 2\phi \qquad (2.43)$$

2.4 Proposed Study

In this thesis, a dual-mode circular waveguide antenna is selected as a primary feed for an offset reflector antenna. The feed is placed at the focal point of an offset reflector. It will be shown that the phase centre location of the compound antenna can be displaced by controlling mode content factors of the primary feed, as well as the polarization of each mode. In other words, one can have virtual antenna by altering sequentially the excitation amplitude, phase, and alignment of each mode. The resultant antenna can then have multiple identical beams with multiple displaced phase centre locations. Such a property is desirable in remote sensing applications, to allow multiple antenna representations [12]. Particularly, different polarizations of a dual-mode feed are studied to establish the idea and show that the phase centre displacement is feasible along any direction.

With a proper selection of the phase difference between the modes, an antenna with a single phase centre location can be obtained. In this case, the mode excitation ratio can be used to control the polarization. This study has also been done. As a single-phase centre antenna application, an analytic model for the primary feed of offset reflector antennas is presented that facilitates a more general investigation of the cross polarization reduction in both asymmetric and inter-cardinal planes. It includes both first and second order azimuthal modes, primarily the TE_{11} and TE_{21} type modes, and allows selection of symmetric and asymmetrical patterns, with different field tapers in the principal planes. It is shown that minimizing the cross polarization in the asymmetric plane does not necessarily reduce it globally, as in the inter-cardinal plane it remains high. The procedure for reduction of the cross polarization globally and its effects on the sidelobe

levels of the reflector antenna are also investigated. Finally, the effect of phase errors associated with the primary feed on the cross polarization is presented.

2.5 Summary

In this chapter, a brief background theory on the offset reflector, as well as the circular horn antenna was provided. Analysis of the offset reflector, based on physical optics and aperture theory, was reviewed. With respect to the primary feed, multimode circular waveguide antennas were explained with their far-field radiation properties. Finally, the proposed multi-phase centre antenna concept was introduced, in which by varying the mode content factor and polarization of the primary feed, the phase centre location of the offset reflector antenna could be displaced along any axis. As for the single-phase centre antenna, a simplified feed model is proposed to study the offset reflector antenna radiation properties. Emphasis is placed on cross polarization reduction at both asymmetry and inter-cardinal planes.

Chapter 3

Single-Phase Centre Reflector Antennas

3.1 Introduction

In this chapter, offset reflector antennas are studied for single-phase centre antenna applications. As known, such antennas suffer from high cross polarization level when illuminated by a conventional linear polarized feed. To overcome this deficiency, the idea of a matched feed was proposed in [10]. Essentially, the primary feed should conjugately match the focal region of the reflector to reduce or cancel the cross polarization. The tri-mode conical horn feed [10], utilizing the TE_{11}, TE_{21} and TM_{11} modes, is the most popular example of such matched feeds which have been recently revisited in [37-38] for balanced back-to-back reflectors with a reduced moment of inertia.

In this thesis, the cross polarization reduction is further investigated by expressing the feed radiation patterns in terms of analytic functions. Appropriate trigonometric functions are used, based on the general waveguide theory, to represent the first and second order azimuthal modes with arbitrary excitation coefficients. The representation is general and enables the generation of both symmetric and asymmetric radiation patterns, similar to those of TE_{11} and TE_{21} type modes. It also decouples the reflector performance from that of the feed, thus allowing a more general investigation of the reflector antenna cross polarization and its dependence on the second mode. It will be shown that the asymmetrical aperture distribution of the fundamental mode in the presence of the higher TE_{21} mode is sufficient to reduce the cross polarization of offset reflector antenna even

for small *F/D* ratios. First several examples for circular rim offset reflector antennas of different *F/D* ratios are presented. The results are based on the aperture distribution method [22] and are verified by the commercial software TICRA's GRASP v.7 [18], using the physical optics, geometrical optics, and geometrical theory of diffraction. Then, elliptical-rim offset reflectors cases are also selected and studied to further investigate the concept. The effect of cross polarization reduction is also studied on the sidelobe levels and aperture efficiencies of offset reflector antennas. With the proposed feed model, the aperture efficiency of the reflector antenna is improved compared with a standard Gaussian feed with the same edge taper. Finally, the results of this investigation are used to design practical dual mode feeds using simple circular waveguide geometries. Their performance on an offset reflector antenna are then investigated and shown that the reflector cross polarization is significantly reduced within a respectable frequency band. To complete the study, the effects of linear and quadratic phase errors associated with the optimized primary feed are also investigated on the cross polarization of the offset reflector antennas.

3.2 Analytical Model of the Primary Feed [39]

In general, inside a waveguide an infinite number of *TE* and *TM* modes can exist and their radiated field can be expressed by double summations in the form:

$$\begin{aligned} E_\theta &= \sum_n \sum_m \left[A_{nm}^{TE} \; f_{nm}^{TE}(\theta,\phi) + A_{nm}^{TM} \; f_{nm}^{TM}(\theta,\phi) \right] \\ E_\phi &= \sum_n \sum_m \left[B_{nm}^{TE} \; g_{nm}^{TE}(\theta,\phi) + B_{nm}^{TM} \; g_{nm}^{TM}(\theta,\phi) \right] \end{aligned} \tag{3.1}$$

where A_{nm} and B_{nm} are the complex numbers in general to express both amplitude ratios and phase differences of the nm^{th} mode. The $f_{nm}(\theta,\phi)$ and $g_{nm}(\theta,\phi)$ represent radiation properties of the nm^{th} mode and they can be functions of spherical angles of θ and ϕ. The

remarkable property of the round open-ended waveguides and horns is that both $f_{nm}(\theta,\phi)$ and $g_{nm}(\theta,\phi)$ functions are the multiplication of two independent functions of θ and ϕ, in the forms of $f_{nm}(\theta,\phi)=F_{nm}(\theta)\sin(n\phi)$ and $g_{nm}(\theta,\phi)=G_{nm}(\theta)\cos(n\phi)$, assuming the field is *y*-polarized. This allows one to control the pattern of each mode independently in two orthogonal angular spaces, by shaping the waveguide geometry while maintaining its circular cross-section. The required numbers of modes, and their excitation coefficients, normally depend on the application. In addition, the coefficient of each mode can be controlled by the geometry and type of the excitation ports, probes or slots, and the waveguide aperture size which can also cut off the unwanted higher order modes within the operating frequency band.

The modes of special interest in this study are those represented by n=1 and n=2 indices, which are led by TE_{11} and TE_{21} modes in circular waveguides. The first group of modes is led by the TE_{11} mode, the field of which for a *y*-polarized case can be written in the form

$$\begin{aligned} E_\theta &= \left(\sum_{m=1}^{\infty} \left(A_{1m}^{TE}\ F_{1m}^{TE}(\theta) + A_{1m}^{TM}\ F_{1m}^{TM}(\theta) \right) \right) \sin\phi \\ E_\phi &= \left(\sum_{m=1}^{\infty} A_{1m}^{TE}\ G_{1m}^{TE}(\theta) \right) \cos\phi \end{aligned} \qquad (3.2)$$

With an asymmetric excitation, the n=0 mode is not excited and the second group of modes is led by the TE_{21} modes. Their radiated fields form a null along the waveguide axis and can be written as

$$\begin{aligned} E_\theta &= \left(\sum_{m=1}^{\infty} \left(A_{2m}^{TE}\ F_{2m}^{TE}(\theta) + A_{2m}^{TM}\ F_{2m}^{TM}(\theta) \right) \right) \sin 2\phi \\ E_\phi &= \left(\sum_{m=1}^{\infty} A_{2m}^{TE}\ G_{2m}^{TE}(\theta) \right) \cos 2\phi \end{aligned} \qquad (3.3)$$

where F and G are mainly governed by the Bessel functions with the exception of

G_{nm}^{TM}=0 as *TM* modes have no E_ϕ components, as expressed by Eq. 2.34 in chapter 2. The above equations provide exact expressions for the radiated field of an open-ended circular waveguides. However, in practice the excitation port geometry and the filtering property of the waveguide can be used to limit the radiation to the desired modes of operation.

The aim of this chapter is to conduct a general study on the relationship between the feed radiation patterns and the cross polarization of the offset reflector antennas with circular and elliptical rims. For such a study the form of the waveguide radiated field, given by previous equations in term of the waveguide modes, is not suitable. However, the above complex summations can be expressed in terms of simpler sine and cosine functions over the radiation main beams. For instance, since the TE_{11} mode radiates along the waveguide axis, its radiated field along the main beam can be represented by $\cos^{n'}\theta$ [5], where n' is an arbitrary constant and has different values in the two principal planes. The value of this constant can be controlled by several different ways. In a conventional waveguide it can be controlled by the mode excitation coefficients. However, if only the TE_{11} mode must be excited, the beam shaping, i.e. the value of the constant n' can be controlled by shaping the waveguide flare profile, and/or loading it with a suitable dielectric material [1]. It will be shown later that even a simple waveguide discontinuity with proper feed probes and diameter sizes can achieve satisfactory beam controls. Using the same analogy, an analytical model for the TE_{21} lead modes having a null at the boresight may be expressed by $[\sin(2\theta)\cos(\theta-\theta_m)]^p$, where p plays the same role as n', in the previous case for the n=1 modes. Here too, the power p can be controlled by the waveguide mode excitations, or for selected TE_{21} mode, by shaping the feed geometry.

For the sake of generality, we will refer to these two cases as the "TE_{11} type" and "TE_{21} type" modes, i.e. they could refer to the radiated fields of profiled single mode, or dual (multi) mode feeds. The simple sin(2θ) function provides a null at the boresight with the peak located at the θ=45°. The extra factor of cos(θ-θ_m) is multiplied by sin(2θ) to move the beam peak to around the θ=45°. In other words, the angle θ_m also depends on the aperture radius supporting the TE_{21} type mode. Therefore, assuming both mode types are polarized along the y-axis, the analytical model describing the combined TE_{11} type and TE_{21} type modes can be expressed as follows

$$\begin{aligned} E_\theta &= C_1 \cos^{n1}\theta \sin\phi + jC_2\left(\sin(2\theta)\cos(\theta-\theta_m)\right)^{p1}\sin(2\phi) \\ E_\phi &= C_1 \cos^{n2}\theta \cos\phi + jC_2\left(\sin(2\theta)\cos(\theta-\theta_m)\right)^{p2}\cos(2\phi) \end{aligned} \tag{3.4}$$

wherein C_1 and C_2 are the content factors of TE_{11} type and TE_{21} type modes, respectively, and they can be complex numbers in general to represent both amplitude ratio and phase difference of these modes. In the present study, we have selected two separate coefficients to simplify understanding the excitation level of each mode type. However, mathematically one only needs the mode ratio C_2/C_1 to describe the feed function completely. Herein, the feed parameter is shown by the mode ratio C_2/C_1. The exponential terms n_1, n_2, and p_1, p_2 define the tapering function in the E- and H-planes. Since the second term is led by the TE_{21} type mode, the factor j in the second term of Eq. 3.4 represents a 90° phase shift, and is considered in order to be consistent with the radiation pattern of the TE_{21} mode according to Silver [5], Eqs. 2.42 and 2.43. As an example, the normalized amplitude patterns of both TE_{11} type and TE_{21} type modes are illustrated in Fig. 3.1, when it is assumed that each mode type has symmetric patterns at the principal planes. That is, n_1=n_2=p_1=p_2=1 and θ_m=0°. As shown, the first term has a

broadside radiation pattern whereas the second term has a null at the boresight angle of θ=0^o. They correspond closely to the radiation patterns of the TE_{11} and TE_{21} modes.

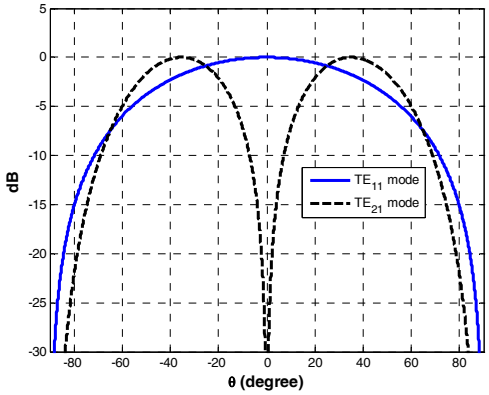

Fig. 3.1. Normalized amplitude patterns of the feed model expressed by Eq. 3.4 for both TE_{11} and TE_{21} modes, when n_1=n_2=p_1=p_2=1 and θ_m=0^o.

3.3 Cross Polarization Reduction in Circular-rim Offset Reflector Antennas [39-40]

The geometry of an offset reflector antenna with a circular-rim is shown in Fig. 3.2. The reflector is defined by the focal length F, the offset angle θ_0, the half-angle subtended by the reflector rim θ*, the diameter of the projected aperture of the offset reflector D, and the offset clearance distance d_c, which is the distance between the axis of the parent parabola and the lower edge of the reflector rim as shown in Fig. 3.2, [2], [23]. The analytic feed described by Eq. 3.4 is located at the focal point f of the reflector shown in Fig. 3.2a. It is shown that with appropriate amplitude and phase excitation of these two type modes, the cross polarization can be reduced at the far-field region. As reported in [10], the TE_{21} mode should have -90^o phase shift with the TE_{11} mode to reduce the cross polarization of the secondary pattern, provided an appropriate amplitude ratio, and more importantly tapering factors for each mode at each principal plane are determined. To conduct an investigation on the cross polarization, offset reflector antennas with different

F/D ratios are studied with $D=20\lambda$, $d_c=\lambda$, where λ is the wavelength at the selected frequency of 10GHz. After an extensive study, it is found that the angle θ_m in Eq. 3.4 is equal to zero, the TE_{21} type mode should have symmetric patterns at the principal planes, and both p_1 and p_2 are equal to unity. Therefore, the remaining parameters are the exponential terms n_1 and n_2 of the TE_{11} type modes, and the amplitude ratio C_2/C_1.

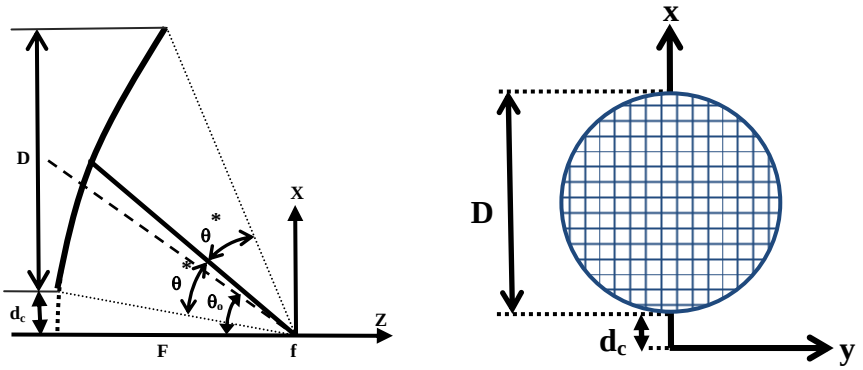

(a) (b)

Fig. 3.2. The geometry of a circular-rim offset reflector antenna (a) cross-section view (b) front view.

Tables 3.1 and 3.2 summarize the cross polarization levels of the secondary patterns of the offset reflector fed by the model given by Eq. 3.4 at the $\phi=90^o$ asymmetry plane and the diagonal $\phi=45^o$ plane, respectively, and compared with the single TE_{11} mode feed, i.e. $C_2=0$. As can be seen, with the dual-mode feed model given by Eq. 3.4, the cross polarization component is reduced to about -47dB even for the large offset angles, at both the asymmetry and $\phi=45^o$ planes. Moreover, the value of C_2/C_1 increases as *F/D* decreases, to obtain the minimum cross polarization level at both above-mentioned planes. This implies that a larger fraction of the TE_{21} type mode is needed to cancel the unwanted cross polarization at the far-field zone for large offset angles. Also, the tapering factor n_2 remains constant for all values of *F/D* ratios, whereas n_1 varies from 2.4 to 2.1 as *F/D* changes from 1.1 to 0.6. As a result, more asymmetric patterns of the

TE_{11} type mode are required to minimize the cross polarization for larger offset angles. It should be mentioned that the required phase difference between the TE_{21} and the TE_{11} type modes is always -90° as explained earlier.

Table 3.1: Reduced cross polarization of offset reflector antennas in the asymmetry ϕ=90° plane, for different *F/D* ratios with $D=20\lambda$, $d_c=1\lambda$, fed by the model given by Eq. 3.4 at f=10GHz.

F/D	θ_o	XPOL (C_2=0)	XPOL by Eq. 3.4	C_2/C_1	n_1	n_2
1.1	26.80°	-28.76	-77.77	0.126	2.4	2.6
1.0	29.12°	-26.89	-77.21	0.139	2.3	2.6
0.8	35.06°	-23.55	-65.18	0.175	2.2	2.6
0.6	43.57°	-19.46	-50.03	0.243	2.1	2.6

Table 3.2: Reduced cross polarization of offset reflector antennas in the inter-cardinal ϕ=45° plane, for different *F/D* ratios with $D=20\lambda$, $d_c=1\lambda$ fed by the model given by Eq. 3.4 at f=10GHz.

F/D	θ_o	XPOL (C_2=0)	XPOL by Eq. 3.4	C_2/C_1	n_1	n_2
1.1	26.80°	-31.24	-55.00	0.126	2.4	2.6
1.0	29.12°	-29.62	-53.55	0.139	2.3	2.6
0.8	35.06°	-26.22	-50.88	0.175	2.2	2.6
0.6	43.57°	-22.15	-47.25	0.243	2.1	2.6

To conduct an investigation on the effect of tapering factors n_1 and n_2 on the cross polarization, an offset reflector antenna is selected with *F/D*=0.595, *D*=66.5cm, d_c=-6.25cm, θ^*=41.80°, and θ_0=32.77°. The operating frequency is 10GHz as before. Fig. 3.3 shows the cross polarization and sidelobe levels of the secondary patterns in terms of C_2/C_1 in both the asymmetry plane of ϕ=90° and the ϕ=45° plane. Different values of n_1 and n_2 are considered as: i) $n_1=n_2=1$, ii) $n_1=n_2=2$, iii) n_1=2.2, n_2=2.6, and iv) n_1=2.0, n_2=3.0. Cases i and ii correspond to the symmetric *E*- and *H*-plane patterns for the TE_{11} type mode and cases iii and iv generate asymmetric ones. As can be seen, the sidelobe levels are almost unchanged for different amplitude ratios of C_2/C_1 and it is minimum when there is stronger tapered distribution for the TE_{11} type mode, i.e. n_1=2.0 and n_2=3.0,

as expected based on the aperture theory. However, the cross polarization levels mainly depend on C_2/C_1 and are well below -50dB at both planes when n_1=2.2 and n_2=2.6, and C_2/C_1=0.177.

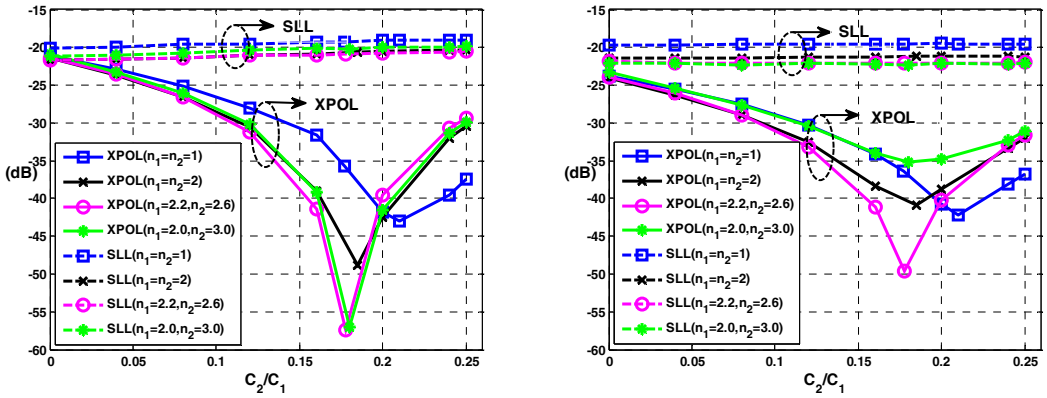

(a) (b)

Fig. 3.3. Cross polarization and sidelobe levels of the circular-rim offset reflector antenna (F/D=0.595, D=66.5cm, d_c=-6.25cm, θ^*=41.80°, and θ_0=32.77°), fed by the tapered dualmode feed given by Eq. 3.4 at the frequency of 10GHz (a) ϕ=90° (b) ϕ=45° plane.

The normalized copolar and crosspolar radiation patterns are shown in Fig. 3.4 for the optimum case, when n_1=2.2, n_2=2.6 and C_2/C_1=0.177, with a -90° phase shift. They are also compared with a standard Gaussian feed with a -12dB edge illumination. As can be seen, the cross polarization level of the secondary patterns is reduced from -25dB, when fed by the Gaussian feed, to less than -50dB when fed by the proposed tapered feed in Eq. 3.4, at both ϕ = 90° and 45° planes. The radiation patterns of the primary feed are shown in Fig. 3.5 for the optimized case of n_1=2.2, n_2=2.6 and C_2/C_1=0.177 with a -90° phase shift. As can be seen, the feed mostly illuminates the upper section of the offset reflector antenna aperture, with its phase centre located at the focal point of the reflector.

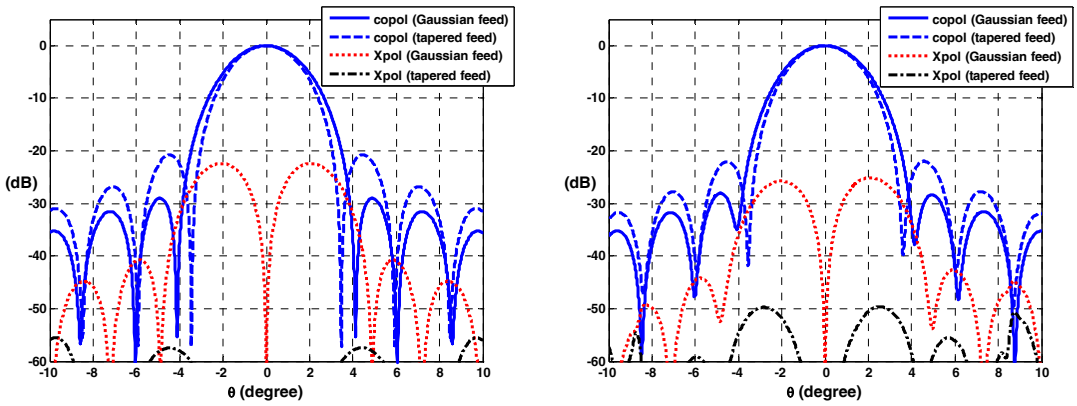

Fig. 3.4. Normalized copolar and crosspolar radiation patterns of the circular-rim offset reflector antenna (F/D=0.595, D=66.5cm, d_c=-6.25cm, θ^*=41.80°, and θ_0=32.77°), fed by a Gaussian feed (-12dB edge illumination) and the optimized tapered dualmode feed operating at TE_{11} and TE_{21} with C_2/C_1=0.177∠-90°, n_1=2.2, and n_2=2.6 (a) ϕ=90° (b) ϕ=45°.

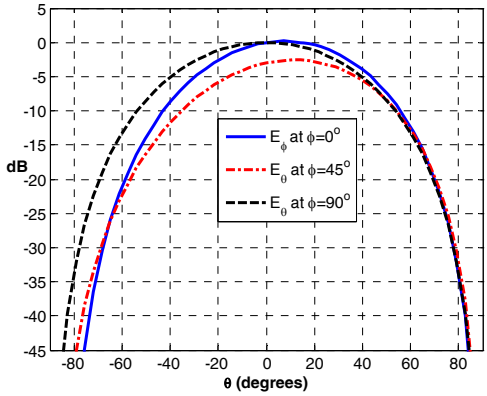

Fig. 3.5. Normalized radiation patterns of the feed model defined by Eq. 3.4 with n_1=2.2, n_2=2.6, and C_2/C_1 =0.177∠-90°.

3.4 Cross Polarization Reduction in Elliptical-rim Offset Reflector Antennas [39]

In this section, the effect of the proposed feed is studied on the elliptic-rim offset reflector antenna shown in Fig. 3.6. The focal length and d_c remain similar to the example of circular-rim offset reflector discussed in section 3.3. The minor axis, D_H, is selected to be equal to the diameter of the circular-rim offset reflector which is 66.5cm. First, the major axis of the ellipse, D as shown in Fig. 3.6, changes from D_H to 90cm, to gradually

form an elliptical projected aperture. The resulting sidelobe levels and cross polarizations are shown in Fig. 3.7, for the same values of n_1 and n_2 stated in the previous section at both asymmetry and inter-cardinal planes, when C_2/C_1=0.18 with a -90° phase shift. The sidelobe level decreases as the major axis of the ellipse increases and it is minimum when n_1=2.2 and n_2=2.6. As for cross polarization, the same tapering numbers yield the minimum value of cross polarization at both ϕ-planes. They are less than -50dB and -48dB at the ϕ=90° and the ϕ=45° planes, respectively. Therefore, it has been shown that the same tapering numbers can minimize the cross polarization of the elliptic-rim offset reflector antenna under study.

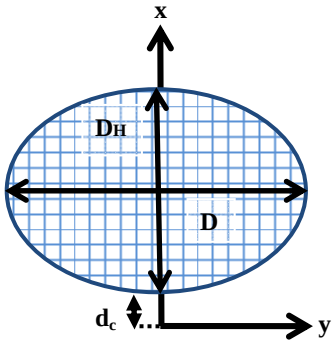

Fig. 3.6. Cross-section view of the projected aperture of an elliptic-rim offset reflector antenna.

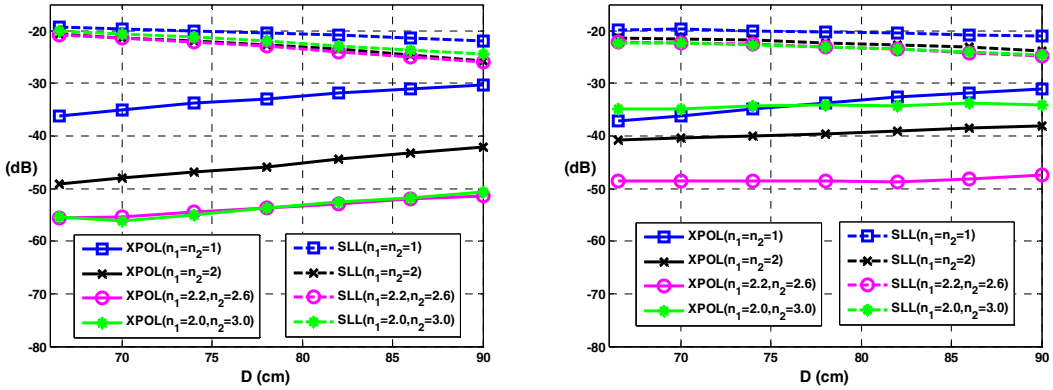

(a) (b)

Fig. 3.7. Cross polarization and sidelobe levels of the elliptical-rim offset reflector antenna fed by the tapered dualmode feed operating at TE_{11} and TE_{21} when C_2/C_1=0.18∠-90° at (a) ϕ=90° (b) ϕ=45° planes.

Now, the major axis of D = 90cm is selected to conduct study on the sidelobe and

cross polarization levels, in terms of the amplitude ratio C_2/C_1, for the same tapering numbers of i) $n_1=n_2=1$, ii) $n_1=n_2=2$, iii) $n_1=2.2$, $n_2=2.6$, and iv) $n_1=2.0$, $n_2=3.0$ as before. The results are shown in Fig. 3.8 at both ϕ-planes of 90^o and 45^o. As can be seen, the cross polarization reaches to less than -48dB at both planes when $C_2/C_1=0.18$, $n_1=2.2$, and $n_2=2.6$. The corresponding secondary patterns of this optimized case are depicted in Fig. 3.9 and are compared with a standard Gaussian feed with a -12dB edge illumination, as a primary feed. As can be seen, the cross polarization decreases from almost -23dB to about -48dB at both planes. The feed radiation patterns are almost the same as the ones shown in Fig. 3.5.

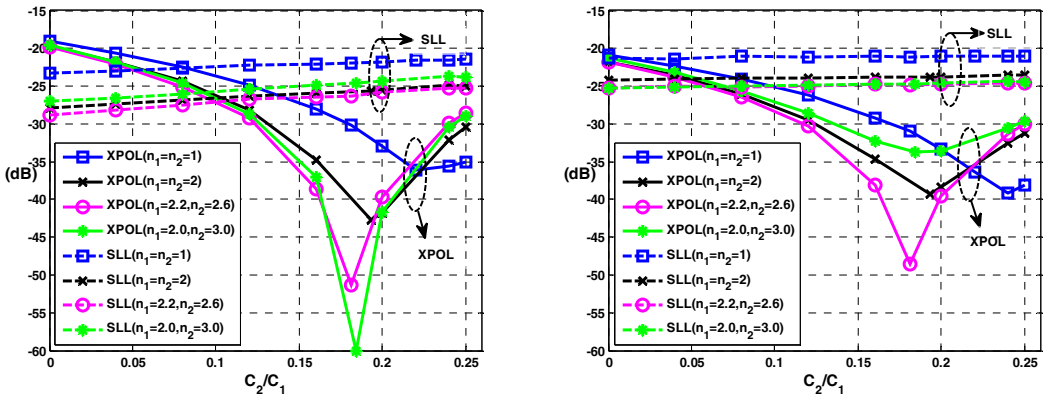

(a) (b)

Fig. 3.8. Cross polarization and sidelobe levels of the elliptical-rim offset reflector antenna (F=39.6cm, D=90cm, D_H=66.5cm, and d_c=-6.25cm) fed by the tapered feed given by Eq. 3.4, (a) $\phi=90^o$ (b) $\phi=45^o$planes.

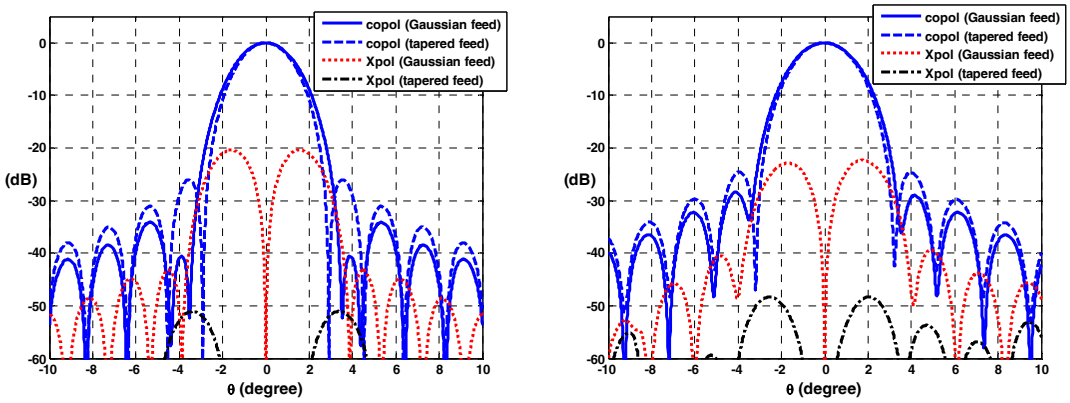

(a) (b)

Fig. 3.9. Normalized copolar and cross polar radiation patterns of the elliptical-rim offset reflector antenna (F=39.6cm, D=90cm, D_H=66.5cm, and d_c=-6.25cm), fed by a Gaussian feed with -12dB edge illumination and the optimized tapered dualmode feed, with $C_2/C_1=0.181\angle-90^o$, $n_1=2.2$, and $n_2=2.6$ (a) $\phi=90^o$ (b) $\phi=45^o$.

The performance of the offset reflector antennas with the matched primary feed proposed in this section was also compared with three different primary feeds: the tapered feed with -12dB, the Gaussian feed with -5dB, and the Gaussian feed with -12dB edge illuminations. The results are summarized in Tables 3.3 and 3.4 for the circular- and elliptical-rim reflectors, the two examples discussed earlier as illustrated in Figs. 3.4 and 3.9, respectively. As can be seen, the proposed feed provides better aperture efficiencies, illumination and spillover factors, compared with a standard Gaussian feed of -5dB edge illumination for both circular- and elliptical-rim reflectors with much reduced cross polarized components and comparable sidelobe levels. The -5dB edge illumination have been considered in order to make a valid comparison. According to Fig. 3.5, the value of the primary radiation pattern at the half-angle subtended by the rim (θ^*), which is around 40^o, is approximately 5dB below its value at the $\theta=0^o$. If the standard -12dB Gaussian feed were to be used, the proposed tapered feed given by Eq. 3.4 needs to provide the same edge illumination of -12dB according to the new mode content factor and exponential terms as denoted in the footnote of Tables 3.3 and 3.4. The corresponding results are listed under columns 3 and 5 of above-mentioned tables. For the circular-rim case, with the -12dB tapered feed the cross polarization levels are still below -35dB compared with the Gaussian feed of -12dB edge illumination, whereas their sidelobe levels and efficiencies are pretty much the same. However, for the elliptic-rim case, the -12dB tapered feed results in low cross polarization at only the asymmetry plane and lower efficiency. It should be noted that the Gaussian feed #1 provides -5dB at the $\theta=41.80^o$ and -7.35dB edge illuminations at the $\theta=51.11^o$, the two half-angles subtended by the elliptical-rim case. Similarly, the edge illumination of the Gaussian feed #2 is -

8.25dB at the θ=41.80^o and -12dB at the θ=51.11^o.

Table 3.3. Gain, Aperture efficiencies, cross polarization, and SLL of the Circular-rim offset reflector discussed in Fig. 3.4 with the proposed tapered feed and standard Gaussian feeds.

		Proposed Tapered feed	Tapered feed with ~ -12dB*	Gaussian feed -5dB	Gaussian feed -12dB
Gain		**35.54dB$_i$**	35.69dB$_i$	34.90dB$_i$	35.80dB$_i$
η_{ap}		**73.84%**	76.44%	63.72%	78.40%
Xpol	**ϕ=45^o**	**-49.80dB**	**-36.63dB**	**-24.07dB**	**-25.22dB**
	ϕ=90^o	**-56.54dB**	**-39.96dB**	**-21.38dB**	**-22.41dB**
SLL	**ϕ=45^o**	**-22.02dB**	-27.93dB	-21.38dB	-28.17dB
	ϕ=90^o	**-20.87dB**	-28.31dB	-21.76dB	-29.06dB

*-12dB edge taper at θ=41.80^o with n_1= n_2=5.2 and C_2/C_1=0.1$\angle$-90^o

Table 3.4. Gain, Aperture efficiencies, cross polarization, and SLL of the elliptical- rim offset reflector discussed in Fig. 3.9 with the proposed tapered feed and standard Gaussian feeds.

		Proposed Tapered feed	Tapered feed with ~ -12dB*	Gaussian feed #1 -5dB	Gaussian feed #2 -12dB**
Gain		**37.05dB$_i$**	36.62dB$_i$	36.62dB$_i$	36.94dB$_i$
η_{ap}		**77.25%**	69.96%	69.96%	75.31%
Xpol	**ϕ=45^o**	**-48.38dB**	**-23.48dB**	**-21.51dB**	**-22.38dB**
	ϕ=90^o	**-51.12dB**	**-41.04dB**	**-19.64dB**	**-20.51dB**
SLL	**ϕ=45^o**	**-24.68dB**	-31.49dB	-24.25dB	-29.18dB
	ϕ=90^o	**-26.11dB**	-40.12dB	-28.09dB	-40.70dB

*-12dB edge taper at θ=51.11^o with n_1=5.2, n_2=3.2, and C_2/C_1=0.1$\angle$-90^o
** First side lobe levels are given.

3.5 Dual-Mode Feed Design

In section 3.2, simple mathematical expressions for the radiation field of the feed were selected to allow a complete investigation of the reflector performance. In general, the required radiation patterns of the optimum feed can be generated by a suitable combination of the *TE* and *TM* modes, or by selecting the first two TE_{11} and TE_{21} modes and shaping the cross section profile of the feed, as well as loading it preferentially by dielectrics [1]. However, it will be shown that such a feed can also be designed simply by a proper selection of circular waveguides of different diameters and lengths, and exciting efficiently the TE_{11} and TE_{21} modes. It will also be shown that such a simple feed can

effectively improve the offset reflector performance. Traditionally, the input impedance matching of a multimode waveguide is adversely affected by exciting a higher order mode. It will be demonstrated that the higher order TE_{21} mode has a negligible impact on the return losses of the proposed dual-mode feeds.

In this section, two novel dual mode circular waveguide feeds are proposed. They generate both TE_{11} and TE_{21} modes with a quadrature -90^{o} phase difference in different amplitude ratios. Feed #1 is a simple choke excited circular waveguide. It consists of a central round waveguide with a single longitudinal slot opening to a surrounding single choke of circular cross-section. It generates the dominant TE_{11} mode inside the waveguide and the higher order TE_{21} mode inside the choke. Therefore, it separates the two modes spatially, and isolates the input waveguide from the detrimental effects of the higher order TE_{21} mode providing a wide impedance bandwidth, without the need for a matching network. Feed #2 is a compact circular waveguide antenna with a small discontinuity step and two blocks to excite the TE_{21} mode. These blocks are tangent to the aperture of the second waveguide, as opposed to the traditional case where they are usually located right at the discontinuity step, which results in high reflections. It is shown that the proposed feed provides a good impedance match, over a wide frequency band, similar to its counterpart for the single mode antenna with no blocks. All simulations are carried out using ANSOFT HFSS v.12 [19], which is based on the Finite Element method. The prototypes of both antennas are fabricated and tested. There is an excellent agreement between the simulated and measured results.

3.5.1 Feed #1: Choke Excited Circular Waveguide with Slot [41-42]

The geometry of the antenna under study is shown in Fig. 3.10. It consists of a central round waveguide with a single longitudinal slot opening on its wall into a single round choke. The physical dimension of the slot is defined by its half-angular opening and its height, as denoted by α and h in Fig. 3.10, respectively. The desired modes of operation are a combination of the TE_{11} and TE_{21} modes. The radius of the central waveguide is designed to excite the dominant TE_{11} mode. The slot is to couple some of its energy into the higher order TE_{21} mode inside the choke. In other words, the required cross-sectional change is made through the slot, right at the junction of the central cylinder and the choke. The outer radius of the choke is selected judiciously to support only the TE_{21} mode and suppress all other higher order modes. The inner and outer radii were optimized to be a=13mm and b=17.7mm, respectively, to meet the above-mentioned criteria. With a y-polarized wave port excitation, the antenna finds an asymmetrical structure, which is needed for the excitation of the TE_{21} mode. This structure can now operate as a dual-mode antenna. For this antenna to work as a primary feed for offset reflector antennas, the phase difference between the two modes must be -90^{o} [10]. Therefore, the lengths of the choke and the waveguide are optimized to provide such a phase shift and they are equal to 19mm and 77.5mm, respectively. That is, L_{ch}=19mm and L=77.5mm.

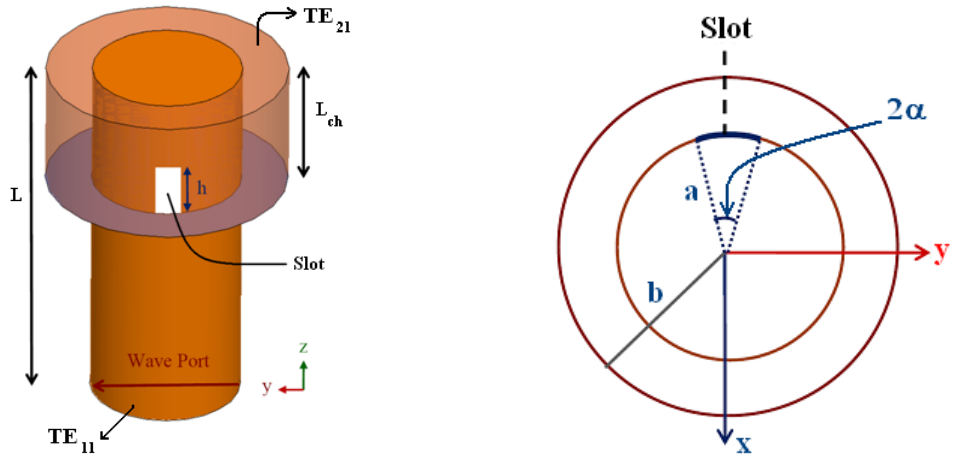

(a) (b)

Fig. 3.10. Geometry of the feed#1 operating at the TE_{11} mode inside the waveguide and TE_{21} mode inside the choke, with a=13mm, b=17.7mm, L_{ch}=19mm, and L=7.75cm (a) 3-D view (b) top-view.

3.5.1.1 Feed #1: Numerical Results

To simplify understanding the contribution of each mode in the far-field region, especially the mode content factor, Eq. 3.4 is used to model the radiation patterns of the proposed dual-mode feed based on the curve-fitting method. Several studies were performed to investigate the effect of the slot height and its angular width on the mode content factor and exponential terms in the analytical model expressed by Eq. 3.4. It is found that the angle θ_m in Eq. 3.4 is equal to zero, the TE_{21} type mode should have symmetric patterns at the principal planes, and both p_1 and p_2 are equal to unity. Therefore, the remaining parameters are the exponential terms n_1 and n_2 of the TE_{11} type modes, and the amplitude ratio C_2/C_1 and Eq. 3.4 can be rewritten as,

$$E_\theta = C_1 \cos^{n1}\theta \sin\phi + jC_2 \sin(2\theta)\cos\theta \sin(2\phi)$$
$$E_\phi = C_1 \cos^{n2}\theta \cos\phi + jC_2 \sin(2\theta)\cos\theta \cos(2\phi) \qquad (3.5)$$

Fig. 3.11a shows the effect of the slot height on the amplitude ratio of C_2/C_1 over the frequency range of 7.0 to 9.0GHz, for a fixed value of α=6.8°. As can be seen, the amplitude ratio increases with frequency. Also, the larger the height of the slot, the

stronger the TE_{21} mode is as expected. Similarly, the effect of angular width of the slot, α, is shown in Fig. 3.11b. It follows almost the same trend as explained for the height, except for α=4°, where the mode content factor decreases up to 8.0GHz, and starts increasing thereafter.

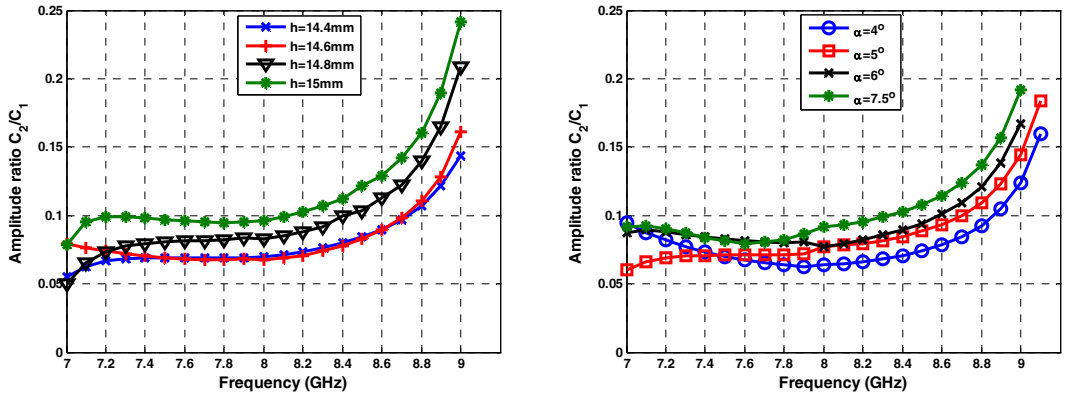

(a) (b)

Fig. 3.11. Amplitude ratio of C_2/C_1 of the feed #1 shown in Fig. 3.10 versus frequency, (a) effect of h when α=6.8°, (b) effect of α when h=14.6mm.

The exponential terms of the dominant mode are also determined by Eq. 3.5. The corresponding results are illustrated in Fig. 3.12. The impact of the slot height and its angular opening are shown in Figs. 3.12a-b, and Figs. 3.12c-d, respectively. As can be seen, the exponential terms of n_1 and n_2 are equal to each other up to 8.7GHz, and become slightly different thereafter. This implies that the TE_{11} mode of the proposed feed generates symmetric E- and H-plane radiation patterns over the frequency range of 7.0-8.7GHz. Therefore, the beamwidth of this mode is not sensitive to the slot's physical dimensions. However, the generated TE_{21} mode causes the antenna beam tilt and increased cross polarization, the amount of which depends on the slot size, in terms of the percentage energy conversion to the TE_{21} mode through the slot. To clarify this, the normalized copolar and crosspolar radiation patterns of the antenna under study, with and without slot, are compared in Fig. 3.13 at the operating frequency of 9.0GHz. The slot

size is selected as h=14.4mm and α=6.8°. The copolar patterns with no slot are completely symmetric, as shown in Fig. 3.13a, with their main beam located at the boresight direction, whereas the main beam of the copolar pattern with the slot at the ϕ=0° is scanned due to the presence of the TE_{21} mode, as shown in Fig. 3.13b. In addition, the crosspolar component increases when the slot is present. In fact, such an asymmetry and high cross polarization level, in the primary feed, are required to reduce the inherent cross polarization of the offset reflector antenna as will be explained shortly.

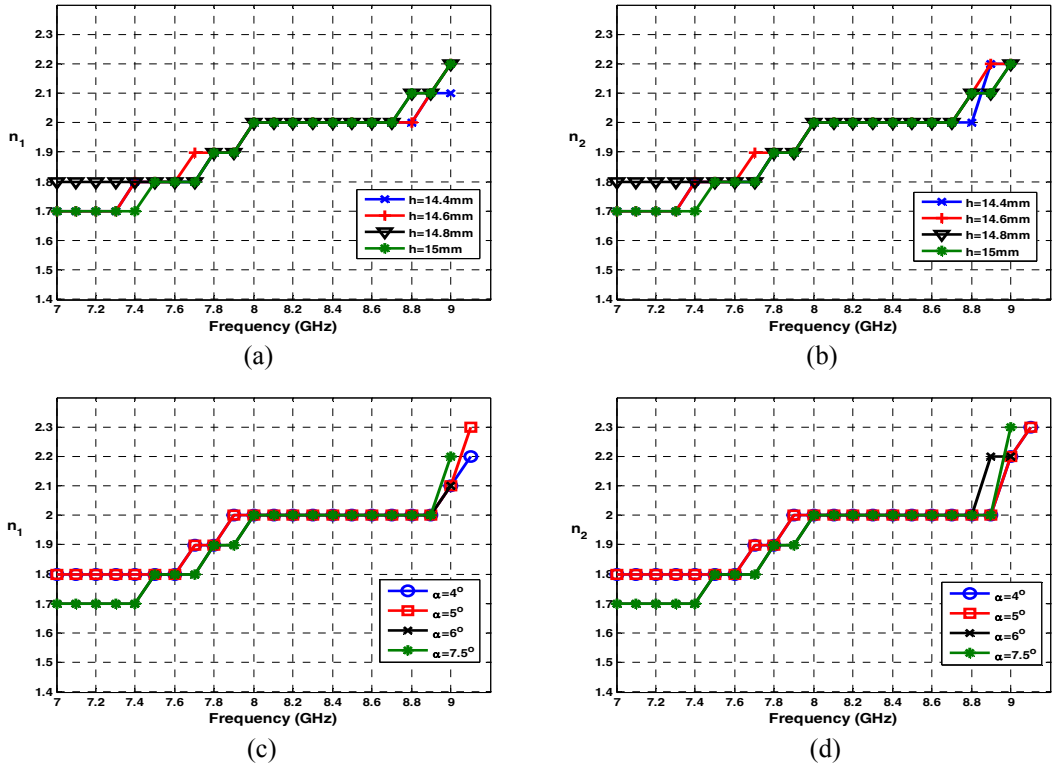

Fig. 3.12. The exponential terms for the TE_{11} mode of the feed #1 versus frequency, (a)-(b) effect of h when α=6.8°, (c)-(d) effect of α when h=14.6mm.

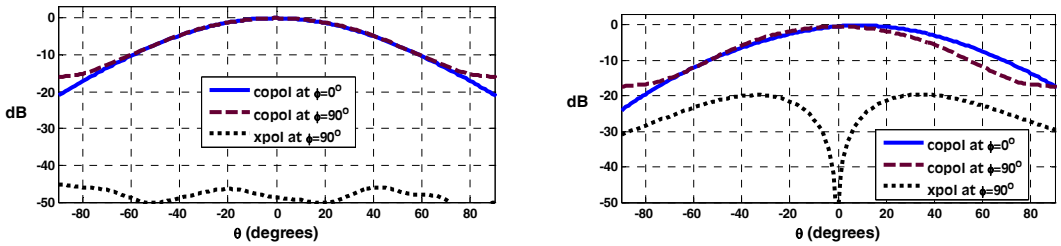

Fig. 3.13. Normalized copolar and crosspolar patterns of the feed #1 at f=9.0GHz (a) no-slot (α=h=0), (b) with slot h=14.4mm and α=6.8°.

The boresight gains of the antenna are also studied for different slot sizes. Fig. 3.14 shows the boresight gain variations as the slot height varies from 14.4mm to 15mm for a fixed value of α=6.8°. As can be seen, the boresight gain changes smoothly from 8.5 to 10dB$_i$. The feed performance is therefore stable over the frequency range of 7.0-9.0GHz, and the gain change is only 1.5dB. The effect of angular opening of the slot, i.e. α, on the gain is the same as the one shown in Fig. 3.14.

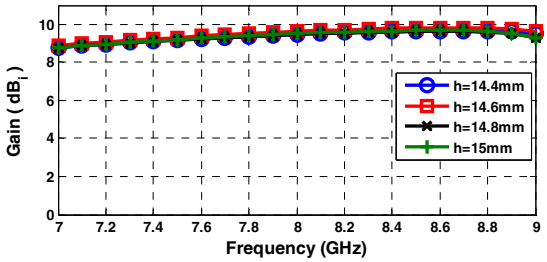

Fig. 3.14. Boresight gain of the feed #1 versus frequency for different h when α=6.8°.

As indicated in Section 3.5, the antenna proposed in Fig. 3.10 can be used as a primary feed for offset reflector dishes to reduce their inherent high cross polarization components. To verify this, the dual-mode feed with a slot height of 14.4mm has been used as a primary feed to illuminate a commercial elliptic-rim offset reflector of 36"×27" and F/D=0.6, at the frequency of 9.0GHz. The copolar and cross-polar radiation patterns at the asymmetry plane, i.e. ϕ=90° plane, are plotted in Fig. 3.15 and compared with the case when the primary feed is a conventional single mode circular waveguide with a radius of 18mm. As can be seen, the cross polarization of the compound reflector and the feed improves by about 13dB when the proposed dual-mode feed is used to illuminate the offset reflector antenna. At the frequency of 9.0GHz, C_2/C_1= 0.15$\angle$-90° with n_1=2.1 and n_2=2.2, which gives almost symmetric E- and H-plane TE_{11} mode patterns. To further reduce the cross polarization, the desired values of n_1 and n_2 are 2.2 and 2.6, respectively,

as obtained in section 3.4. The reflector gains, when illuminated by the dual-mode and single mode feeds, are in the same order and equal to 35.45dB$_i$ and 35.43dB$_i$, corresponding to aperture efficiencies of 62.97% and 62.68%, respectively. It should be noted that the required amplitude ratio of C_2/C_1, to reduce the cross polarization of offset reflectors, depends mainly on the offset reflector geometry, while the required phase difference between the two modes must always be -90^o [10].

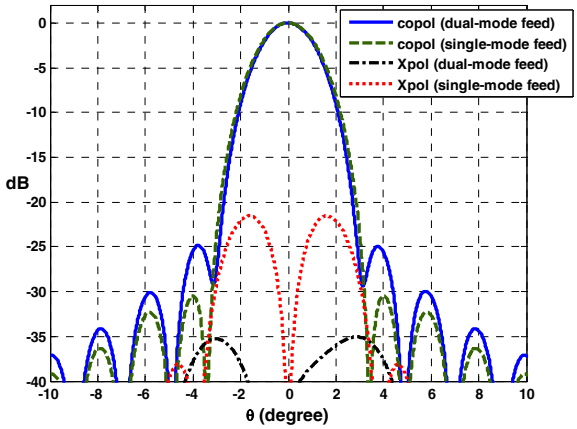

Fig. 3.15. Copolar and crosspolar radiation patterns of an elliptic offset reflector antenna with *F/D*=0.6 at the ϕ=90^o plane and f=9GHz fed by a conventional single mode circular waveguide and the feed #1 with the slot height of 14.4mm.

3.5.1.2 Feed #1: Measurement Results

To verify the simulation results, a prototype of the antenna shown in Fig. 3.10 was built. Photograph of the fabricated antenna is shown in Fig. 3.16. The antenna parameters were the same as those in Fig. 3.10, with the slot length of 14.5mm and half-angular opening of 6.8^o. The resulting mode content factor, which is the ratio of TE_{21}/TE_{11}, is around $0.15\angle$-90^o at the frequency of 9.0GHz. The measured co-polar and cross-polar radiation patterns of the fabricated antenna are compared with the corresponding simulated results at the principal planes and the operating frequency of 9.0GHz. They are illustrated in Fig. 3.17. As can be seen, they are in excellent agreement. The asymmetry

of the co-polar pattern in $\phi = 0$ plane is due to the TE_{21} mode, and is necessary for reduction of the cross polarization of the offset reflectors. The boresight gain of this antenna is near $10dB_i$ similar to the simulation result. The minor undulations on the measured data are due to small reflections from the support structure, holding it on the tower. Because there is no discontinuity inside the central waveguide, the antenna remains well matched to a standard 50Ω input. The measured and simulated scattering parameters of the antenna are compared in Fig. 3.18, over the frequency range of 8.0-9.2GHz, which agree well. The waveguide transition, from a rectangular cross-section to a circular one, available in the laboratory was designed to work over the X-band frequency range from 8GHz to 12GHz. Thus, the measured S_{11} is shown only for frequencies above 8GHz. The antenna bandwidth is much wider, as shown by the simulated S_{11}, exhibiting a broad 10dB bandwidth from 7.1 to 9.2GHz.

Fig. 3.16. Photograph of the prototype feed #1 (choke excited circular waveguide with slot).

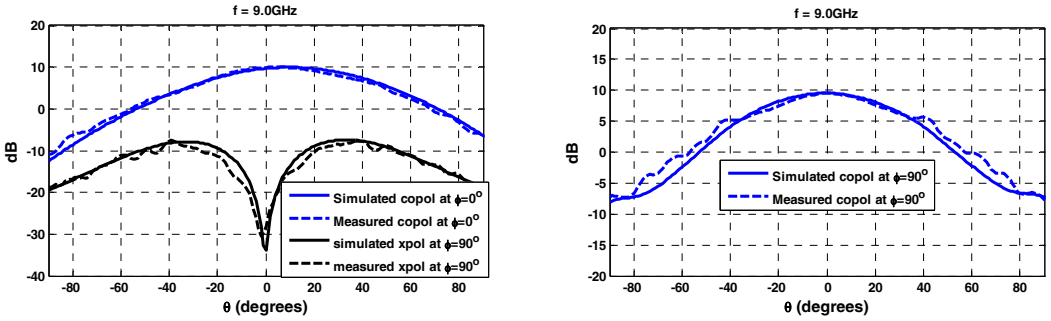

(a) (b)

Fig. 3.17. Measured and predicted co-polar and cross-polar radiation patterns of the proposed antenna at the frequency of 9.0GHz, (a) co-polarization at the ϕ=0° and cross-polarization at the ϕ=90°, (b) co-pol at the ϕ=90° plane.

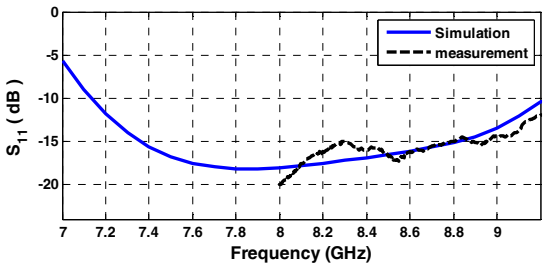

Fig. 3.18. Measured and simulated S_{11} of the proposed antenna versus frequency.

3.5.2 Feed #2: Stepped Circular Waveguide with two Tuning Screws [43]

The geometry of proposed feed is shown in Fig. 3.19. It consists of only two waveguide sections. The diameter of the larger waveguide is selected as smaller as possible so that only the TE_{11} and TE_{21} modes can propagate and the latter higher mode can be excited efficiently. Its excitation sources are two radial blocks/screws, which can be placed at any arbitrary axial position. In the present design, they are placed on the feed aperture, to be far from the waveguide discontinuity, to cause maximum attenuation of the higher order modes at the junction. In this manner, the input waveguide port is not influenced by their presence and the feed can be designed easily to be broadband. The radial excitation screws do not excite the *TM* modes efficiently [44] and the main operating modes are the TE_{11} and TE_{21} modes. However, a step discontinuity used in the

proposed feed may excite the next higher order TM_{11} mode. This has been taken care of by selecting the appropriate aperture size to cut off the TM_{11} mode over the frequency band of interest. As a result, the TM_{11} mode ratio will be very small and its contribution on the cross polarization of the offset reflector is negligible. In addition, if a tri-mode feed is to illuminate an offset reflector to reduce its cross polarization, the TM_{11} mode ratio should be almost the same level as the TE_{21} mode ratio as reported in [10], [38]. The length of the larger waveguide is selected such that the phase difference between the two modes is -90^{o} over the frequency range of interest, which is from 8.0 to 9.1GHz. This frequency band was selected to enable experimental verification, because a waveguide transition at this band was available in the laboratory. The antenna dimensions can be scaled readily for operation at any other band. After optimizing the antenna design, the inner and outer radii were found to be 13 and 17.3mm, respectively. The length of the larger waveguide was 24mm to provide the required -90^{o} phase shift between the modes, and the total antenna length and waveguide wall thickness were 77.5 and 2mm, respectively. This structure can now operate as a dual-mode feed with different mode content ratios using tuning screws.

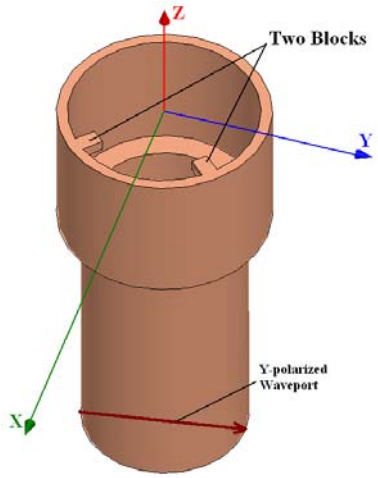

Fig. 3.19. The geometry of the proposed dual-mode circular waveguide horn (feed#2) with tuning blocks/screws to use as a primary feed in offset reflector antennas.

3.5.2.1 Feed #2: Numerical Results

In this section, first the impact of the length of the tuning blocks/screws on the mode amplitude ratio of the proposed antenna shown in Fig. 3.19 is presented. Then, the input impedance matching of the proposed dual-mode antenna is compared with those of the same antenna, when it generates only the dominant TE_{11} mode, i.e. with no tuning blocks, as well as when the blocks are placed right at the discontinuity step. As mentioned earlier, the phase shift between the two modes is -90^{o}. Therefore, the remaining parameters to be studied are the amplitude mode ratio, C_2/C_1, and exponential terms of the TE_{11} mode expressed by n_1 and n_2 as given by Eq. 3.5. It should be mentioned that the two blocks shown in Fig. 3.19 are identical and their heights and widths are fixed and equal to 2 and 3mm, respectively. Fig. 3.20 illustrates how the amplitude ratio of C_2/C_1 varies as the length of the blocks changes from 3mm to 5mm, over the frequency range of 8.0-9.1GHz. As can be seen, the longer the blocks, the stronger the TE_{21} mode is, as expected. The exponential terms n_1 and n_2 of the TE_{11} mode are shown in Fig. 3.21 and increase with frequency. For the block lengths of 3 and 4mm, the antenna has symmetric radiation patterns, i.e. equal in *E*- and *H*-planes, over the entire frequency range of 8.0-9.1GHz, as the exponential terms of n_1 and n_2 are equal. However, for the block length of 5mm, it generates slightly asymmetric radiation patterns up to 8.5GHz, which is required for cross polarization reduction in offset reflectors.

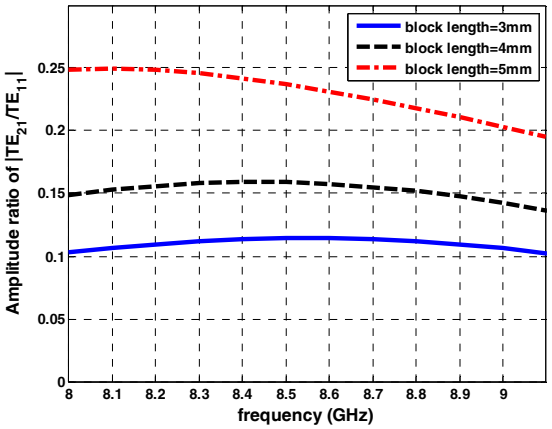

Fig. 3.20. Effect of the block lengths on the amplitude ratio of TE_{21}/TE_{11} of the feed #2 versus frequency.

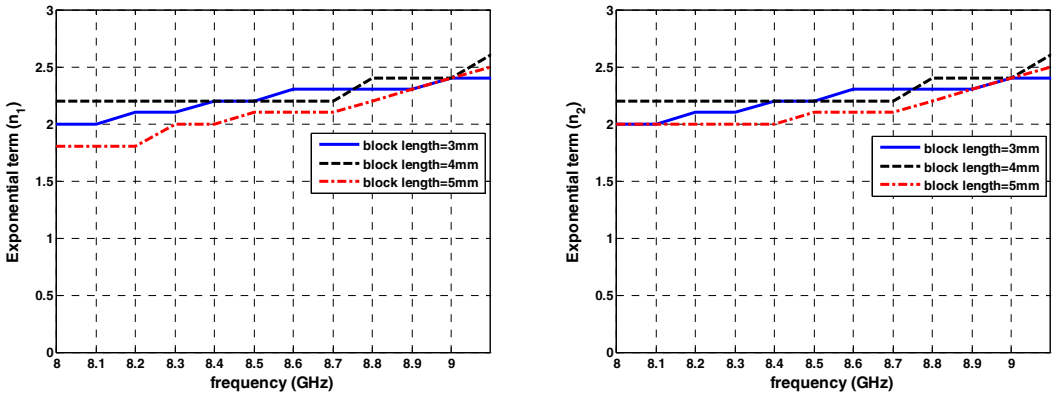

(a) (b)

Fig. 3.21. Effect of the block lengths on the exponential terms of the TE_{11} mode as given by Eq. 3.5 of the feed #2 versus frequency (a) n_1, (b) n_2.

The results of the input impedance matching with different block lengths are shown in Fig. 3.22, and compared with those of two other antennas, namely, the same antenna with no blocks present and the same geometry when the 5mm blocks are placed right at the discontinuity, as in traditional designs. As can be seen, when blocks are at the aperture their reflections have negligible effects on the S_{11} of the proposed dual-mode antenna, as compared to the case when the blocks are inside the waveguide structure at the discontinuity, which significantly deteriorates S_{11} to above -10dB, over the entire

frequency range of interest. For the proposed antenna S_{11} remains well below -15dB, for all block lengths, including the zero value, which implies no block is present.

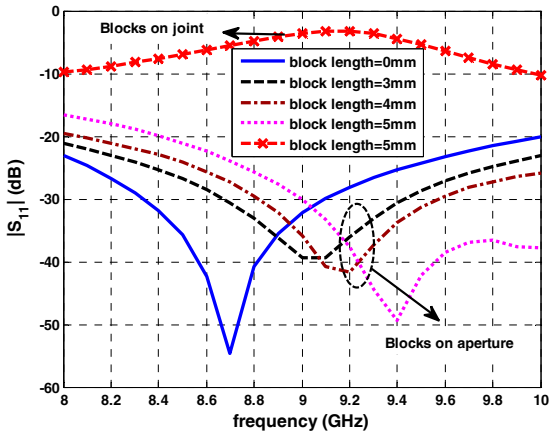

Fig. 3.22. S_{11} of the feed #2 with different block lengths compared with the same antennas with no blocks and with 5mm blocks placed right at the discontinuity joint.

The proposed dual-mode feed shown in Fig. 3.19 is also used to illuminate the commercial elliptic-rim offset reflector of 36"×27" and F/D=0.6. The resulting reduced cross polarization levels versus frequency are shown in Fig. 3.23 at both the ϕ=90^o and 45^o planes. They are well below -30dB over the frequency range of 8.0-8.6GHz. As an example, the secondary radiation patterns of the composite reflector and the proposed feed shown in Fig. 3.19 are plotted in Fig. 3.24 at the frequency of 8.3GHz at both previously-mentioned ϕ-planes. The cross polarization components are less than -35dB and -42dB at the inter-cardinal and asymmetry planes, respectively. This can be compared with the single TE_{11} mode feed case when the cross polarization components are in the order of -22dB.

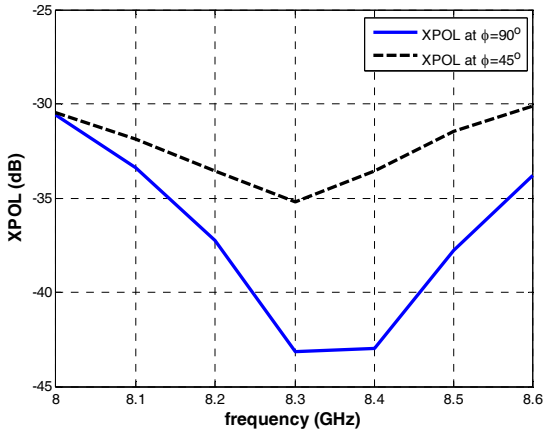

Fig. 3.23. Reduced cross polarization levels at both ϕ=90° and ϕ=45° planes with the simulated primary feed shown in Fig. 3.19 illuminating the elliptical-rim offset reflector antenna used in Fig. 3.9.

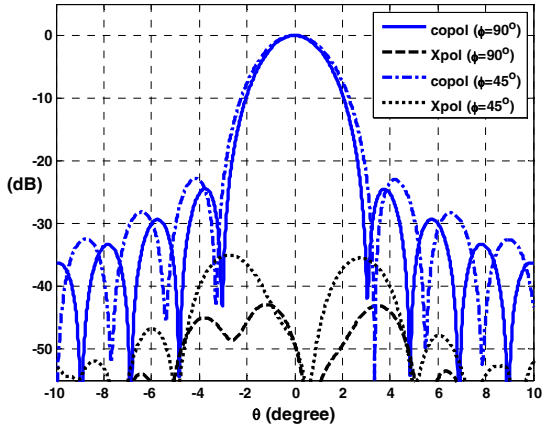

Fig. 3.24. Normalized copolar and cross polar radiation patterns of the elliptical-rim offset reflector antenna used in Fig. 3.9, when fed by simulated feed shown in Fig. 3.19 at both ϕ=90° and ϕ=45° planes at f=8.3GHz.

3.5.2.2 Feed #2: Measurement Results

To verify the numerical results discussed in the previous section, a prototype antenna was fabricated and tested. Photograph of the prototype antenna is shown in Fig. 3.25. The measured co-polar and cross-polar far-field radiation patterns are plotted in Fig. 3.26 at the start and end frequencies of interest, 8.0 and 9.0GHz, when the length of the blocks is 4mm. The remaining parameters are the same as those described in section 3.5.2. As can be seen, the measurement and simulated results agree quite satisfactorily

with each other at both end frequencies. The measured S_{11} are shown in Fig. 3.27a and compared with corresponding simulated ones, when the block length is 4mm. They both follow almost the same trend and are well below -18dB over the frequency range of 8.0 to 10.0GHz. Note that the cross polarization is high due to the presence of the TE_{21} mode, which cancels or minimizes the inherent cross polarization of the offset reflector as shown in Fig. 3.24. The measured copolar and cross-polar radiation patterns of the compound reflector and the feed is shown in Fig. 3.27b at the frequency of 8.43GHz. The measured cross polarization is -30dB, which is close to the cross polarization of the compact range in the anechoic chamber at this frequency.

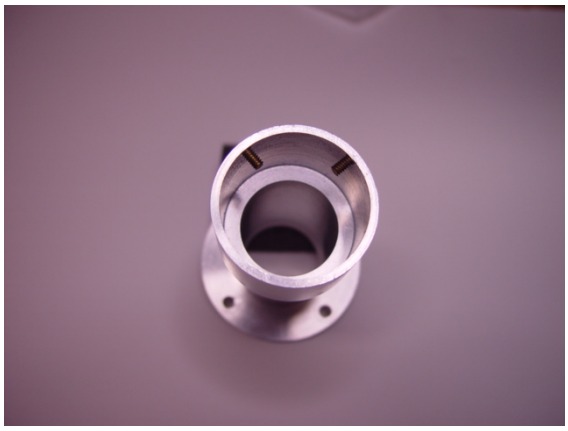

Fig. 3.25. Photograph of the prototype feed #2 (stepped waveguide with two tuning screws).

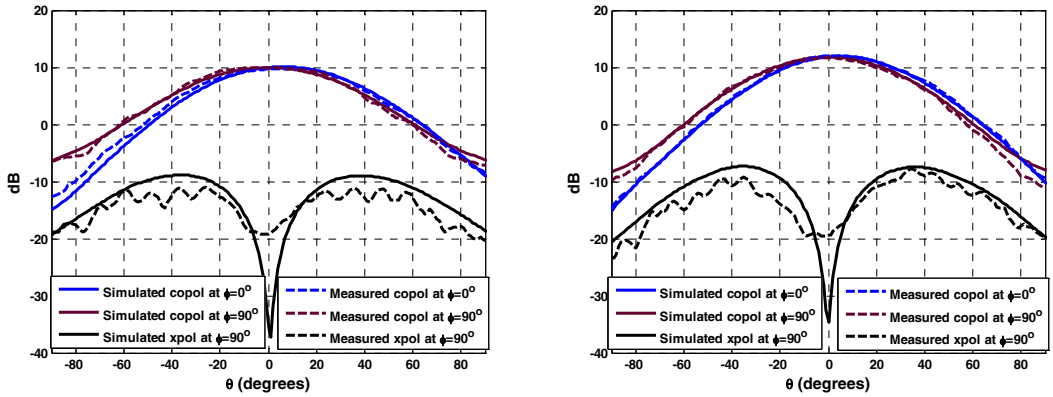

(a) (b)

Fig. 3.26. Measured and simulated copolar and crosspolar radiation patterns at the principal planes for the feed #2 with the block length of 4mm (a) f=8.0GHz, (b) f=9.0GHz.

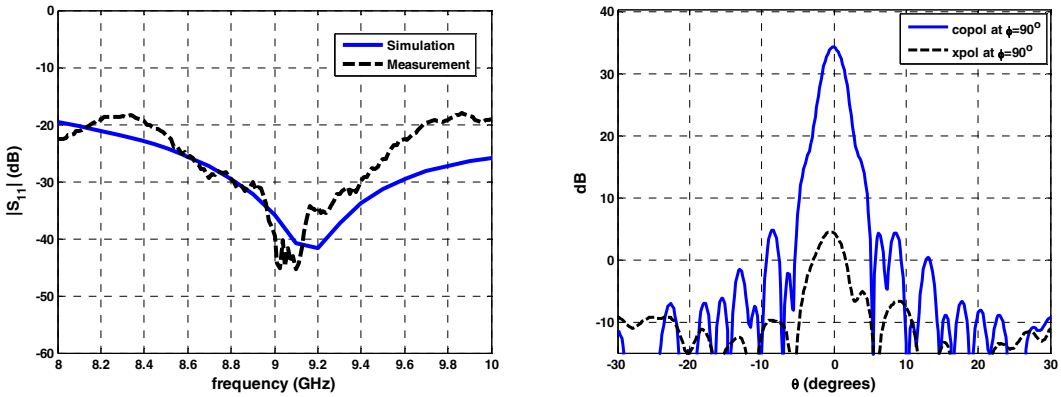

Fig. 3.27. (a) Measured and simulated S_{11} of the feed #2 with the block length of 4mm (b) Measured radiation patterns of the elliptic reflector and the feed at the ϕ=90° plane and f=8.43GHz.

3.6 Effect of Feed Phase Errors on the Cross Polarization of Offset Reflector Antennas [45]

It is known that the reflector antenna gain maximizes with uniform amplitude and phase distributions over its aperture plane. To ensure phase uniformity on the reflector aperture, the phase centre of the feed must coincide with the focal point of the reflector [5]. In practice, however, the primary feed may not have a unique phase centre location, which results in phase errors on the reflector aperture. In addition, the reflecting surface itself may introduce some phase variations due to its imperfection, or deviations from a parabola. The effect of phase error on the gain factor for symmetric reflector antennas has been studied in [5]. Its impact on the cross polarization of center-fed parabolas was numerically investigated in [46]. It was shown that a slightly right-left asymmetric feed phase pattern can significantly degrade the cross polarization of symmetrical-cut reflectors. As for asymmetrical-cut geometries, such as offset structures, the above study was done to investigate the impact of the phase error applied to the primary feed, which was a single TE_{11} mode, on the cross polarization in [47]. It was shown that the linear phase error significantly degraded the cross polarization, whereas the quadratic phase

error had less impact on the cross polarization.

In this section, the cross polarization of offset reflector antennas is studied in the presence of phase errors, which are introduced in the proposed dual-mode feed model by Eq. 3.5. The feed is *y*-polarized and operates at the TE_{11} and TE_{21} type modes. Two cases are studied in terms of how the modes are affected by the phase errors. The phase errors applying to the resultant dual-mode feed is studied as the first case. The second case includes the effect of phase error only on the higher order TE_{21} mode resulting in different phase centre locations for each mode. A broad range of focal length to diameter ratios, *F/D* from 0.5 to 1.1, is considered to investigate the reduced cross polarization properties in the presence of phase errors. Asymmetric right-left phase patterns with respect to the angle ϕ are used to conduct the study. Both linear and quadratic phase variations are studied and they are expressed as,

Linear phase:
$$\psi(\theta) = \begin{cases} 0 & , 0 \le \phi < \pi \\ \alpha\,\theta & , \pi \le \phi < 2\pi \end{cases} \qquad (3.6)$$

Quadratic phase:
$$\psi(\theta) = \begin{cases} 0 & , 0 \le \phi < \pi \\ \alpha\,\theta^2 & , \pi \le \phi < 2\pi \end{cases} \qquad (3.7)$$

wherein α determines the non-uniformity of the phase pattern. That is, there is no phase error when α=0, which will be considered as a reference case for our study. In practice, such phase errors may occur when the primary feed has an asymmetrical geometry or multi-port excitations [46]. As mentioned earlier, we have also considered two cases in terms of how phase errors will affect the primary feed and they are given as:

Case A:
$$\begin{aligned} E_\theta &= [C_1 \cos^{n1}\theta \sin\phi + jC_2 \sin(2\theta)\cos\theta\, \sin(2\phi)]\, e^{j\psi} \\ E_\phi &= [C_1 \cos^{n2}\theta \cos\phi + jC_2 \sin(2\theta)\cos\theta\, \cos(2\phi)] e^{j\psi} \end{aligned} \qquad (3.8)$$

Case B:

$$E_\theta = C_1 \cos^{n1}\theta \sin\phi + [\, jC_2 \sin(2\theta)\cos\theta \, \sin(2\phi)]e^{j\psi}$$
$$E_\phi = C_1 \cos^{n2}\theta \cos\phi + [\, jC_2 \sin(2\theta)\cos\theta \, \cos(2\phi)] \, e^{j\psi} \qquad (3.9)$$

With the above definitions, the phase error affects both modes in Case A, whereas it only influences the TE_{21} mode pattern in Case B. Thus, Case A corresponds to coincident phase centre locations for both modes, while Case B will implicitly include different phase centre locations for each mode. First, the cross polarization level of offset reflector antennas with F/D from 0.5 to 1.1, $D=50\lambda$, $d_c=5\lambda$ will be minimized with no phase error in the primary feed. According to [10], the TE_{21} mode should have -90° phase shift with the TE_{11} mode. Therefore, the cross polarization of the secondary pattern will be reduced by finding an appropriate amplitude ratio (C_2/C_1) and more importantly different tapering factors, n_1 and n_2, at each principal plane. They are plotted in Fig. 3.28 versus F/D with $D=50\lambda$ and $d_c=5\lambda$ at the frequency of 10GHz. The reduced cross polarization levels are well below -47dB and -50dB at inter-cardinal and asymmetry planes, ϕ=45° and ϕ=90°, respectively. The parameters shown in Fig. 3.28 will be used to investigate the phase error effect on the cross polarization of offset reflector antennas.

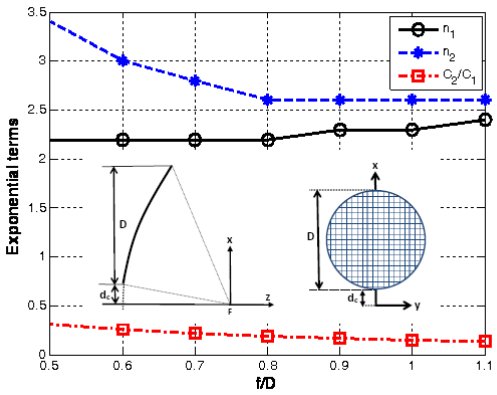

Fig. 3.28. Amplitude ratio of TE_{21}/TE_{11} and exponential terms of TE_{11} mode versus F/D ratio to minimize the cross polarization of offset reflector antennas of $D=50\lambda$, $d_c=5\lambda$ with no phase error on the primary feed defined by Eq. 3.5.

3.6.1 Results for Case A with Linear Phase Errors [45]

With the primary feed model defined by Eq. 3.8 and linear phase errors given by Eq. 3.6, α in Eq. 3.6 changes from 0 to 1 with a step of 0.25 to include the phase errors in both TE_{11} and TE_{21} modes. The secondary far-field crosspolar components are numerically calculated at both diagonal and asymmetry planes, i.e. ϕ=45^o and 90^o. They are plotted in Fig. 3.29 in terms of different *F/D* ratio when D=50λ and d_c=5λ at the frequency of 10GHz. The case with α=0 has no phase error with reduced cross polarization levels using the parameters shown in Fig. 3.28 for the corresponding *F/D* ratio. As α grows, the cross polarization levels increase at both above-mentioned planes. The degradation is more significant at the plane of asymmetry when *F/D* increases. This indicates that the cross polarization will get easily deteriorated when the primary feed having asymmetric phase patterns even for large *F/D* ratios, which usually has low crosstalk. As an example, the secondary radiation patterns with and without phase errors, α=0 and α=1, are shown in Fig. 3.30, for the offset reflector antenna with *F/D*=0.8, D=50λ, and d_c=5λ, at both ϕ=45^o and 90^o planes. The cross polarization levels deteriorate about 12dB and 25dB at the diagonal and asymmetry planes, respectively. However, the phase error has no significant impact on the copolar components as well as side lobes.

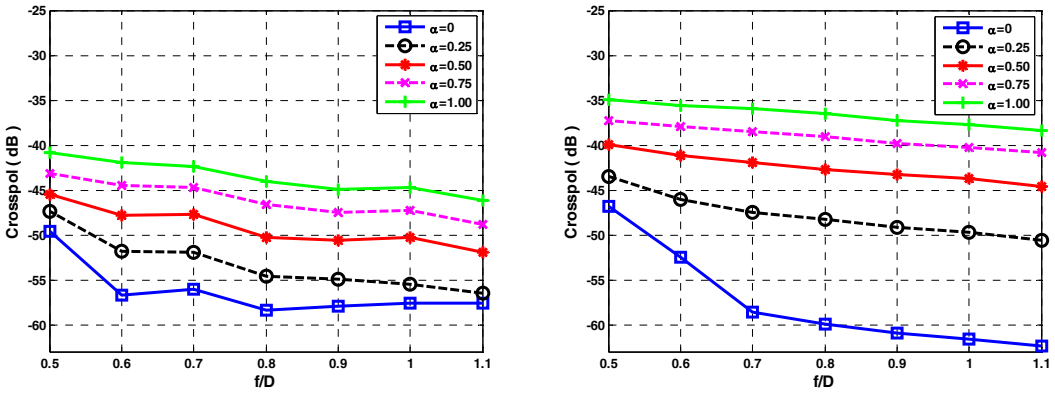

(a) (b)

Fig. 3.29. Effect of linear phase errors on cross polarization with the primary feed model defined by Eq. 3.8 with the associated mode content factors and tapering levels shown in Fig. 3.28 (a) ϕ=45^o (b) ϕ=90^o planes.

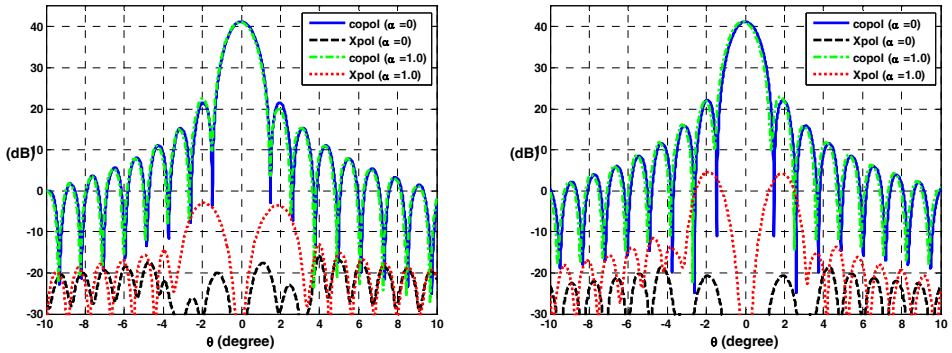

(a) (b)

Fig. 3.30. Copolar and cross polarization radiation patterns with and without the presence of linear phase errors for F/D =0.8, D=50λ, and d_c=5λ (a) ϕ=45^o (b) ϕ=90^o planes.

3.6.2 Results for Case A with Quadratic Phase Errors [45]

In this section, the same feed model discussed in previous sections is used as the primary feed defined by Eq. 3.8 with the quadratic phase errors given by Eq. 3.7. The results are illustrated in Fig. 3.31, for both ϕ-planes under study. As shown, the cross polarization degradation is less at the diagonal plane than the one in the asymmetry plane. The maximum degradation of 17dB occurs in the latter plane when F/D=0.8. The far-field secondary patterns have the same features as the one shown in Fig. 3.31 and they are not repeated here for brevity.

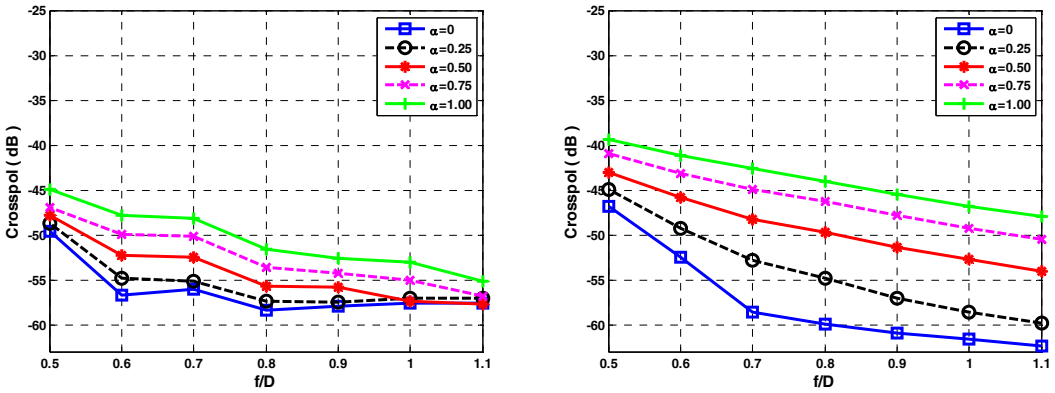

(a) (b)

Fig. 3.31. Effect of quadratic phase errors on cross polarization with the primary feed model defined by Eq. 3.8 with the associated mode content factors and tapering levels shown in Fig. 3.28 (a) ϕ=45^o (b) ϕ=90^o planes.

3.6.3 Results for Case B [45]

The primary feed model for Case B is defined by Eq. 3.9, in which the phase errors are only applied to the second azimuthal mode, i.e. TE_{21}. This case can be interpreted as a dual-mode feed having different phase centre locations for each individual mode. With the linear phase errors described by Eq. 3.6, the secondary cross polarization levels are calculated at both ϕ=45^o and 90^o planes as before. The results are depicted in Fig. 3.32 for different *F/D* ratios with the same aperture diameter and offset clearance distance as before. As can be seen, the levels of cross polarization components drastically increase for small *F/D* ratio at both above-mentioned planes. More importantly, the secondary far-field radiation patterns for *F/D*=0.8, illustrated in Fig. 3.33, show the cross polarization component having now a broadside shape rather than a usual boresight-null pattern in the no phase error case. The end effect of such phase errors on the cross polarization is similar to the one reported in [48], wherein the tracking errors due to the radome de-polarization effect caused additional broadside-shape cross polarization in monopulse systems. With the quadratic phase errors, the results are

approximately the same as the linear ones and are not repeated here. Comparing with the linear phase error, which has the highest level of -27dB crosspol when α=1 and F/D=0.5, the quadratic phase error results in a maximum cross polarization of about -32dB for the α=1 and F/D=0.5.

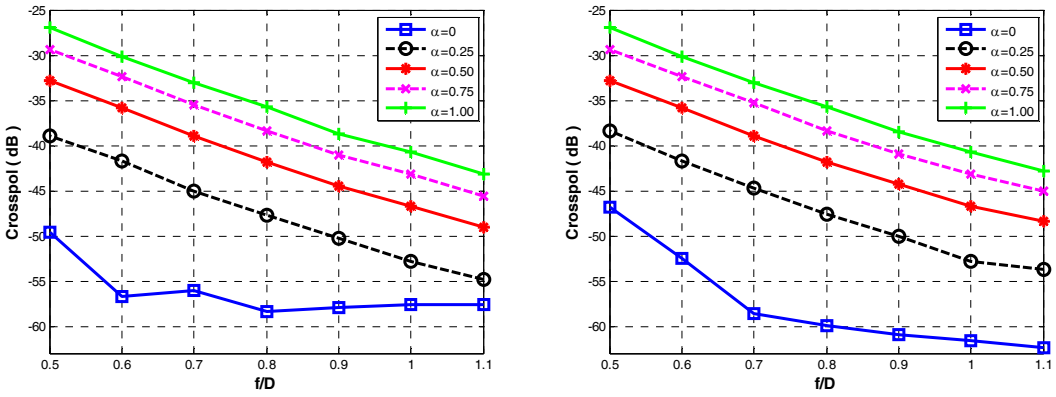

(a) (b)

Fig. 3.32. Effect of linear phase errors on cross polarization with the primary feed model defined by Eq. 3.9 with the associated mode content factors and tapering levels shown in Fig. 3.28 (a) ϕ=45^o (b) ϕ=90^o planes.

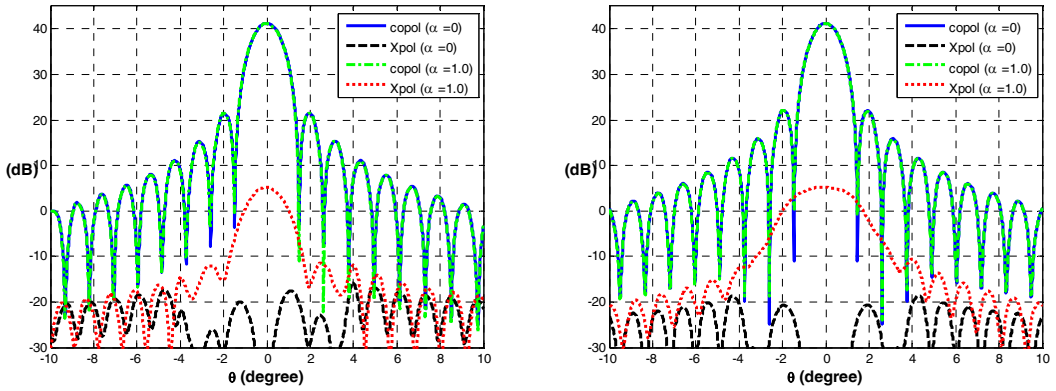

(a) (b)

Fig. 3.33. Copolar and cross polarization radiation patterns with and without the presence of linear phase errors (only applied to the TE_{21} mode) for F/D =0.8, D=50λ, and d_c=5λ at (a) ϕ=45^o (b) ϕ=90^o planes.

3.7 Summary

As for single-phase centre antenna application, the side lobe level, aperture efficiency, and cross polarization responses of offset reflector antennas were studied in both asymmetry and inter-cardinal planes, i.e. ϕ=90^o and 45^o. The primary feed was a dual-mode circular waveguide operating at the TE_{11} and the TE_{21} type modes. To exclude the feed imperfections, the feed under study was modeled by trigonometric functions such that the TE_{11} type mode had asymmetric *E*- and *H*-plane patterns. Consequently, the secondary cross polarization was minimized by adjusting the amplitude ratio and phase difference of the two modes, and more importantly by selecting different tapering levels of the TE_{11} type mode in the principal planes. The concept provided a simple dual-mode primary feed model to reduce the unwanted cross polarization of offset reflector antennas, which is high in the plane of asymmetry when illuminated by a conventional linearly polarized feed. Moreover, the proposed dual-mode feed model improved the aperture efficiency of the reflector in comparison with a standard Gaussian feed of the same edge illumination. To verify the concept, two novel dual mode feeds were designed. The traditional dual-mode feeds suffer from the deteriorating impact of the higher order TE_{21} mode on the S_{11}. The distinct advantage of these feeds over the traditional dual-mode feed is that the higher order TE_{21} mode is isolated from the input port resulting in a wide impedance bandwidth. The resulting radiation patterns of the proposed feeds were then used to illuminate an elliptical offset reflector antenna and determine its far field patterns. Feed #1 was a choke excited circular waveguide with a single slot. Feed #2 was a stepped circular waveguide with two tuning screws. Of these two feeds, the feed #2 provided better response to the cross polarization reduction technique as the mode content factor

and the tapering numbers of the dominant mode were easily adjusted by the tuning screws.

The effect of asymmetric phase errors applied to the proposed primary feed model on the cross polarization of offset reflector antennas was also investigated. A broad range of *F/D* ratios was studied. Both linear and quadratic phase errors with asymmetric patterns were applied to the primary feed. Two cases were considered. Case A included phase errors to both modes, whereas only the TE_{21} mode was affected by the phase error in Case B. It was shown that, both cases drastically increased the cross polarization levels at both inter-cardinal and asymmetry planes. More interestingly, the patterns of the cross polarization component had a broadside shape rather than a boresight-null in Case B, wherein the two modes had different phase centre locations. The results were the same as the radome effect on the cross polarization of monopulse systems reported in [48].

Chapter 4

Multi-Phase Centre Antennas: Theory and Design

4.1 Introduction

Multi-phase centre antennas have found increasing interest in a variety of applications such as virtual array antennas, remote sensing, radars, and military applications. In certain applications, e.g. moving target indicator (MTI) radars, where the antenna part is mounted on a moving platform, the forward motion of the moving platform changes the effective phase centre location of the operating antenna. This could result in errors as significant as missing low-velocity objects [6, 49]. One of the techniques to reduce the platform motion noise and scanning modulation noise is the displaced phase centre antenna (DPCA) processing technique [6]. The principle idea is to make the antenna appear stationary in space. Traditionally, DPCA technique exploits multi–aperture antennas, which provide displaced phase centre locations. This will, in turn, increase the hardware and complexity of the antenna systems.

In this chapter, a novel multi-phase centre offset reflector antenna is investigated that utilizes a single hardware system to displace the antenna phase centre location electronically. The primary feed is a dual-mode circular waveguide operating at the dominant TE_{11} and the higher order TE_{21} type modes. The fundamental mode has a broadside radiation pattern whereas the higher order mode produces a null at the boresight. The combination of these modes with different polarizations, amplitude ratios, and phase shift differences are considered. The resulting feed is placed at the focal point tipped toward the center of the offset reflector. For simplicity, each mode of the feed is modeled by the closed-form analytical equations explained in detail in

chapter 3, section 3.1. Four cases of different mode alignments or polarizations are studied. It will be shown that the phase centre location of the antenna can be displaced from the physical center of its geometry by changing the excitation amplitude and phase of each mode, as well as employing different mode orientations. This will result in a virtual array antenna with a phase centre location that can be displaced in any direction, depending on the polarization of each mode by a simple signal processing procedure without mechanically moving the antenna itself. The antenna developed using this technique has a potential application as a transceiver antenna in GMTI radar applications. The operating frequency is chosen as the center of the X-band frequency range, which is 10GHz. All required simulations for the reflector antenna are carried out using the physical optics, geometrical optics, and geometrical theory of diffraction software, TICRA's GRASP v.7 [18].

4.2 Multi-phase Centre Virtual Antennas versus Traditional DPCA

As defined in section 2.2.4, the phase centre location of an antenna is the effective source of radiation providing a uniform phase pattern at the far-field region over a finite angular range in space, which is normally around the main beam. Therefore, any phase centre displacement will move the apparent location of the antenna. Traditionally, multi-aperture antennas were used to provide separate phase centre locations as required in MTI radars with moving platforms. The main objective of this thesis is to develop a virtual array antenna with electronically adjustable multi-phase centre locations within a single aperture to allow multiple antenna representation. This is illustrated in Fig. 4.1. As a result, the cost and complexity of the antenna system will be

reduced through the use of simple signal processing procedure to control the phase centre location of the operating antenna.

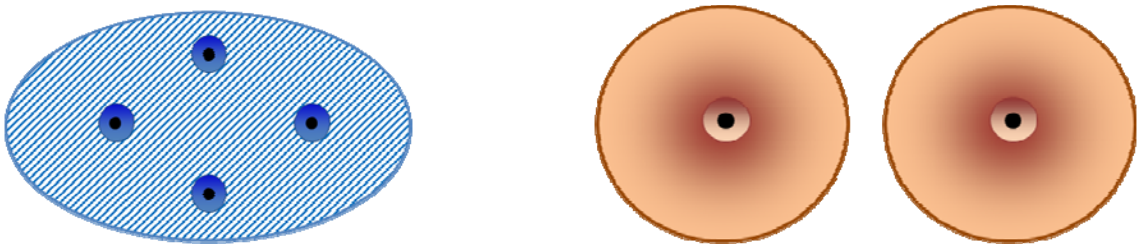

(a) (b)

Fig. 4.1. (a) Virtual array antenna with multi-phase centre locations versus (b) Traditional DPCA multi–aperture antennas.

Among aperture antennas, parabolic antennas are the best candidates for our study because of their unique focusing properties, as well as their wide range of applications in most modern systems. Because of the profound advantages of asymmetrical-cut paraboloids over its symmetrical-cut counterpart, as discussed in section 2.1, an offset reflector antenna is selected to develop the virtual array antenna with multiple-phase centre locations. Figure 4.2 shows the geometry of the offset reflector antenna under investigation. The aperture diameter, offset clearance distance, half-angle subtended by the rim, and offset angle are denoted by D, and, d_c, θ^*, θ_o, respectively. The operating frequency is 10GHz. The software TICRA's GRASP v.7 used here assumes that the offset reflector is the intersection between the paraboloid and a circular cone tilted the angle of θ_o. Therefore, θ_f shown in Fig. 4.2 represents the feed tilt angle which can be expressed as [23]:

$$\tan(\theta_f/2)= (d_c + D/2)/2F \qquad (4.1)$$

As illustrated in Fig. 4.2, the plane of symmetry is the *x*-axis or ϕ=0^o and the asymmetry plane is the *y*-axis or ϕ=90^o.

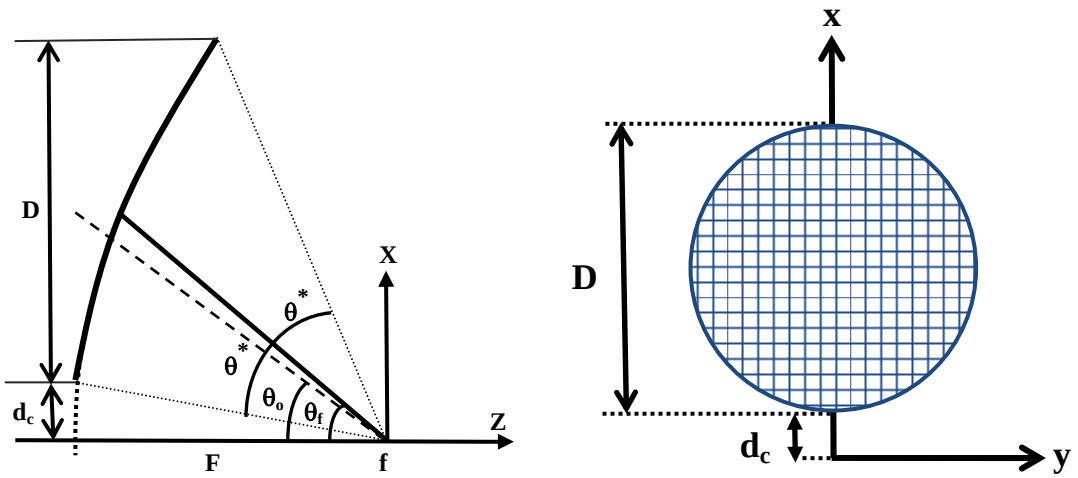

Fig. 4.2. Geometry of an offset reflector antenna with F/D=1.10, D=20λ, d_c=1λ, θ*=24.20^o, θ_o=26.80^o, and θ_f=28.073^o.

As mentioned earlier, the DPCA technique is employed in MTI applications to lessen the deleterious impacts of moving platforms. In general, the required phase centre displacement depends on the application. It is mainly determined by the speed of the moving platform, *v*, and the pulse repetition interval, *T*. That is, $d=vT$, where *d* is the phase centre location [6]. The typical value of *v* changes from 36m/sec to 176m/sec for airborne applications and that of *T* is either 0.25msec or 0.5msec [50]. For example, for v=176m/sec and T=0.25msec, the required phase centre displacement is 4.4cm. We will show that with controlling the mode power ratio such phase centre movement is easily achievable without considerable loss in antenna performance.

4.3 Analytical Feed Model and Calibration Procedure

In order to develop a virtual array antenna, the phase centre location of the composite reflector and the feed should be displaced from the physical center of the reflector aperture while their corresponding secondary radiation patterns remain identical to each other. To this end, the primary feed should asymmetrically illuminate the reflector aperture with its phase centre located at the focal point of the reflector. Multimode feeds are the best candidates for this application because controlling their mode content factors, both amplitude and phase, as well as mode polarization alignments provides extra degrees of freedom to control the shaping of the primary feed patterns and eventually to displace the phase centre locations of the composite reflector and the feed. Essentially, multimode antennas use the combination of two or more transverse magnetic (*TM*) and/or transverse electric (*TE*) modes. The well-known examples of such antennas are the waveguide and microstrip antennas with arbitrary cross-sectional geometry. The remarkable property of the round open-ended waveguide, as well as circular microstrip patch antennas is that their principal-cut radiation functions are the multiplication of two independent functions of θ and ϕ. This allows one to control the pattern of each mode independently in two orthogonal angular spaces. The results for the circular microstrip antenna are presented in [51]. In this chapter, the emphasis is placed on the circular waveguide antennas utilizing the first two transverse electric type modes, leading by the TE_{11} and TE_{21} type modes, whose closed-form equations are given by Eqs. 2.34-35. They are mainly governed by Bessel Functions of order *n*. For simplicity, however, they can be expressed by simple trigonometric sine and cosine functions as discussed in section 3.2 in detail. Without loss of generality, it is assumed that the primary feed has identical *E*- and *H*-plane patterns. The resulting analytical model is given as,

$$E_\theta = C_1 \cos^n \theta \sin\phi + jC_2 \sin(2\theta)\cos\theta \sin(2\phi)$$
$$E_\phi = C_1 \cos^n \theta \cos\phi + jC_2 \sin(2\theta)\cos\theta \cos(2\phi) \quad (4.1)$$

wherein the tapering number of the TE_{11} type mode is denoted by n, which is different from the index numbers of the waveguide nm^{th} mode. The normalized amplitude and phase patterns of both TE_{11} and TE_{21} type modes are illustrated in Fig. 4.3, when n=1. As shown, the fundamental mode has a broadside radiation pattern whereas the higher order TE_{21} mode has a null at the boresight angle of θ=0°. Both modes have uniform phase variations over each half-observation angle.

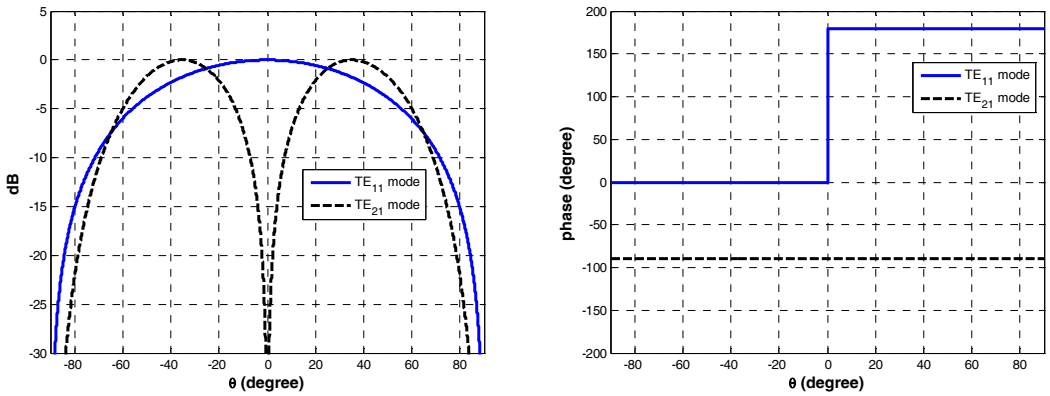

(a) (b)

Fig. 4.3. (a) Normalized amplitude (b) phase patterns of the TE_{11} and TE_{21} modes of Eq. 4.1, when n=1.

The above equations define the mode content factor in terms of amplitude ratio of C_2/C_1. In practice, however, it is more convenient to deal with power ratios instead. Therefore, Eq. 4.1 is normalized first to total power of 4π, as follows.

$$E_\theta = \sqrt{2n+1}\, C_1 \cos^n \theta \sin\phi + j\sqrt{35/8}\, C_2 \sin 2\theta \cos\theta \sin 2\phi$$
$$E_\phi = \sqrt{2n+1}\, C_1 \cos^n \theta \cos\phi + j\sqrt{35/8}\, C_2 \sin 2\theta \cos\theta \cos 2\phi \quad (4.2)$$

As a result, the mode power ratio, which is the ratio of the power content factor of the TE_{21} to that of the TE_{11} mode, can be stated as,

$$P_{TE21} / P_{TE11} = \frac{35/8\ C_2^2}{(2n+1)C_1^2} \qquad (4.3)$$

where P_{TE11} and P_{TE21} represent mode power ratios of the TE_{11} and TE_{21} type modes, respectively. Now, the above feed is placed at the focal point of the offset reflector antenna under study. To investigate the phase centre location, the aperture field of the reflector is studied. Due to the asymmetrical geometry of the offset reflector antenna, the aperture distribution of the reflector, when illuminated by a single TE_{11} mode, may be asymmetric for the feed tilt angle defined by Eq. 4.1. Consequently, the phase centre location will move off the physical center of the aperture. This is illustrated in Fig. 4.4a for an offset geometry of F/D=1.1, D=20λ, d_c=1λ, and θ_f=28.073^o at the frequency of 10GHz, excited by a single TE_{11} mode feed as given by Eq. 4.2 with n=1 and C_2=0. Therefore, the feed tilt angle, θ_f, needs to be re-adjusted accordingly. For the above example, the feed tilt angle is increased to 40.5^o in order to have a symmetric aperture distribution for a pure mode feed as depicted in Fig. 4.4b. That is, the peak amplitude intensity occurs at the center of the aperture. In short, the required feed tilt angle is dependent on the geometry of the offset reflector as well as the edge illumination determined by n in Eq. 4.2. This calibration procedure will be used for any given offset geometry discussed in chapters 4 and 5.

To conduct the virtual array antenna investigation, four cases of different mode alignments or polarizations of the primary feed are studied. Also, two F/D ratios of 1.1 and 0.6 with D=20λ and d_c=λ are considered at the frequency of 10GHz with different edge illuminations. They are discussed in the next sections. The offset angles, half angle subtended by the rim, and corresponding edge illuminations are given in Table 4.1. The case with n=1 in Eq. 4.2 is studied for both F/D ratios, which give low edge illuminations. Then, the -10dB edge illumination is also studied for both F/D ratios resulting in different tapering number n. The

results for F/D=1.1 and n=1 will be shown in details and the summarized versions will be presented for the others.

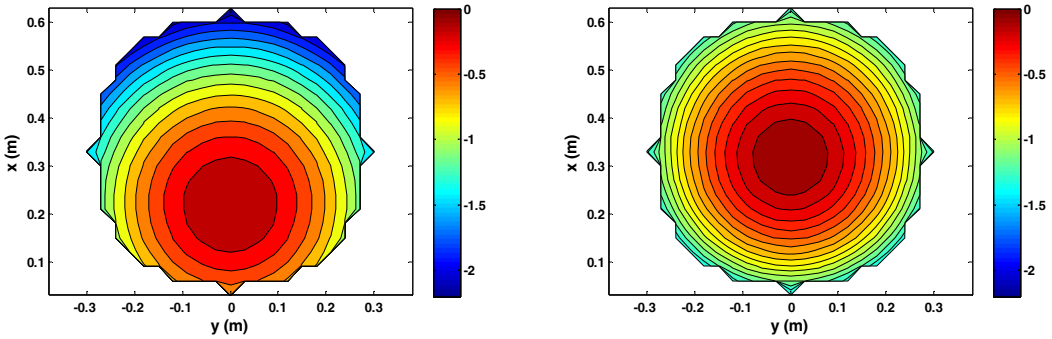

(a) (b)

Fig. 4.4. Aperture distribution of the offset reflector fed by a single mode y-polarized TE_{11} mode (n=1, C_2=0) when f=10GHz, F/D=1.1, D=20λ, and d_c=1λ (a) θ_f=28.073^o (b) θ_f=40.5^o.

Table 4.1. Geometrical angles, θ^* and θ_0, defining offset reflector structure with D=20λ and d_c=λ and edge illuminations.

F/D	**1.1**		**0.6**	
θ^*	**24.20^o**		**38.80^o**	
θ_o	**26.80^o**		**43.57^o**	
Edge illumination	***n*=1**	**-0.8dB**	***n*=1**	**-2.16dB**
	***n*=12**	**-10dB**	***n*=4.5**	**-10dB**

It is worth mentioning that a symmetrical-cut parabola produces a symmetric aperture distribution, when fed by a single mode antenna. Therefore, there is no need to calibrate the feed tilt angle.

4.4 Case I: *Y*-polarized TE_{11} and TE_{21} Modes

In this section, both modes are aligned along the y-axis, i.e. y-polarized, as shown in Fig. 4.5. The rotation angles of the TE_{11} and TE_{21} type modes with respect to the y-axis are represented by δ_{11} and δ_{21}. For the current case, these angles are equal to zero, i.e. δ_{11}=δ_{21}=0^o. The far-field radiation pattern of each mode can be described by the following equations, which have identical E-plane and H-plane patterns.

$$\textbf{TE}_{11}\textbf{ mode } (\delta_{11}=0^{o}):\quad \left\{\begin{aligned} E_\theta &= \sqrt{P_{TE11}}\,\cos^n\theta\,\sin(\phi-\delta_{11}) = \sqrt{P_{TE11}}\,\cos^n\theta\,\sin\phi \\ E_\phi &= \sqrt{P_{TE11}}\,\cos^n\theta\,\cos(\phi-\delta_{11}) = \sqrt{P_{TE11}}\,\cos^n\theta\,\cos\phi \end{aligned}\right\} \tag{4.4}$$

$$\textbf{TE}_{21}\textbf{ mode } (\delta_{21}=0^{o}):\left\{\begin{aligned} E_\theta &= j\sqrt{P_{TE21}}\,\sin 2\theta\,\cos\theta\,\sin 2(\phi-\delta_{21}) = j\sqrt{P_{TE21}}\,\sin 2\theta\,\cos\theta\,\sin 2\phi \\ E_\phi &= j\sqrt{P_{TE21}}\,\sin 2\theta\,\cos\theta\,\cos 2(\phi-\delta_{21}) = j\sqrt{P_{TE21}}\,\sin 2\theta\,\cos\theta\,\cos 2\phi \end{aligned}\right\} \tag{4.5}$$

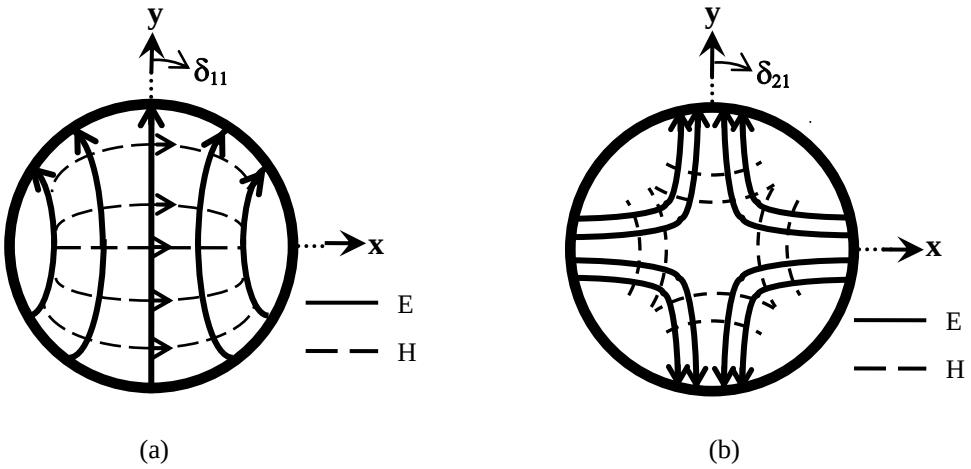

(a) (b)

Fig. 4.5: Aperture distribution of the *y*-polarized (a) TE_{11} mode ($\delta_{11}=0^{o}$) (b) TE_{21} mode ($\delta_{21}=0^{o}$).

The primary amplitude and phase patterns, which are due to the feed only with combined TE_{11} and TE_{21} type modes with n=1, are shown in Fig. 4.6 and Fig. 4.7, respectively, for a power ratio of P_{TE21}/P_{TE11}=0.5 with four phase excitation values of 0^{o}, 180^{o}, and $\pm 90^{o}$. As can be seen, the main beam is tilted at the ϕ=0^{o} plane only if there is a quadrature phase difference between the two modes. The direction of the main beam is opposite the sign of the phase difference. That is, it moves to a positive observation angle with a -90^{o} phase excitation and a negative observation angle with a $+90^{o}$. Thus, the phase excitation of $+90^{o}$ and -90^{o} moves the illumination to lower and higher parts of the offset reflector, respectively. In terms of phase patterns, the phase excitations of 0^{o} and 180^{o} will make a non-uniform shape at each half-observation angle. It should be mentioned that the negative θ represents the same positive observation angle at a given ϕ-cut, except that ϕ has been changed to $\phi+\pi$.

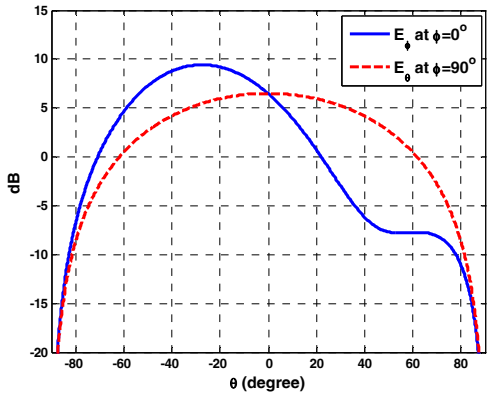

$P_{TE21}/P_{TE11}=0.5\angle +90^{o}$

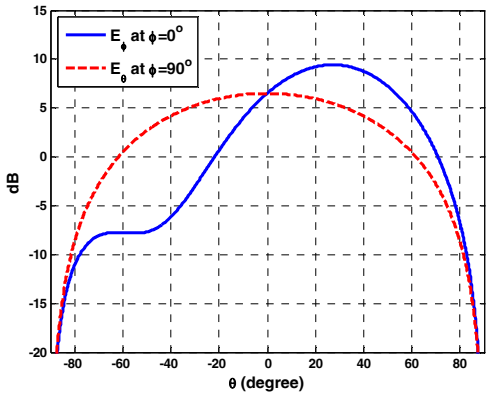

$P_{TE21}/P_{TE11}=0.5\angle -90^{o}$

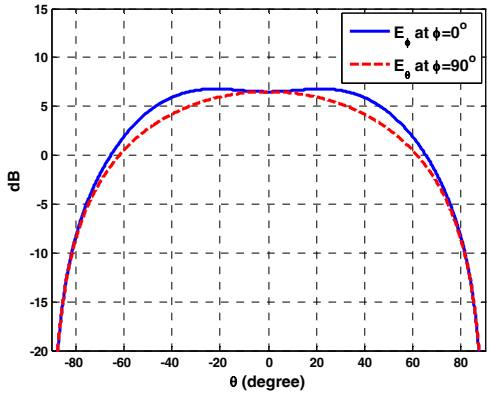

$P_{TE21}/P_{TE11}=0.5\angle 0^{o}$

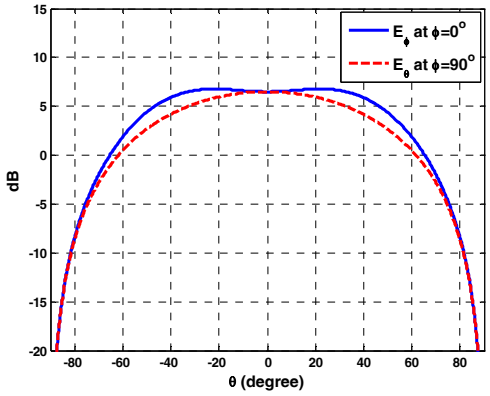

$P_{TE21}/P_{TE11}=0.5\angle 180^{o}$

Fig. 4.6. Radiation patterns of the feed defined by Eqs. 4.4-5 operating at the combined *y*-polarized TE_{11} and TE_{21} modes, $\delta_{11}=\delta_{21}=0^{o}$, and n=1 at f=10GHz.

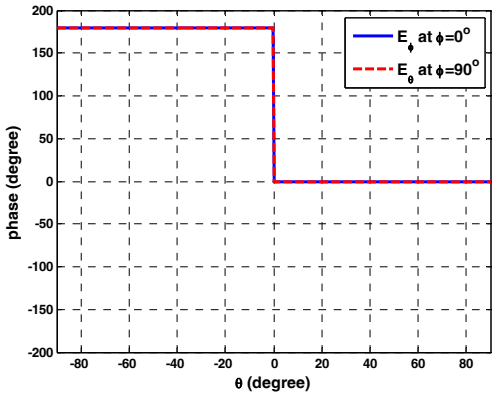

$P_{TE21}/P_{TE11}=0.5\angle +90^{o}$

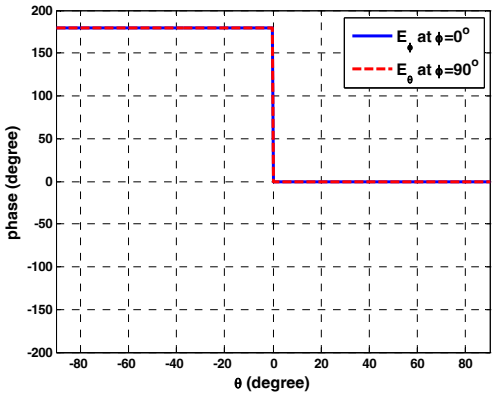

$P_{TE21}/P_{TE11}=0.5\angle -90^{o}$

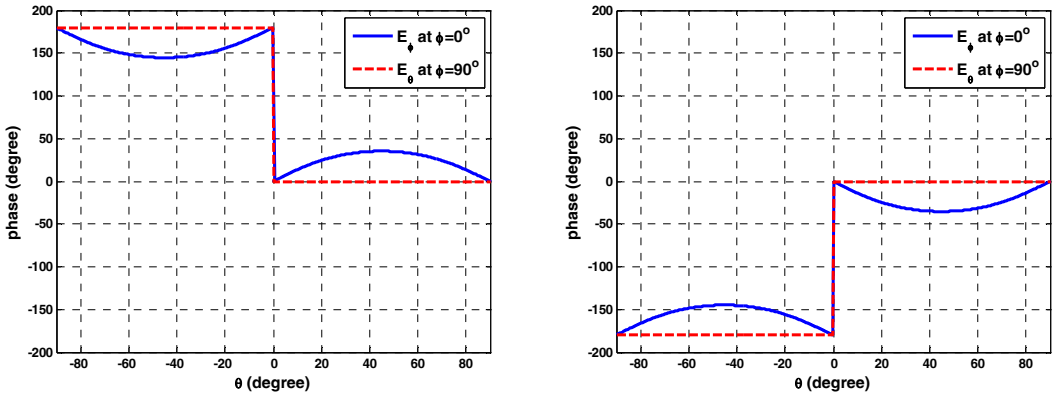

$P_{TE21}/P_{TE11}=0.5\angle 0^{o}$ $P_{TE21}/P_{TE11}=0.5\angle 180^{o}$

Fig. 4.7. Phase patterns of the feed the feed defined by Eqs. 4.4-5 operating at the combined *y*-polarized TE_{11} and TE_{21} modes, $\delta_{11}=\delta_{21}=0^{o}$, and n=1 at f=10GHz.

To show how the phase centre location is affected by the primary feed, the aperture amplitude and phase distributions are studied. Figure 4.8 shows the aperture distribution for different phase shifts with a fixed power ratio of 0.5, i.e. $|P_{TE21}/P_{TE11}|=0.5$. As can be seen, the phase centre location changes when the excitation phase is $\pm 90^{o}$ and it moves along the *x*-axis. Due to the asymmetrical geometry of the offset reflector, the aperture distributions with $+90^{o}$ and -90^{o} phase shifts are not identical mirror images with respect to the *y*-axis. This is not the case if a symmetric parabola is used. The excitation phases of 0^{o} and 180^{o} do not displace the phase centre, even though the peak intensity has been moved from the physical center. The reason that the phase centre of the reflector is not displaced is that the phase centre location of the feed itself is changed according to Fig. 4.7, resulting in an off-focus feed or a laterally displaced feed. Consequently, the main beam of the secondary pattern will be off the boresight as reported in [52-54]. The aperture phase distribution is also used to study the phase behavior of each case. They are all given in Fig. 4.9. The quadrature phases produce uniform phase distributions over the aperture, which confirm the phase centre movement along the *x*-axis. The in-phase and out-of-phase excitations of 0^{o} and 180^{o} have a non-uniform phase distribution.

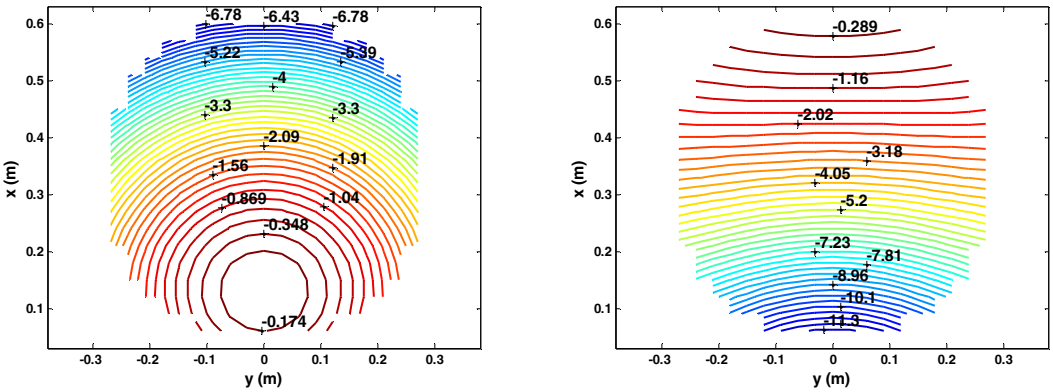

$P_{TE21}/P_{TE11}=0.5\angle +90^{o}$ $P_{TE21}/P_{TE11}=0.5\angle -90^{o}$

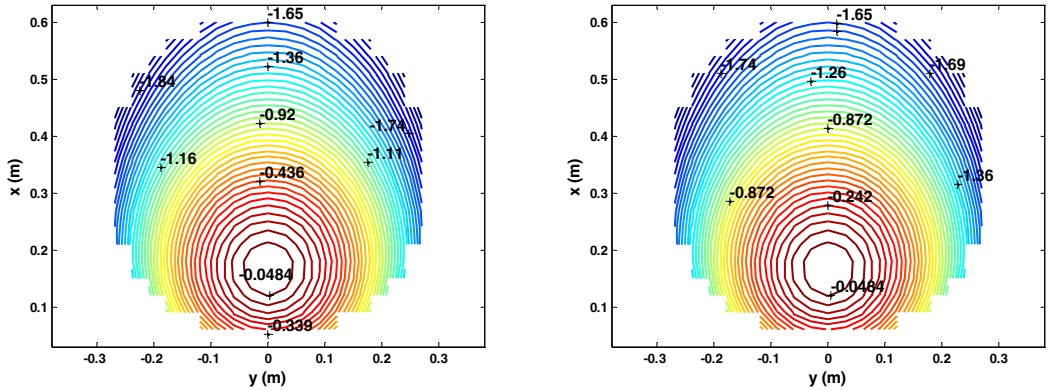

$P_{TE21}/P_{TE11}=0.5\angle 0^{o}$ $P_{TE21}/P_{TE11}=0.5\angle 180^{o}$

Fig. 4.8. Aperture distributions of the offset reflector fed by the feed model, defined by Eqs. 4.4-5 operating at the combined *y*-polarized TE_{11} and TE_{21} modes, $\delta_{11}=\delta_{21}=0^{o}$ and n=1, when F/D=1.1, $D=20\lambda$, $d_c=1\lambda$, and $\theta_f=40.5^{o}$ at f=10GHz.

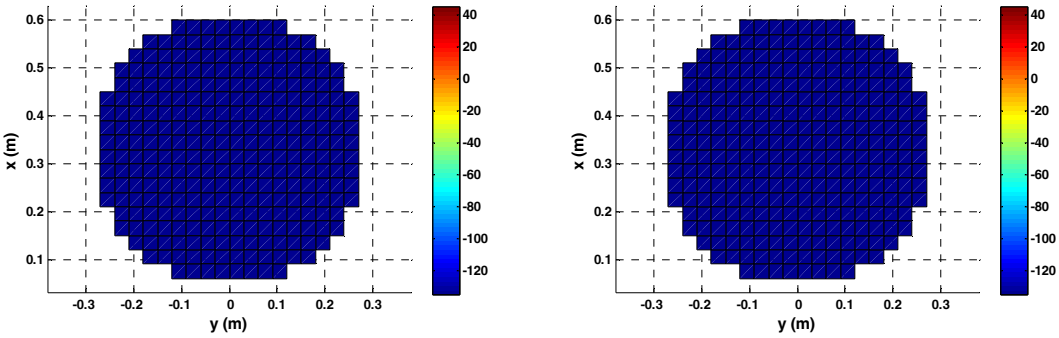

$P_{TE21}/P_{TE11}=0.5\angle +90^{o}$ $P_{TE21}/P_{TE11}=0.5\angle -90^{o}$

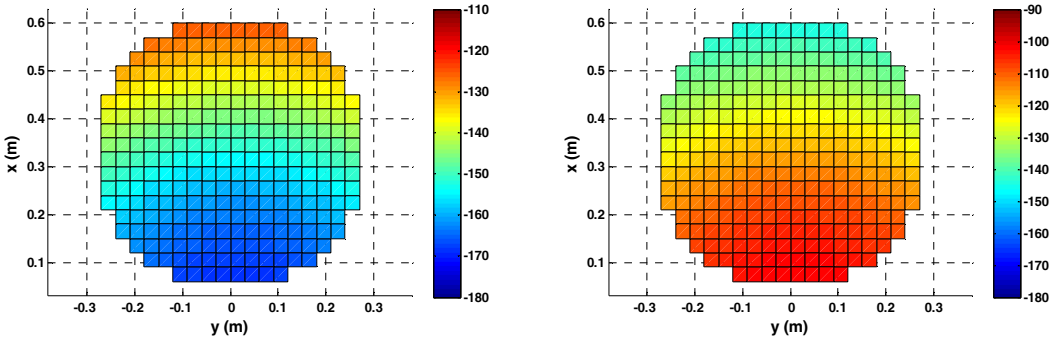

$P_{TE21}/P_{TE11}=0.5\angle 0^{o}$ $P_{TE21}/P_{TE11}=0.5\angle 180^{o}$

Fig. 4.9. Aperture phase distributions of the offset reflector fed by the feed model, defined by Eqs. 4.4-5 operating at the combined *y*-polarized TE_{11} and TE_{21} modes, $\delta_{11}=\delta_{21}=0^{o}$ and n=1, when F/D=1.1, $D=20\lambda$, $d_c=1\lambda$, and $\theta_f=40.5^{o}$ at f=10GHz.

Finally, the secondary far-field radiation patterns are plotted in Fig. 4.10. As expected, the main beams are at the boresight angle for both $\pm 90^{o}$ excitation phases and their radiation patterns are identical, whereas it is tilted at $\phi=0^{o}$ plane for in-phase, 0^{o}, and out-of-phase, 180^{o}, excitations. The main beam is tilted toward negative θ and positive θ for 0^{o} and 180^{o} phase excitations, respectively. Therefore, the quadrature phase shifts generate identical secondary radiation patterns with two separate phase centre. This leads to a virtual array antenna.

From the aperture distribution plots, the direction of the phase centre motion of the composite reflector and the feed is well predicted so far. However, the exact phase centre location needs to be determined as well. To do so, the coordinate origin of the reflector is displaced such that the far-field phase patterns are uniform over the main beam, which covers a small angular range in space around the main beam, i.e. $-5^{o}<\theta<+5^{o}$. For the example under study here, the phase centre moved along the *x*-axis. Thus, the coordinate origin needs to be displaced along the *x*-axis. The amount of this displacement is equal to the exact phase centre location. This procedure is done for the quadrature phase excitation of $\pm 90^{o}$ for different mode power

ratios to find the exact phase centre location. The quadrature phase shifts are selected as they produce identical secondary patterns with main beams at the boresight required for virtual array antennas, whereas the other possible phase shifts result in scanned beams. The gain, sidelobe levels, and maximum cross polarization are also studied. The results of gain and phase centre location are shown in Fig. 4.11a. As can be seen, the antenna gain is almost unchanged as the mode power ratio increases when there is a $+90^{o}$ phase shift between the two modes, whereas it drops with the power ratio for the -90^{o} phase shift. The reason is that the $+90^{o}$ phase shift generates more uniform aperture distribution as illustrated in Fig. 4.8. This also affects the phase centre location in a way that the -90^{o} phase shift displaces the phase centre more than that of the $+90^{o}$ phase shift for a fixed mode power ratio. It should be noted that the zero phase centre location refers to the physical center of the reflector aperture. The phase centre location normalized to the half aperture diameter is also shown in Fig. 4.11b to show the ratio of the phase centre displacement with respect to the aperture size of the reflector antenna. The phase centre displacement itself is denoted by *d*.

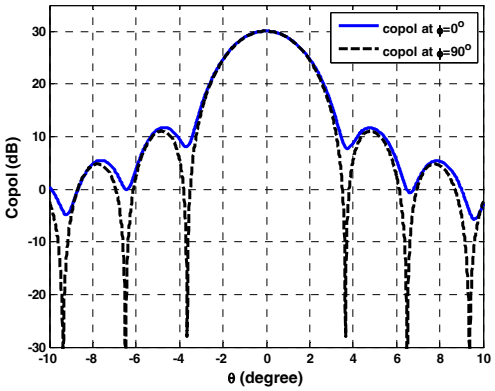

$P_{TE21}/P_{TE11}=0.5 \angle +90^{o}$

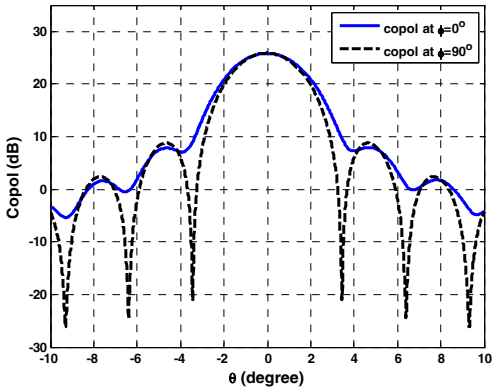

$P_{TE21}/P_{TE11}=0.5 \angle -90^{o}$

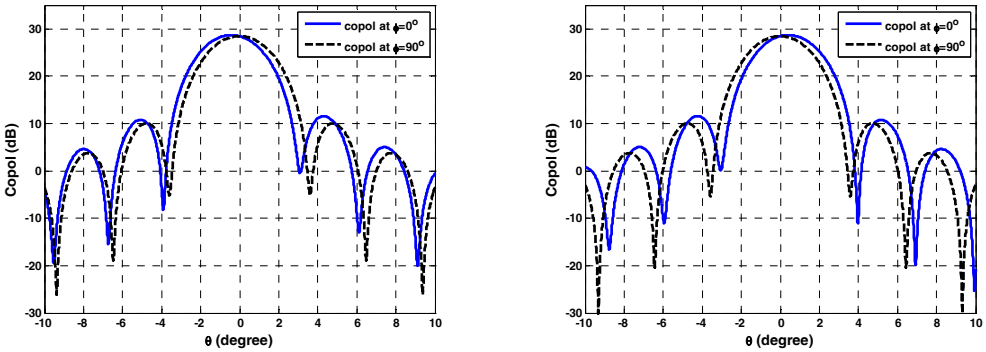

$P_{TE21}/P_{TE11}=0.5\angle 0^{o}$ $P_{TE21}/P_{TE11}=0.5\angle 180^{o}$

Fig. 4.10. Far-field radiation patterns of the offset reflector fed by the feed model, defined by Eqs. 4.4-5 operating at the combined *y*-polarized TE_{11} and TE_{21} modes, $\delta_{11}=\delta_{21}=0^{o}$ and n=1, when F/D=1.1, $D=20\lambda$, $d_c=1\lambda$, and $\theta_f=40.5^{o}$ at f=10GHz.

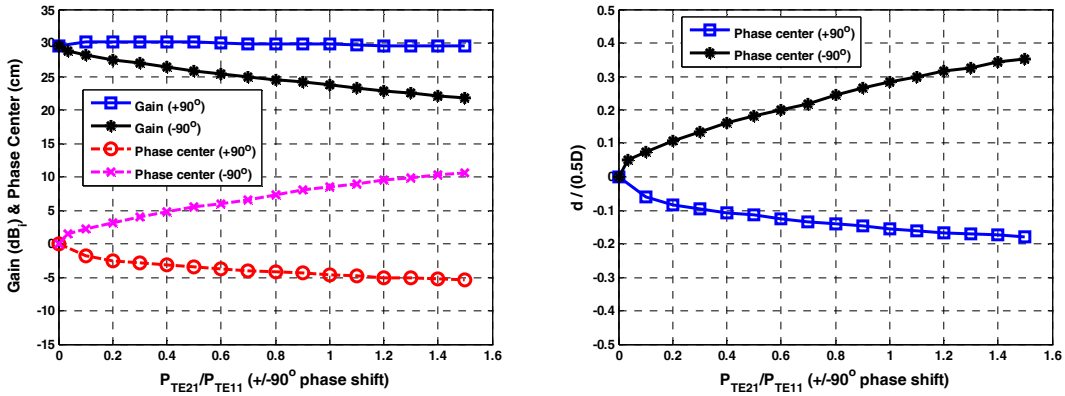

(a) (b)

Fig. 4.11. (a) Gain and phase centre location (b) normalized phase centre location of the offset reflector fed by the feed model, defined by Eqs. 4.4-5 operating at the combined *y*-polarized TE_{11} and TE_{21} modes, $\delta_{11}=\delta_{21}=0^{o}$ and n=1, when F/D=1.1, $D=20\lambda$, $d_c=\lambda$, and $\theta_f=40.5^{o}$ at f=10GHz. Phase centre moves along *x*-axis with reference to the center of offset reflector aperture.

It is instructive to study the sidelobe levels and cross polarization of the offset reflector antenna as its phase centre is displaced in term of different mode power ratios with quadrature phase shifts. They are plotted in Fig. 4.12. As can be seen, the sidelobe levels are almost unchanged as the mode power ratio grows at both principal planes of $\phi=0^{o}$ and 90^{o} planes. As for the cross polarization, it reaches to its minimum value when P_{TE21}/P_{TE11} is near 0.05 with a -90^{o} phase shift between the two modes and starts increasing thereafter at both asymmetry and inter-

cardinal planes, i.e. ϕ=90^o and 45^o. The sidelobe levels plotted in Fig. 4.12 represent the first side lobe. This lobe is merged with the main lobe for the P_{TE21}/P_{TE11} from 0.7 to 1.3 with a -90^o phase shift, as it is left blank in Fig. 4.12b at the ϕ=0^o plane.

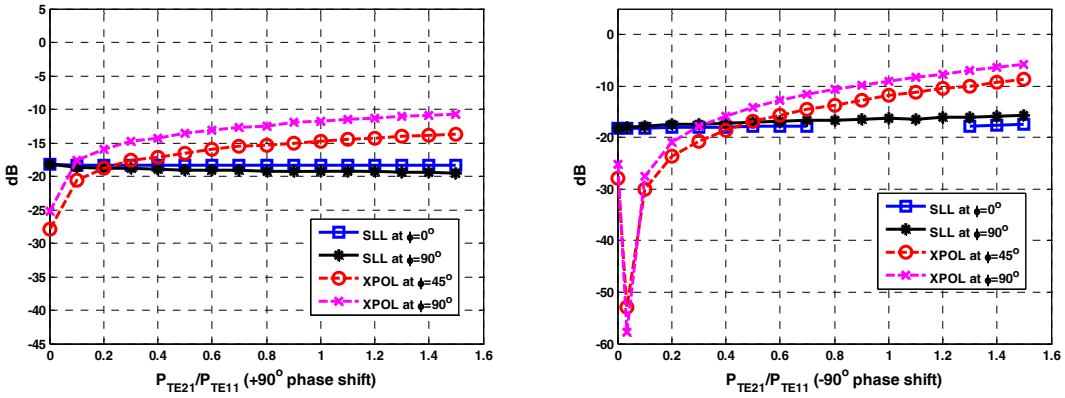

(a) (b)

Fig. 4.12. SLL and cross polarization of the offset reflector fed by the feed model, defined by Eqs. 4.4-5 operating at the combined *y*-polarized TE_{11} and TE_{21} modes, $\delta_{11}=\delta_{21}$=0^o and n=1, when F/D=1.1, D=20λ, $d_c=\lambda$, and θ_f=40.5^o at f=10GHz (a) +90^o (b) -90^o phase shifts.

Based on Table 4.1, the n=1 case for F/D=1.1 results in a low edge illumination. However, for most reflector antennas the -10dB edge taper gives the best performance in terms of gain and spillover efficiencies. Therefore, the effect of -10dB edge illumination, with n=12 for F/D=1.1, on the phase centre location, SLL and cross polarization is also studied. The results are shown in Figs. 4.13-14. For this case, the feed tilt angle is adjusted to 28.5^o based on the procedure explained in section 4.3. As can be seen, the phase centre location is now symmetrically displaced along the *x*-axis with respect to the aperture center for +90^o and -90^o phase shifts, as they reach to a maximum of ±10cm away from the aperture center. The SLL at the ϕ=90^o plane is below -22dB due to the larger tapered edge. At the ϕ=0^o plane, the SLL slowly increases as a function of the mode power ratio. The cross polarization level reaches to a minimum of -47dB, when the P_{TE21} / P_{TE11}=0.006$\angle$-90^o. As the mode power ratio increases, both SLL and cross polarization level increase.

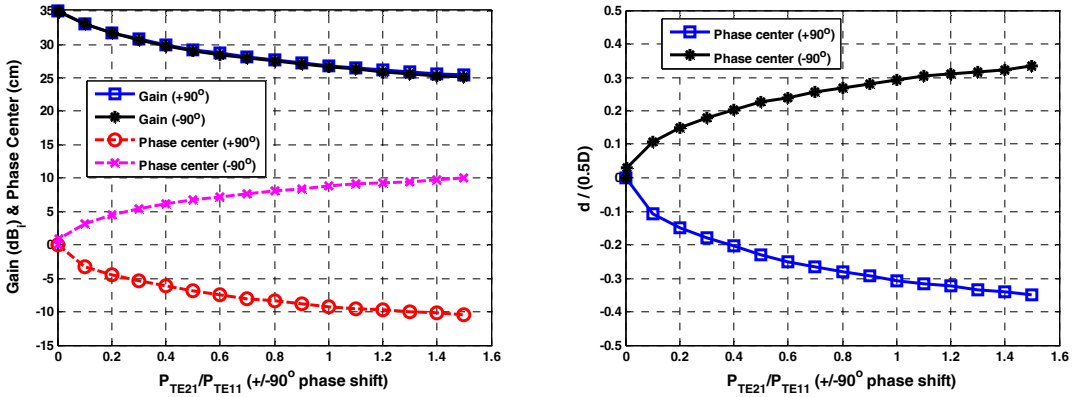

(a) (b)

Fig. 4.13. (a) Gain and phase centre location (b) normalized phase centre location of the offset reflector fed by the feed model, defined by Eqs. 4.4-5 operating at the combined *y*-polarized TE_{11} and TE_{21} modes, $\delta_{11}=\delta_{21}=0^o$ and n=12, when F/D=1.1, $D=20\lambda$, $d_c=\lambda$, and $\theta_f=28.5^o$ at f=10GHz. Phase centre moves along *x*-axis with reference to the center of offset reflector aperture.

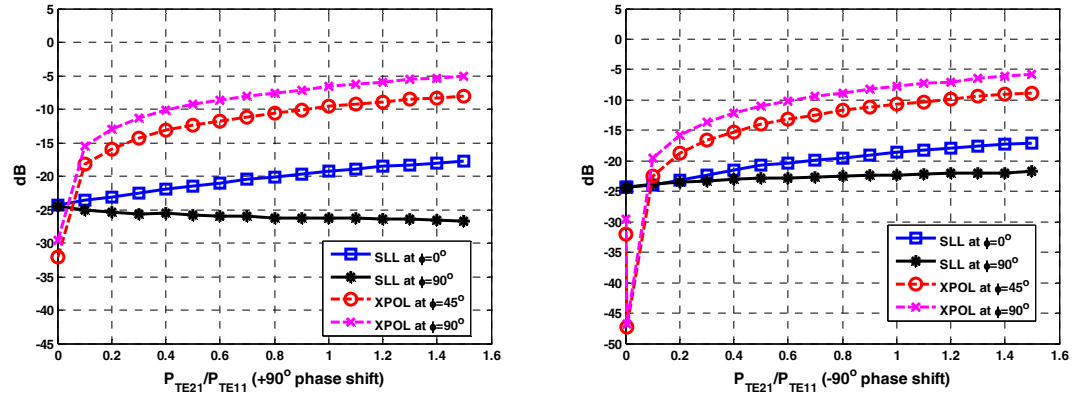

(a) (b)

Fig. 4.14. SLL and cross polarization of the offset reflector fed by the feed model, defined by Eqs. 4.4-5 operating at the combined *y*-polarized TE_{11} and TE_{21} modes, $\delta_{11}=\delta_{21}=0^o$ and n=12, when F/D=1.1, $D=20\lambda$, $d_c=\lambda$, and $\theta_f=28.5^o$ at f=10GHz (a) $+90^o$ (b) -90^o phase shifts.

The above study is also done for F/D=0.6 with n=1 and n=4.5, low and -10dB edge tapers, respectively. For brevity, their normalized phase centre locations versus mode power ratio are only shown in Fig. 4.15. As can be seen, the same trend as the one reported for the F/D=1.1 is observed. The n=1 case results in asymmetric phase centre displacement along the *x*-axis with the aperture center as the origin. The n=4.5 case, which gives -10dB edge illumination along the *H*-plane, makes the phase centre movement symmetric as before. The maximum phase centre displacement is about 2cm more than that of the F/D=1.1.

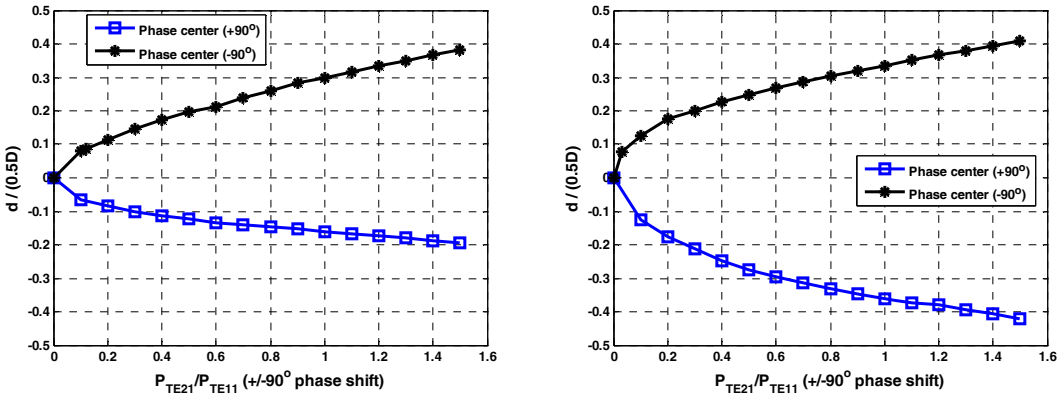

n=1 and θ_f=68.0° **n=4.5 and θ_f=51.2°**

Fig. 4.15. Normalized phase centre location of the offset reflector fed by the feed model, defined by Eqs. 4.4-5 operating at the combined *y*-polarized TE_{11} and TE_{21} modes, $\delta_{11}=\delta_{21}=0^o$, when F/D=0.6, D=20λ, and $d_c=\lambda$, at f=10GHz. Phase centre moves along *x*-axis with reference to the center of offset reflector aperture.

Table 4.2 summarizes the multi-phase centre offset reflector antennas studied above for the case I with F/D=0.6, when P_{TE21} / P_{TE11}=0.5 at the frequency of 10GHz. As can be seen, SLL improves as the aperture distribution tapers off at the edge with n=4.5, as expected based on the aperture theory. The cross polarization level, however, degrades at both planes for n=4.5. It should be noted that the cross polarization of less than -40dB is obtained at the plane of asymmetry, when there is -90° phase shift between the two modes. The corresponding mode power ratios are 0.12 and 0.033, for n=1 and 4.5, respectively.

Table 4.2. Summary of the study of the feed model shown in Fig. 4.5 for the offset reflector with F/D=0.6, D=20λ and $d_c=\lambda$ at f=10GHz. Phase centre moves along *x*-axis with reference to the center of offset reflector aperture.

F/D		**0.6**			
		***n*=1**		***n*=4.5**	
P_{TE21} / P_{TE11}		0.5 ∠ +90°	0.5 ∠ -90°	0.5 ∠ +90°	0.5 ∠ -90°
Gain		**32.7dB$_i$**	**28.8dB$_i$**	**31.6dB$_i$**	**31.5dB$_i$**
Phase centre location		***x*=-3.7cm**	***x*=+5.9cm**	***x*=-8.2cm**	***x*=+7.4cm**
SLL	ϕ=0°	**-19.9dB**	**-17.9dB**	**NA***	**-19.9dB**
	ϕ=90°	**-23.2dB**	**-15.4dB**	**-31.0dB**	**-19.0dB**
XPOL	ϕ=45°	**-11.7dB**	**-17.0dB**	**-9.1dB**	**-13.3dB**
	ϕ=90°	**-8.7dB**	**-14.5dB**	**-6.0dB**	**-10.4dB**

*the 1st side lobe merges with the main lobe

The performance of the virtual array antenna developed for case I is summarized and compared in Table 4.3 for the *F/D* ratios studied above and different edge tapers. In this table, the maximum phase centre location and maximum gain refer to the mode power ratio of 1.5 and 0, respectively. The minimum cross polarizations are also given, along with the required mode power ratio denoted by @, at the asymmetry plane whose cross polarization is usually high with a conventional single mode feed. As can be seen, the smaller the *F/D* ratio, the further the phase centre displaces along the *x*-axis.

Table 4.3. Summary of the case I for the offset reflector antennas with $D=20\lambda$ and $d_c=\lambda$ at f=10GHz. Phase centre moves along *x*-axis with reference to the center of offset reflector aperture. Maximum gain and maximum phase centre displacement are obtained when P_{TE21}/P_{TE11} are 0 and 1.5, respectively. SLL degradation is referred to the increased SLL due to the TE_{21} mode when $P_{TE21}/P_{TE11}=1.5$.

F/D	**1.1**		**0.6**	
	***n*=1**	***n*=12**	***n*=1**	***n*=4.5**
Max. Phase centre displacement	***x*=+10.6cm**	***x*=-10.5cm**	***x*=+11.5cm**	***x*=-12.6cm**
Max. Gain	**29.5dB$_i$**	**35.1dB$_i$**	**32.2dB$_i$**	**34.9dB$_i$**
Gain Loss (due to Max. Phase centre displacement)	**7.7dB**	**9.7dB**	**7.2dB**	**6.4dB**
SLL (single mode feed)	**-18.2dB**	**-24.5dB**	**-19.6dB**	**-25.1dB**
SLL degradation (ϕ=90^o)	**-2.5dB**	**-3.0dB**	**-8.0dB**	**-9.4dB**
Min. XPOL at ϕ=90^o	**-57.8dB @0.035$\angle$ -90^o**	**-46.8dB @0.007$\angle$ -90^o**	**-39.2dB @0.12$\angle$ -90^o**	**-49.0dB @0.033$\angle$ -90^o**

4.5 Case II: *Y*-polarized TE_{11} and 45^o Oriented TE_{21} Modes

Case II is again a dual-mode feed located at the focal point of the same offset reflector antenna shown in Fig. 4.2. The TE_{11} type mode is aligned along the *y*-axis ($\delta_{11}=0^o$), also called copol mode, but the TE_{21} type mode is 45^o orientated ($\delta_{21}=45^o$) called crosspolarized mode. Their corresponding field distributions are shown in Fig. 4.16. The governing far-field patterns are given below for each mode.

$$\textbf{TE}_{11}\textbf{ mode } (\delta_{11}=0^{o}):\quad \left\{\begin{aligned} E_\theta &= \sqrt{P_{TE11}}\,\cos^n\theta\,\sin(\phi-\delta_{11}) = \sqrt{P_{TE11}}\,\cos^n\theta\,\sin\phi \\ E_\phi &= \sqrt{P_{TE11}}\,\cos^n\theta\,\cos(\phi-\delta_{11}) = \sqrt{P_{TE11}}\,\cos^n\theta\,\cos\phi \end{aligned}\right\} \tag{4.6}$$

$$\textbf{TE}_{21}\textbf{ mode } (\delta_{21}=45^{o}):\left\{\begin{aligned} E_\theta &= j\sqrt{P_{TE21}}\,\sin 2\theta\,\cos\theta\,\sin 2(\phi-\delta_{21}) = -j\sqrt{P_{TE21}}\,\sin 2\theta\,\cos\theta\,\cos 2\phi \\ E_\phi &= j\sqrt{P_{TE21}}\,\sin 2\theta\,\cos\theta\,\cos 2(\phi-\delta_{21}) = j\sqrt{P_{TE21}}\,\sin 2\theta\,\cos\theta\,\sin 2\phi \end{aligned}\right\} \tag{4.7}$$

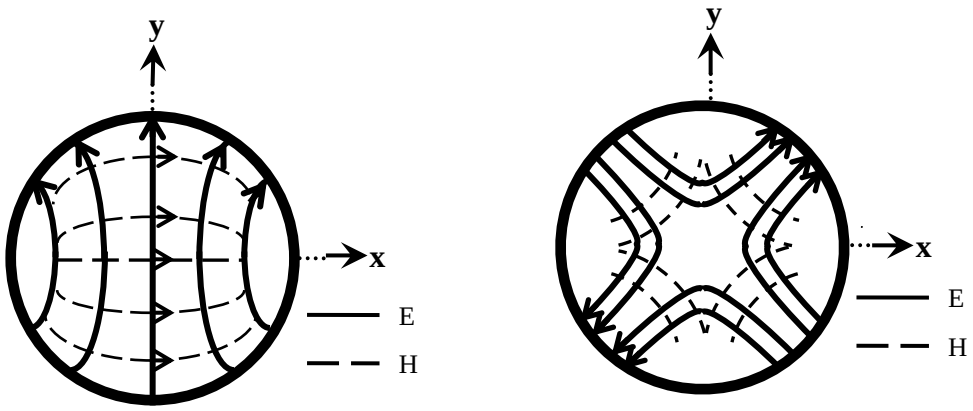

(a) (b)

Fig. 4.16. Aperture distribution of (a) the copol TE_{11} mode (y-polarized or $\delta_{11}=0^{o}$) (b) xpol TE_{21} mode ($\delta_{21}=45^{o}$).

The combination of above field distributions will move the main beam of the primary feed off the boresight at the $\phi=90^{o}$ plane, as shown in Fig. 4.17, only if there exist quadrature phase differences between the two modes. The corresponding phase patterns of the two modes are also given in Fig. 4.18. Again, the quadrature phase excitation will introduce an on-focus feed while the others will laterally displace the feed from the focal point of the offset reflector antenna as discussed before.

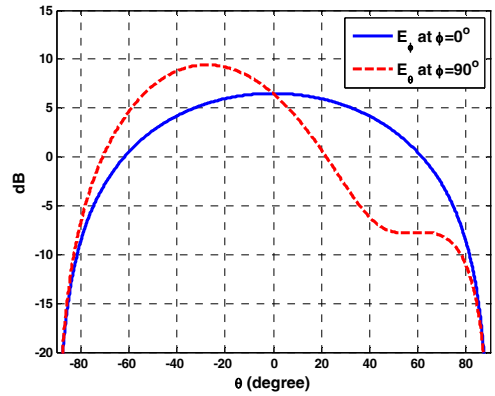

$P_{TE21}/P_{TE11}=0.5\angle +90^{o}$

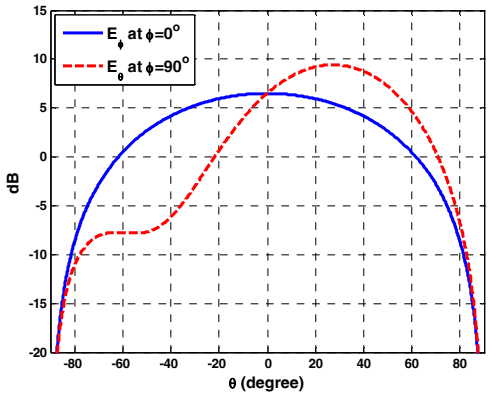

$P_{TE21}/P_{TE11}=0.5\angle -90^{o}$

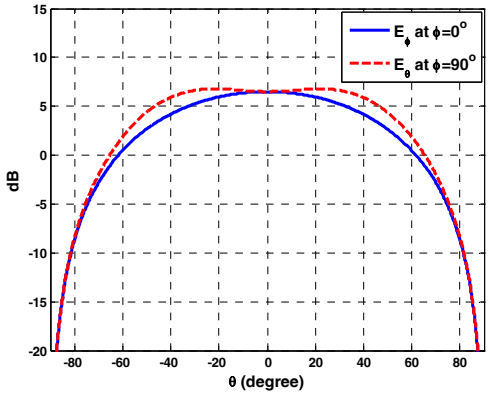

$P_{TE21}/P_{TE11}=0.5\angle 0^{o}$

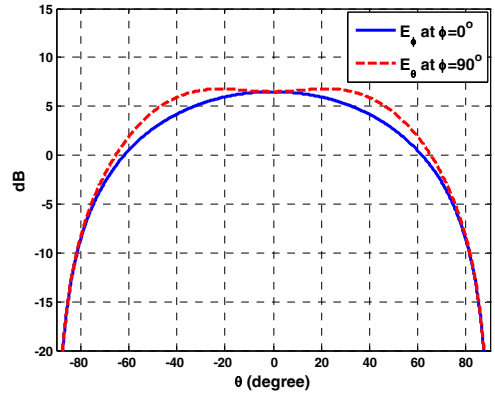

$P_{TE21}/P_{TE11}=0.5\angle 180^{o}$

Fig. 4.17. Radiation patterns of the feed defined by Eqs. 4.6-7 operating at the combined Copol TE_{11} ($\delta_{11}=0^{o}$) and xpol TE_{21} ($\delta_{21}=45^{o}$) modes with n=1 at f=10GHz.

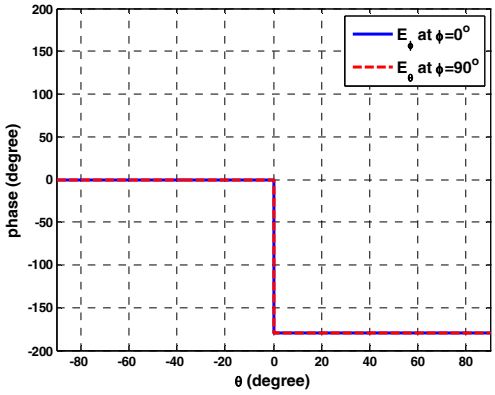

$P_{TE21}/P_{TE11}=0.5\angle +90^{o}$

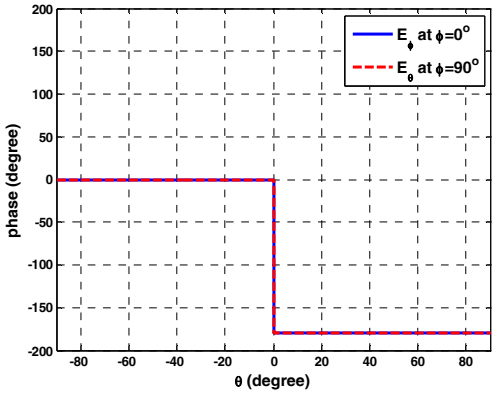

$P_{TE21}/P_{TE11}=0.5\angle -90^{o}$

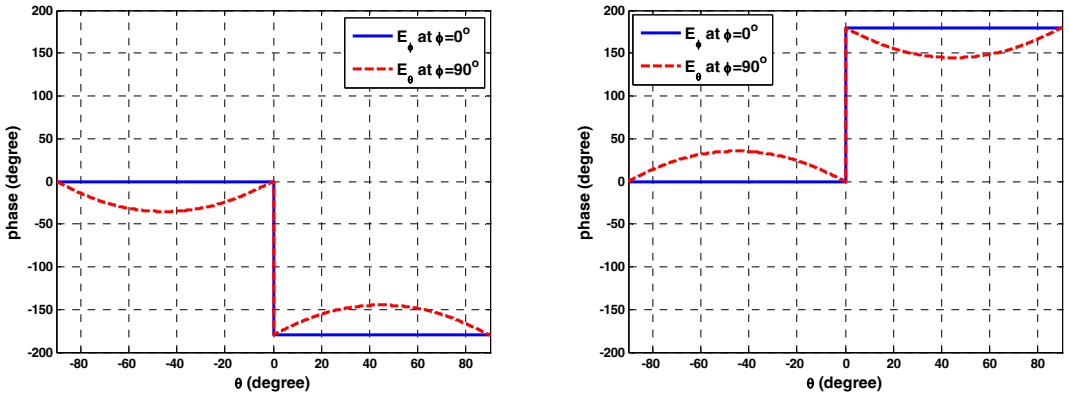

$P_{TE21}/P_{TE11}=0.5\angle 0^{o}$ $P_{TE21}/P_{TE11}=0.5\angle 180^{o}$

Fig. 4.18. Phase patterns of the feed defined by Eqs. 4.6-7 operating at the combined Copol TE_{11} ($\delta_{11}=0^{o}$) and xpol TE_{21} ($\delta_{21}=45^{o}$) modes with n=1 at f=10GHz.

To show the direction of the phase centre movement, both aperture amplitude and phase distributions are investigated similar to the previous case. They are shown in Figs. 4.19-20, respectively, for a fixed power ratio of 0.5 and different excitation phase shifts between the two modes. Similar to the previous section, the phase centre location only changes when the excitation phase is $\pm 90^{o}$. However, it moves along the y-axis for this case, as the peak intensity of the electric field moves along this axis having uniform phase distribution over the aperture. The excitation phases of 0^{o} and 180^{o} produce symmetric aperture distributions with two peaks split along the y-axis, as their primary feed pattern starts having a null at the boresight direction. The phase centre of the reflector, however, does not change for such excitation phases as explained for the case I. The feed tilt angle is still 40.5^{o}. From the aperture phase distributions, shown in Fig. 4.20, it is concluded that the quadrature phase differences between the modes produce uniform phase distributions over the aperture, which confirms the phase centre movement along the y-axis. The in-phase and out-of-phase excitations of 0^{o} and 180^{o} have non-uniform phase distributions.

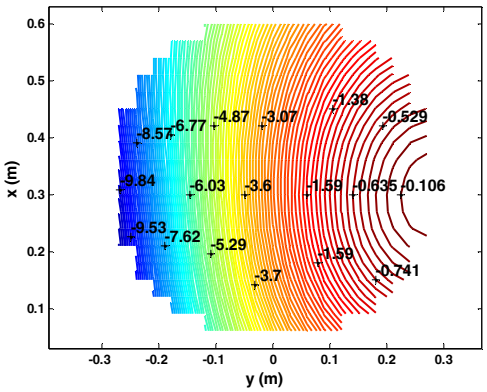

$P_{TE21}/P_{TE11}=0.5\angle +90^{o}$

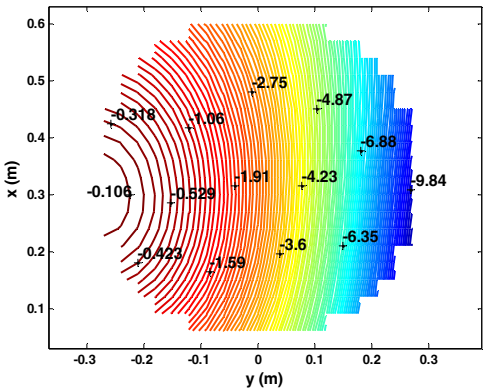

$P_{TE21}/P_{TE11}=0.5\angle -90^{o}$

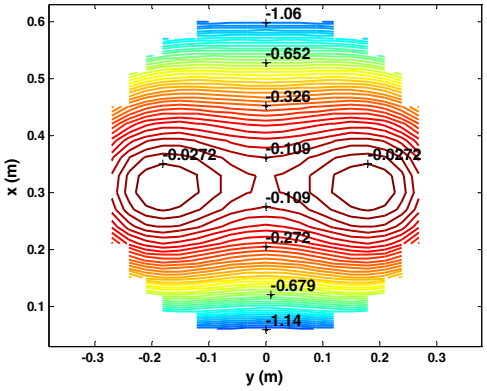

$P_{TE21}/P_{TE11}=0.5\angle 0^{o}$

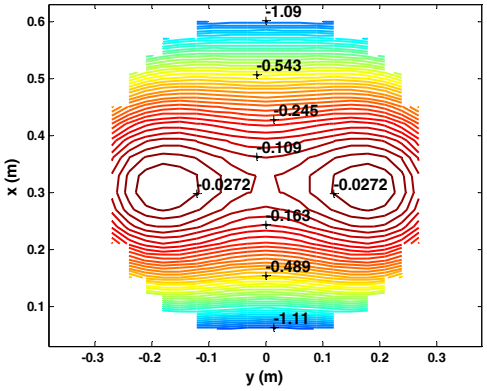

$P_{TE21}/P_{TE11}=0.5\angle 180^{o}$

Fig. 4.19. Aperture distributions of the offset reflector fed by the feed model, defined by Eqs. 4.6-7 operating at the combined TE_{11} and TE_{21} modes, $\delta_{11}=0^{o}$, $\delta_{21}=45^{o}$, and $n=1$, when $F/D=1.1$, $D=20\lambda$, $d_c=1\lambda$, and $\theta_f=40.5^{o}$ at f=10GHz.

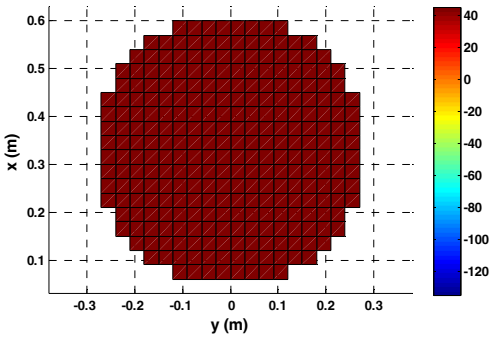

$P_{TE21}/P_{TE11}=0.5\angle +90^{o}$

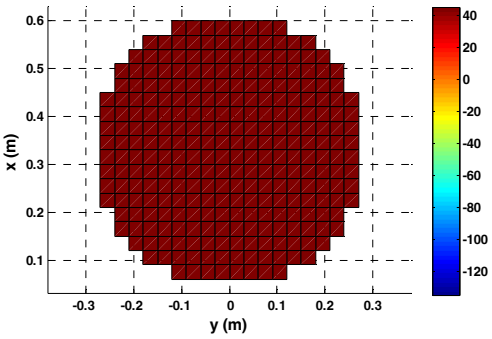

$P_{TE21}/P_{TE11}=0.5\angle -90^{o}$

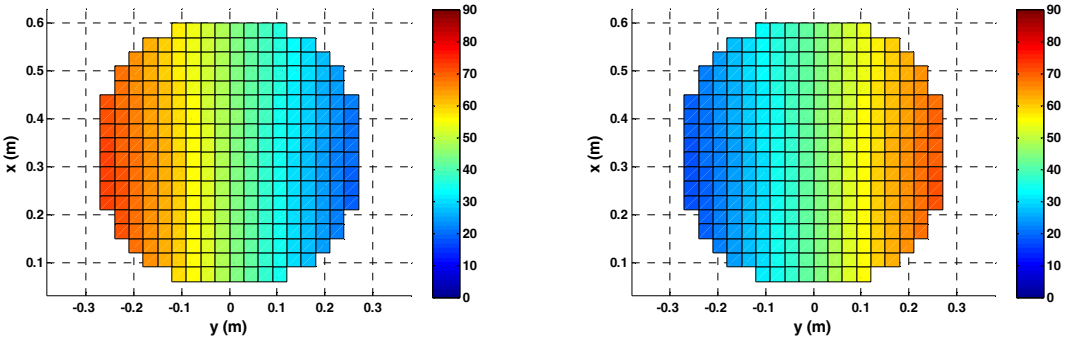

$P_{TE21}/P_{TE11}=0.5\angle 0^{o}$ $P_{TE21}/P_{TE11}=0.5\angle 180^{o}$

Fig. 4.20. Aperture phase distributions of the offset reflector fed by the feed model, defined by Eqs. 4.6-7 operating at the combined TE_{11} and TE_{21} modes, $\delta_{11}=0^{o}$, $\delta_{21}=45^{o}$, and $n=1$, when $F/D=1.1$, $D=20\lambda$, $d_c=1\lambda$, and $\theta_f=40.5^{o}$ at f=10GHz.

The secondary far-field radiation patterns are shown in Fig. 4.21. As expected, the main beam is at the boresight angle for $\pm 90^{o}$ excitation phases and they are identical, whereas it is tilted at $\phi=90^{o}$ plane for in-phase, 0^{o}, and out-of-phase, 180^{o}, excitations. For this case, the main beam is tilted toward positive θ and negative θ for 0^{o} and 180^{o} phase excitations, respectively.

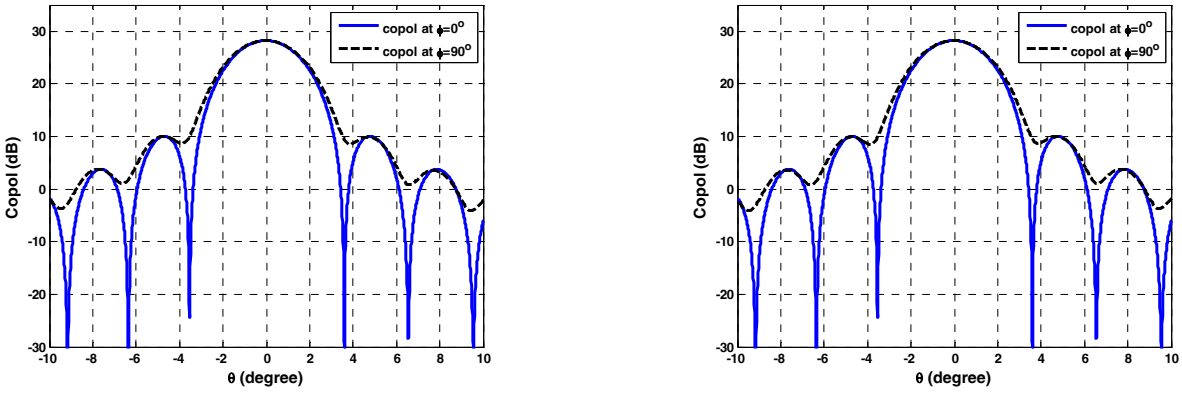

$P_{TE21}/P_{TE11}=0.5\angle +90^{o}$ $P_{TE21}/P_{TE11}=0.5\angle -90^{o}$

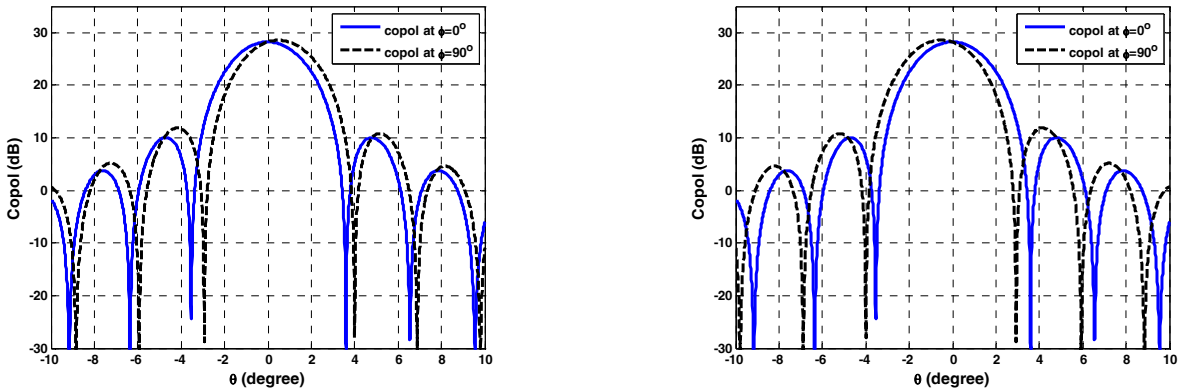

$P_{TE21}/P_{TE11}=0.5\angle 0^{o}$ $P_{TE21}/P_{TE11}=0.5\angle 180^{o}$

Fig. 4.21. Far-field radiation patterns of the offset reflector fed by the feed model, defined by Eqs. 4.6-7 operating at the combined TE_{11} and TE_{21} modes, $\delta_{11}=0^{o}$, $\delta_{21}=45^{o}$, and $n=1$, when $F/D=1.1$, $D=20\lambda$, $d_c=1\lambda$, and $\theta_f=40.5^{o}$ at f=10GHz.

Similar to the case I, the exact phase centre locations are determined using the same procedure explained before for the quadrature phase excitations of $\pm 90^{o}$ and different mode power ratios. For the case II under study here, the phase centre moves along the *y*-axis. The results of gain and phase centre location are shown in Fig. 4.22a. As can be seen, the antenna gain is the same for both $+90^{o}$ and -90^{o} phase shifts. However, it drops by 3.5dB as the mode power ratio increases. For this case, the phase centre moves equally along the *y*-axis for the same mode power ratio with a maximum of 8cm displacement for $P_{TE21}/P_{TE11}=1.5$. The phase centre displacement normalized to the half aperture diameter is also shown in Fig. 4.22b to show the ratio of the phase centre displacement with respect to the half of the reflector aperture size.

The sidelobe levels and cross polarization results are plotted in Fig. 4.23. As can be seen, the sidelobe levels are almost unchanged as the mode power ratio grows at both principal planes of $\phi=0^{o}$ and 90^{o} planes and they are around -18dB. As for the cross polarization, it is less than -20dB for mode power ratio of up to 0.1 and increases thereafter at both asymmetry and inter-cardinal planes, i.e. $\phi=90^{o}$ and 45^{o}.

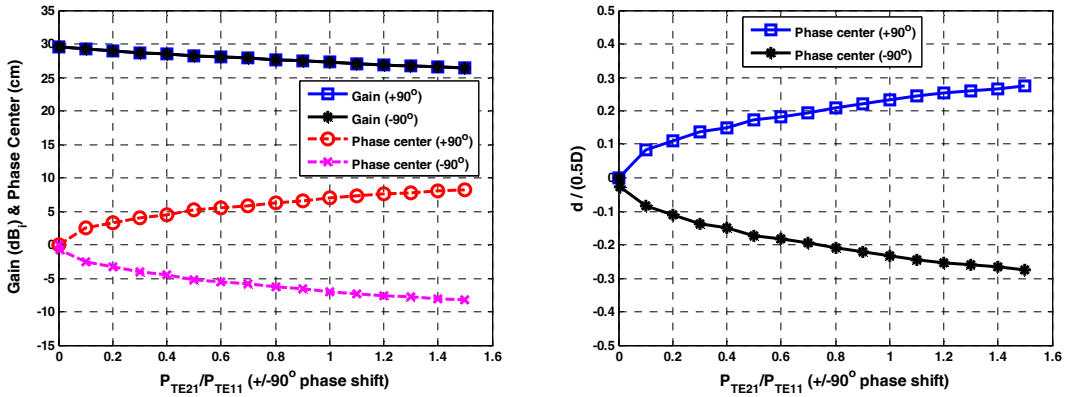

(a) (b)

Fig. 4.22. (a) Gain and phase centre location (b) normalized phase centre location of the offset reflector fed by the feed model, defined by Eqs. 4.6-7 operating at the combined TE_{11} and TE_{21} modes, δ_{11}=0°, δ_{21}=45°, and n=1, when F/D=1.1, D=20λ, d_c=λ, and θ_f=40.5° at f=10GHz. Phase centre moves along y-axis with reference to the center of offset reflector aperture.

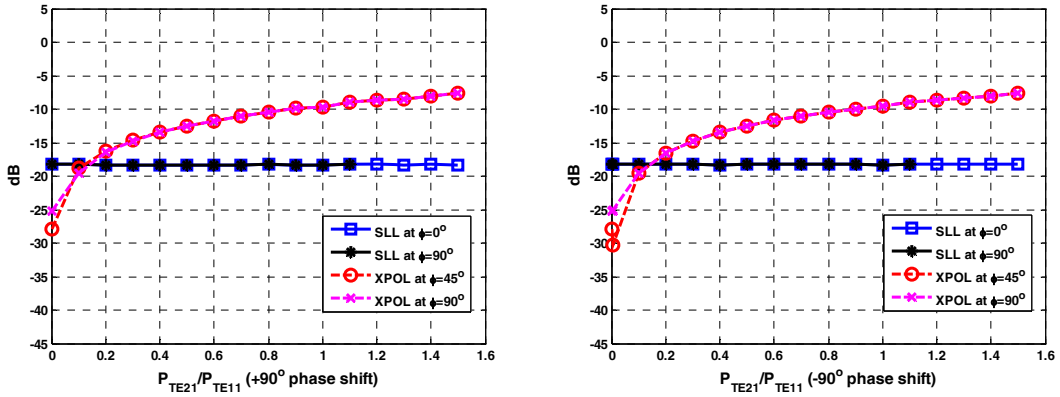

(a) (b)

Fig. 4.23. SLL and cross polarization of the offset reflector fed by the feed model, defined by Eqs. 4.6-7 operating at the combined TE_{11} and TE_{21} modes, δ_{11}=0°, δ_{21}=45°, and n=1, when F/D=1.1, D=20λ, d_c=λ, and θ_f=40.5° at f=10GHz (a) +90° (b) -90° phase shifts.

Similar to the case I, the -10dB edge taper with n=12 and F/D=1.1, based on Table 4.1, is also investigated. The results are shown in Figs. 4.24-25. For this case, the feed tilt angle is adjusted to 28.5° based on the procedure explained in section 4.3. As can be seen, the peak gain is now 35dB$_i$, 5dB more than the n=1 and the gain drop due to the phase centre displacement is about 10dB. The phase centre displaces more for a fixed mode power ratio comparing to the n=1 case, and it moves as far as 11cm away from the center of the aperture along the y-axis. The SLL at the ϕ=0° plane is below -24dB due to the larger tapered edge. At the ϕ=90° plane, the

SLL slowly increases as a function of the mode power ratio. The cross polarization level reaches to a minimum of -49dB, when the P_{TE21} / P_{TE11}=0.003$\angle$ -90^o. As the power ratio increases, both SLL and cross polarization level increase.

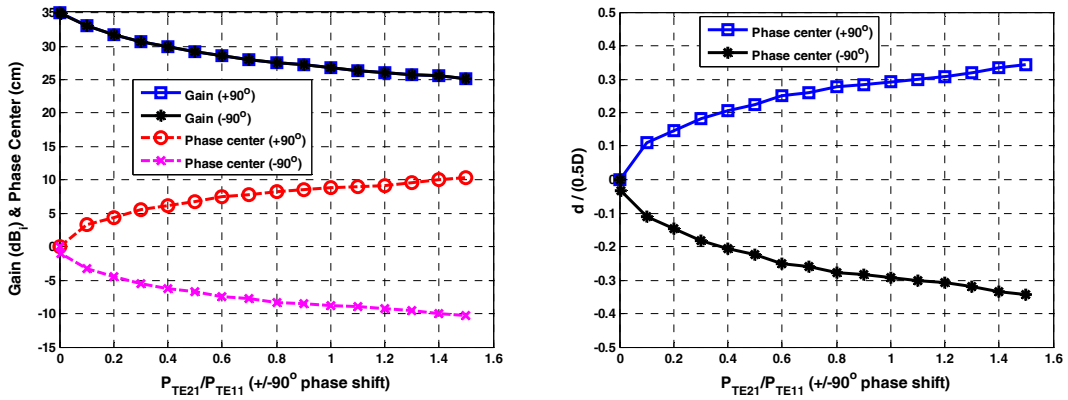

(a) (b)

Fig. 4.24. (a) Gain and phase centre displacement (b) normalized phase centre location of the offset reflector fed by the feed model, defined by Eqs. 4.6-7 operating at the combined TE_{11} and TE_{21} modes, δ_{11}=0^o, δ_{21}=45^o, and n=12, when F/D=1.1, D=20λ, d_c=λ, and θ_f=28.5^o at f=10GHz. Phase centre moves along y-axis with reference to the center of offset reflector aperture.

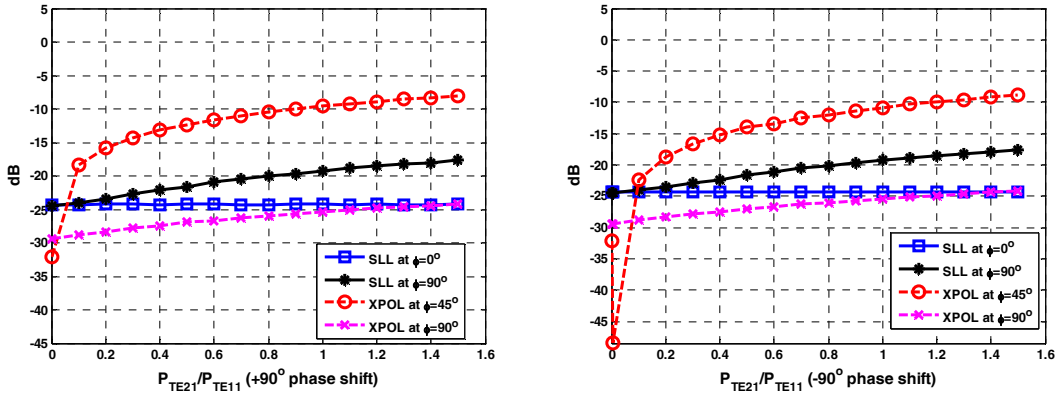

(a) (b)

Fig. 4.25. SLL and cross polarization of the offset reflector fed by the feed model, defined by Eqs. 4.6-7 operating at the combined TE_{11} and TE_{21} modes, δ_{11}=0^o, δ_{21}=45^o, and n=12, when F/D=1.1, D=20λ, d_c=λ, and θ_f=28.5^o f=10GHz (a) +90^o (b) -90^o phase shifts.

The normalized phase centre displacements versus mode power ratio are shown in Fig. 4.26 for F/D=0.6 with n=1 and n=4.5, -2.16dB and -10dB edge tapers as listed in Table 4.1, respectively. The same trend as the one reported for the F/D=1.1 is observed. The n=4.5 moves the phase centre further away from the aperture centre for the same value of mode power ratio. The maximum phase centre displacement for n=4.5 is 3cm more than that of n=1 for F/D=0.6.

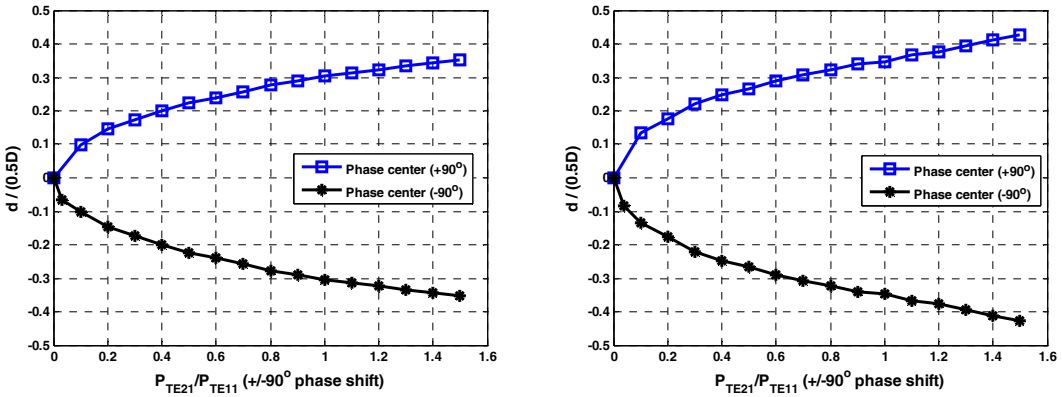

n=1 and θ_f=68.0° **n=4.5 and θ_f=51.2°**

Fig. 4.26. Normalized phase centre displacement of the offset reflector fed by the feed model, defined by Eqs. 4.6-7 operating at the combined TE_{11} and TE_{21} modes, δ_{11}=0°, δ_{21}=45°, when F/D=0.6, D=20λ, and $d_c=\lambda$, at f=10GHz. Phase centre moves along y-axis with reference to the center of offset reflector aperture.

Table 4.4 summarizes the multi-phase centre offset reflector antennas studied above for the case II with F/D=0.6, when P_{TE21} / P_{TE11}=0.5 at the frequency of 10GHz. As can be seen, SLL improves as the aperture distribution tapers off at the edge with n=4.5, as expected based on the aperture theory. The cross polarization level improves by about 4.5dB at the asymmetry plane of ϕ=90° for n=4.5. It should be noted that the cross polarization of -40dB is obtained for n=4.5 at the inter-cardinal plane of ϕ=45°, when there is -90° phase shift between the two modes. The corresponding mode power ratio is 0.037.

Table 4.4. Summary of the study of the case II for the offset reflector with F/D=0.6, D=20λ, and $d_c=\lambda$ at f=10GHz. Phase centre moves along y-axis with reference to the center of offset reflector aperture.

F/D		**0.6**			
		***n*=1**		***n*=4.5**	
P_{TE21} / P_{TE11}		**0.5 ∠ +90°**	**0.5 ∠ -90°**	**0.5 ∠ +90°**	**0.5 ∠ -90°**
Gain		**30.9dB$_i$**	**30.9dB$_i$**	**31.6dB$_i$**	**31.6dB$_i$**
Phase centre location		***y*=+6.7cm**	***y*=-6.7cm**	***y*=+8.0cm**	***y*=-8.0cm**
SLL	**ϕ=0°**	**-19.6dB**	**-19.5dB**	**-24.1dB**	**-24.1dB**
	ϕ=90°	**NA***	**NA***	**-22.6dB**	**-22.6dB**
XPOL	**ϕ=45°**	**-10.9dB**	**-13.6dB**	**-9.1dB**	**-13.5dB**
	ϕ=90°	**-12.6dB**	**-12.6dB**	**-17.1dB**	**-17.1dB**

*the 1st side lobe merges with the main lobe

The performance of the virtual array antenna developed for case II is compared in Table 4.5 for the *F/D* ratios studied above and different edge tapers. The maximum phase centre displacement and maximum gain refer to the mode power ratio of 1.5 and 0, respectively, similar to the previous case. The minimum cross polarizations are also given, along with the required mode power ratio denoted by @, at the asymmetry plane whose cross polarization is usually high with a conventional single mode feed. As can be seen, the phase centre location moves further away from the aperture center along the *y*-axis for the smaller *F/D* ratio.

Table 4.5. Summary of the case II for the offset reflector with $D=20\lambda$ and $d_c=\lambda$ at f=10GHz. Max. gain and max. phase centre displacement are obtained when P_{TE21}/P_{TE11} are 0 and 1.5, respectively. SLL degradation is referred to the increased SLL due to the TE_{21} mode when P_{TE21}/P_{TE11}=1.5.

F/D	**1.1**		**0.6**	
	***n*=1**	***n*=12**	***n*=1**	***n*=4.5**
Max. Phase centre displacement	***y*=8.2cm**	***y*=10.3cm**	***y*=10.6cm**	***y*=12.8cm**
Max. Gain	**29.5dB$_i$**	**35.1dB$_i$**	**32.2dB$_i$**	**34.9dB$_i$**
Gain Loss (due to Max. Phase centre displacement)	**3.1dB**	**9.9dB**	**3.0dB**	**6.5dB**
SLL (single mode feed)	**-18.2dB**	**-24.4dB**	**-19.6dB**	**-25.1dB**
SLL degradation (ϕ=90^o)	**-0.1dB**	**-6.7dB**	**~0dB**	**-6.9dB**
Min. XPOL ϕ=90^o	**-25.0dB @0.006$\angle$-90^o**	**-29.40dB @0.007$\angle$-90^o**	**-16.2dB @0.033$\angle$-90^o**	**-19.5dB @0.037$\angle$-90^o**

4.6 Case III: *X*-polarized TE_{11} and TE_{21} Modes

Case III is a dual-mode feed located at the focal point of the same offset reflector antenna shown in Fig. 4.2. The TE_{11} and TE_{21} type modes are both aligned along the *x*-axis, i.e. *x*-polarized with $\delta_{11}=\delta_{21}=90^o$. Their corresponding field distributions are shown in Fig. 4.27. The governing far-field patterns are given below for each mode.

$$\textbf{\textit{TE}}_{11}\textbf{ mode } (\delta_{11}=90^o): \quad \left\{ \begin{aligned} E_\theta &= \sqrt{P_{TE11}}\,\cos^n\theta\,\sin(\phi-\delta_{11}) = -\sqrt{P_{TE11}}\,\cos^n\theta\,\cos\phi \\ E_\phi &= \sqrt{P_{TE11}}\,\cos^n\theta\,\cos(\phi-\delta_{11}) = \sqrt{P_{TE11}}\,\cos^n\theta\,\sin\phi \end{aligned} \right\} \tag{4.8}$$

$$\textbf{TE}_{21}\textbf{ mode } (\delta_{21}=90^{o}):\begin{cases} E_\theta = j\sqrt{P_{TE21}}\,\sin 2\theta\,\cos\theta\,\sin 2(\phi-\delta_{21}) = -j\sqrt{P_{TE21}}\,\sin 2\theta\,\cos\theta\,\sin 2\phi \\ E_\phi = j\sqrt{P_{TE21}}\,\sin 2\theta\,\cos\theta\,\cos 2(\phi-\delta_{21}) = -j\sqrt{P_{TE21}}\,\sin 2\theta\,\cos\theta\,\cos 2\phi \end{cases} \quad (4.9)$$

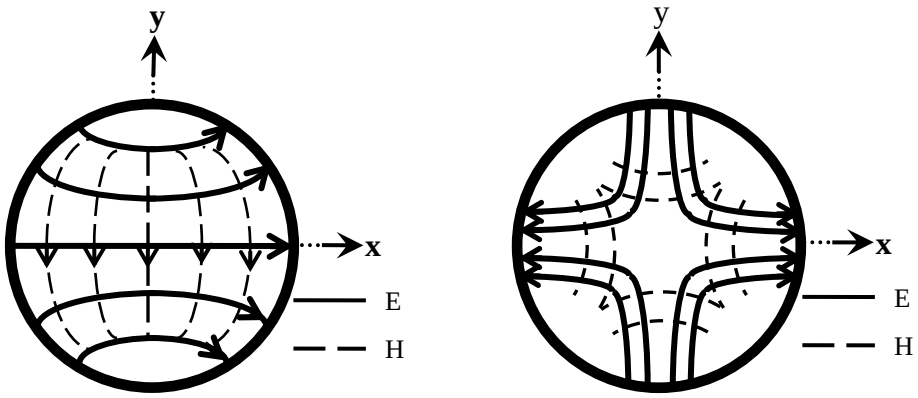

(a) (b)

Fig. 4.27. Aperture distribution of the *x*-polarized (a) TE_{11} mode (δ_{11}=90°) (b) TE_{21} mode (δ_{21}=90°).

The combination of above field distributions will have the main beam of the primary feed scan off the boresight at the ϕ=90° plane, only if there exists a quadrature phase difference between the two modes, as shown in Fig. 4.28. This case is similar to case II studied in section 4.5. The corresponding phase patterns of these two modes are also given in Fig. 4.29. Again, the quadrature phase excitation will introduce an on-focus feed while others will laterally displace the feed from the focal point of the offset reflector antenna as discussed before.

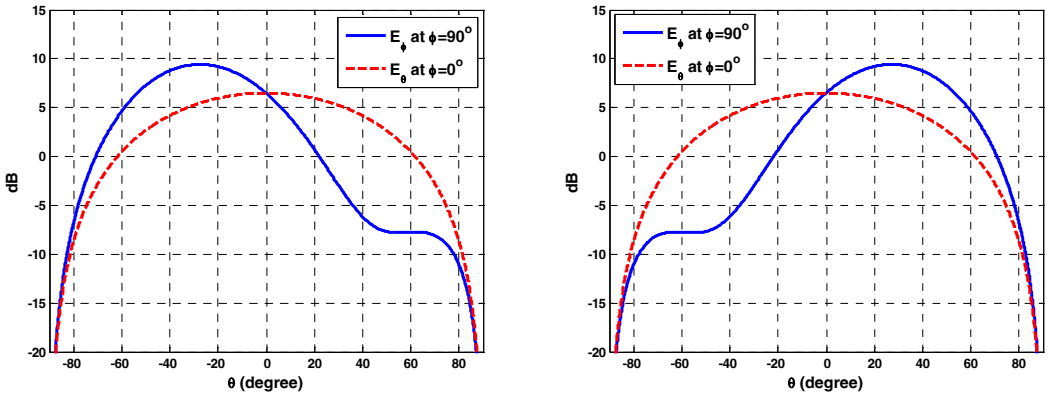

P_{TE21}/P_{TE11}=0.5 ∠ +90° P_{TE21}/P_{TE11}=0.5 ∠ -90°

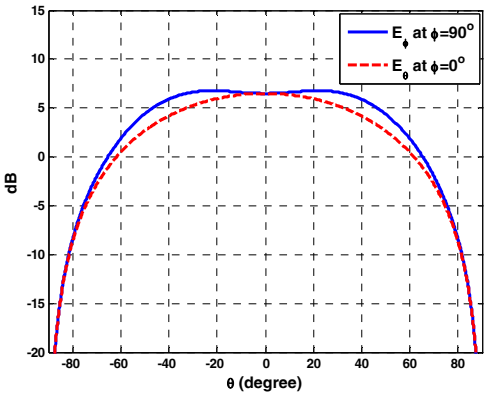

$P_{TE21}/P_{TE11}=0.5\angle 0^{o}$

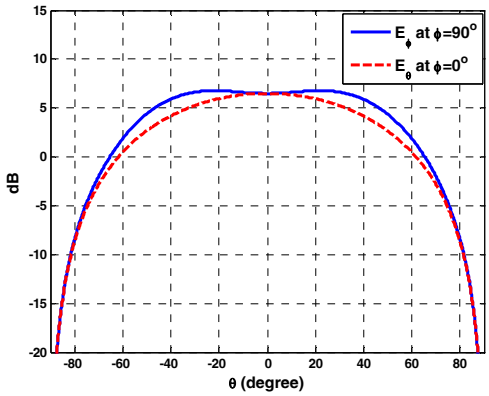

$P_{TE21}/P_{TE11}=0.5\angle 180^{o}$

Fig. 4.28. Radiation patterns of the feed defined by Eqs. 4.8-9 operating at the combined *x*-polarized TE_{11} and TE_{21} modes ($\delta_{11}=\delta_{21}=90^{o}$) with n=1 at f=10GHz.

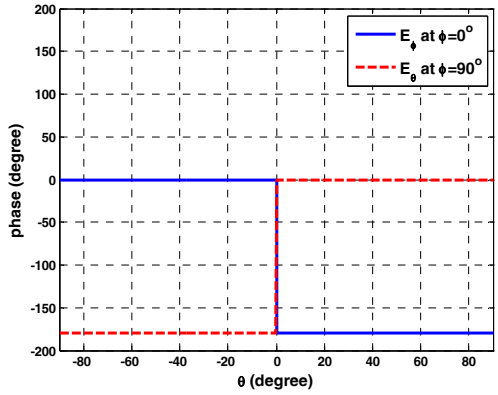

$P_{TE21}/P_{TE11}=0.5\angle +90^{o}$

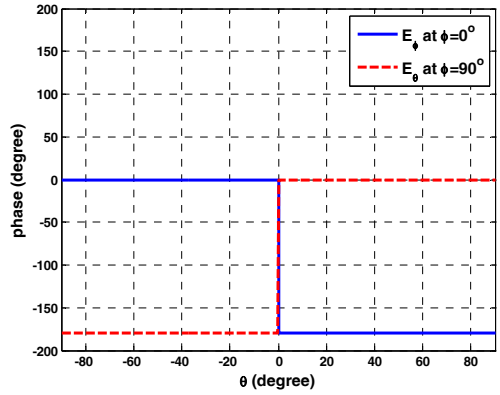

$P_{TE21}/P_{TE11}=0.5\angle -90^{o}$

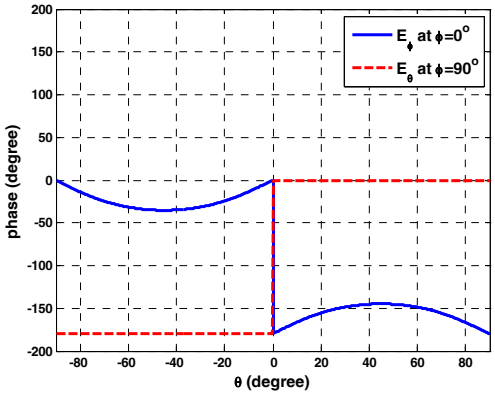

$P_{TE21}/P_{TE11}=0.5\angle 0^{o}$

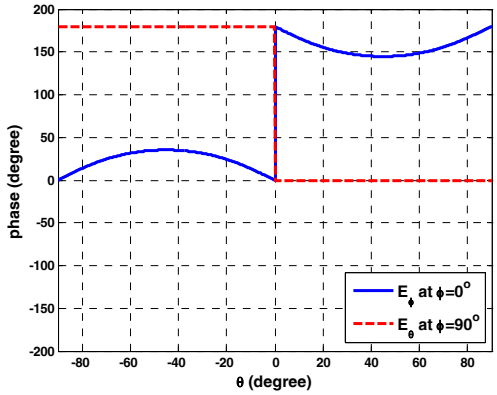

$P_{TE21}/P_{TE11}=0.5\angle 180^{o}$

Fig. 4.29. Phase patterns of the feed defined by Eqs. 4.8-9 operating at the combined *x*-polarized TE_{11} and TE_{21} modes ($\delta_{11}=\delta_{21}=90^{o}$) with n=1 at f=10GHz.

Figure 4.30 shows the aperture distribution for different amplitude and phase excitations of the dual mode feed expressed by Eqs. 4.8 and 4.9. Similar to the previous section, the phase centre location moves along the *y*-axis for the excitation phase of ±90^o. Again, the excitation phases of 0^o and 180^o do not displace the phase centre. The feed tilt angle is still 40.5^o. The aperture phase distributions are depicted in Fig. 4.31. They are uniform for ±90^o phase excitations, which confirm the phase centre location displaces from the aperture center. The in-phase and out-of-phase excitations of 0^o and 180^o generate non-uniform phase distributions.

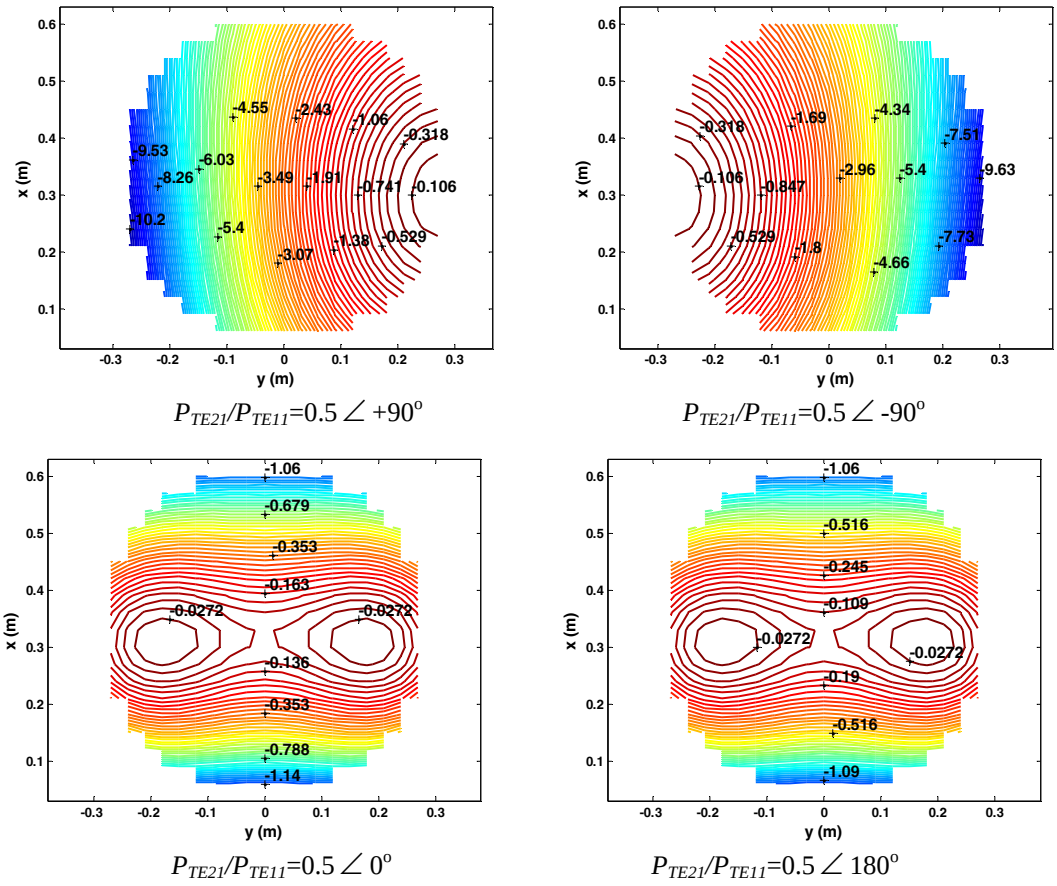

P_{TE21}/P_{TE11}=0.5 ∠ +90^o P_{TE21}/P_{TE11}=0.5 ∠ -90^o

P_{TE21}/P_{TE11}=0.5 ∠ 0^o P_{TE21}/P_{TE11}=0.5 ∠ 180^o

Fig. 4.30. Aperture distributions of the offset reflector fed by the feed model, defined by Eqs. 4.8-9 operating at the combined *x*-polarized TE_{11} and TE_{21} modes ($\delta_{11}=\delta_{21}=90^o$) with n=1, when F/D=1.1, $D=20\lambda$, $d_c=1\lambda$, and θ_f=40.5^o at f=10GHz.

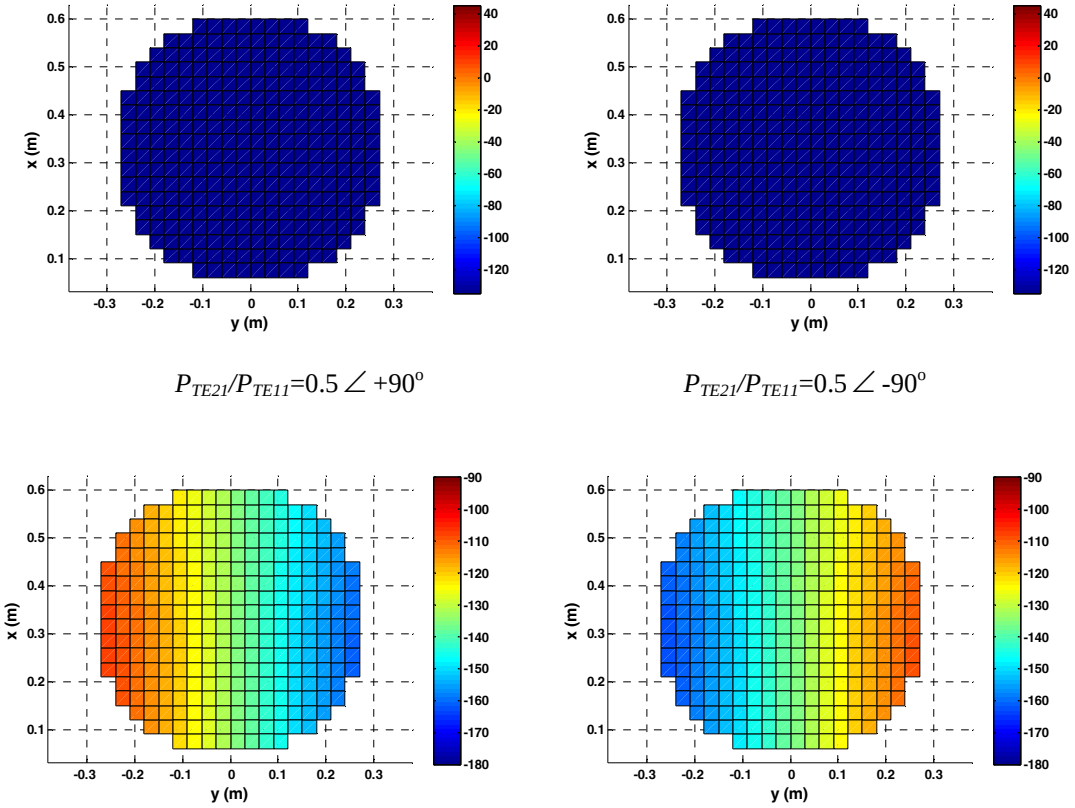

Fig. 4.31. Aperture phase distributions of the offset reflector fed by the feed model, defined by Eqs. 4.8-9 operating at the combined *x*-polarized TE_{11} and TE_{21} modes ($\delta_{11}=\delta_{21}=90^o$) with n=1, when F/D=1.1, $D=20\lambda$, $d_c=1\lambda$, and $\theta_f=40.5^o$ at f=10GHz.

The secondary far-field radiation patterns are shown in Fig. 4.32. As expected, the main beam is at the boresight angle for ±90° excitation phases, whereas it is tilted at ϕ=90° plane for in-phase, 0°, and out-of-phase, 180°, excitations, as they laterally move the feed phase centre away from the focal point of the reflector. Similar to the case II, the main beam is tilted toward positive and negative θ for 0° and 180° phase excitations, respectively. It has been shown that the antenna such developed produces identical main beams at the boresight angle with displaced phase centre locations along the *y*-axis, when there are quadrature phase shifts between the TE_{11} and TE_{21} type modes.

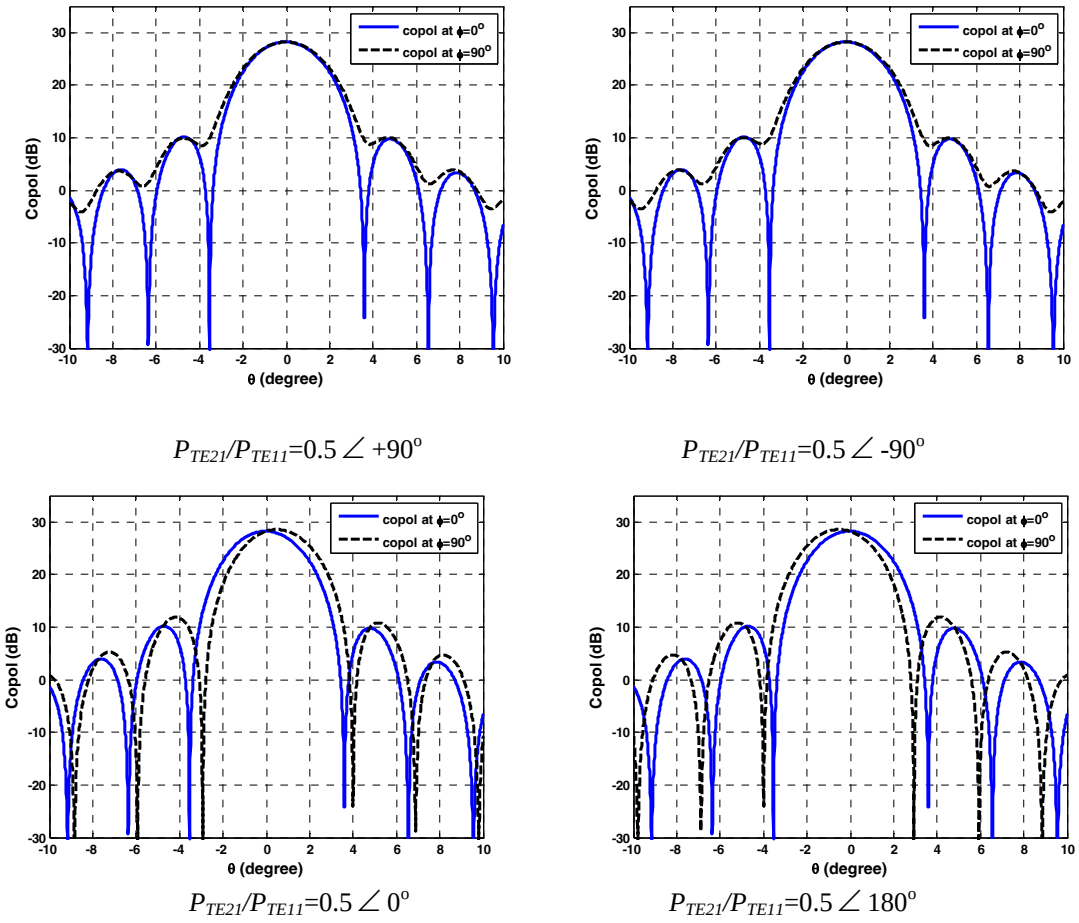

Fig. 4.32. Far-field radiation patterns of the offset reflector fed by the feed model, defined by Eqs. 4.8-9 operating at the combined *x*-polarized TE_{11} and TE_{21} modes ($\delta_{11}=\delta_{21}=90^o$) with n=1, when F/D=1.1, $D=20\lambda$, $d_c=1\lambda$, and $\theta_f=40.5^o$ at f=10GHz.

After an extensive study, the results of case III on the exact phase centre locations, gain, SLL, and cross polarizations versus mode power ratios were found to be the same as those of Case II for each *F/D* ratio, as shown in Figs. 4.22-26 and summarized in Tables 4.4 and 4.5. They are not repeated here for brevity.

4.7 Case IV: *X*-polarized TE_{11} and 45° Oriented TE_{21} Modes

In this section, the TE_{11} mode is aligned along the *x*-axis and the TE_{21} mode is oriented at 45° as shown in Fig. 4.33. That is, δ_{11}=90° and δ_{21}=45°. The far-field radiation patterns of each mode are governed by the following equations:

$$\textbf{TE}_{11}\textbf{ mode } (\delta_{11}=90^{o}):\quad \begin{Bmatrix} E_\theta = \sqrt{P_{TE11}}\,\cos^n\theta\,\sin(\phi-\delta_{11}) = -\sqrt{P_{TE11}}\,\cos^n\theta\,\cos\phi \\ E_\phi = \sqrt{P_{TE11}}\,\cos^n\theta\,\cos(\phi-\delta_{11}) = \sqrt{P_{TE11}}\,\cos^n\theta\,\sin\phi \end{Bmatrix} \tag{4.10}$$

$$\textbf{TE}_{21}\textbf{ mode } (\delta_{11}=45^{o}):\quad \begin{Bmatrix} E_\theta = j\sqrt{P_{TE21}}\,\sin 2\theta\,\cos\theta\,\sin 2(\phi-\delta_{21}) = -j\sqrt{P_{TE21}}\,\sin 2\theta\,\cos\theta\,\cos 2\phi \\ E_\phi = j\sqrt{P_{TE21}}\,\sin 2\theta\,\cos\theta\,\cos 2(\phi-\delta_{21}) = j\sqrt{P_{TE21}}\,\sin 2\theta\,\cos\theta\,\sin 2\phi \end{Bmatrix} \tag{4.11}$$

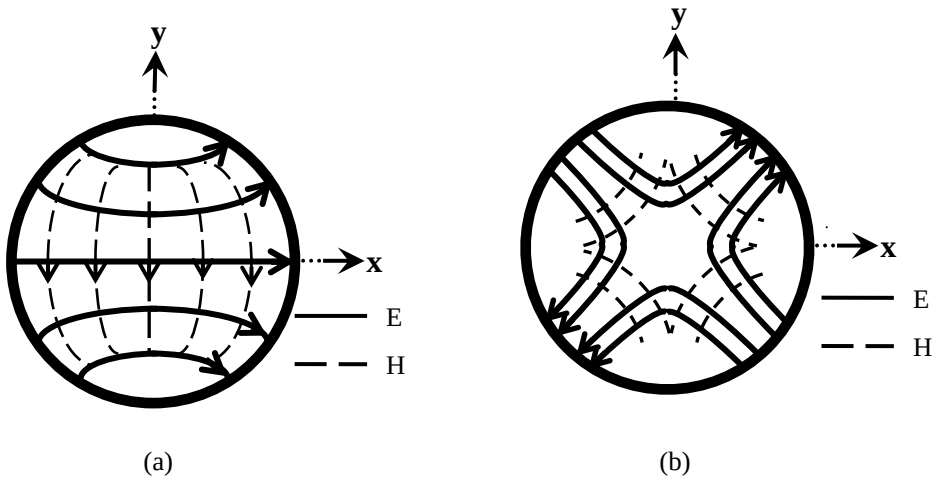

(a) (b)

Fig. 4.33 Aperture distribution of (a) the *x*-polarized TE_{11} mode (δ_{11}=90°) (b) TE_{21} mode (δ_{21}=45°).

The combination of above field distributions will shift the main beam of the primary feed off the boresight at the ϕ=0° plane, as shown in Fig. 4.34, only if there exists a quadrature phase difference between the two modes. This case is similar to the case I studied in section 4.4. The corresponding phase patterns resulting from the alignment stated above are also plotted in Fig. 4.35. Again, the quadrature phase excitation will introduce an on-focus feed while others will laterally displace the feed from the focal point of the offset reflector antenna as discussed before.

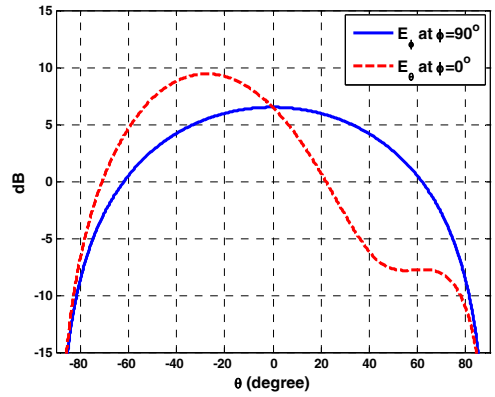

$P_{TE21}/P_{TE11}=0.5\angle +90^{o}$

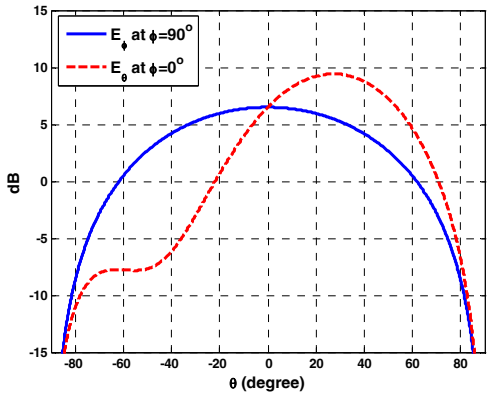

$P_{TE21}/P_{TE11}=0.5\angle -90^{o}$

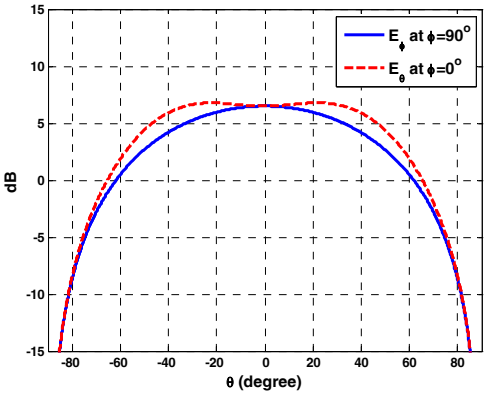

$P_{TE21}/P_{TE11}=0.5\angle 0^{o}$

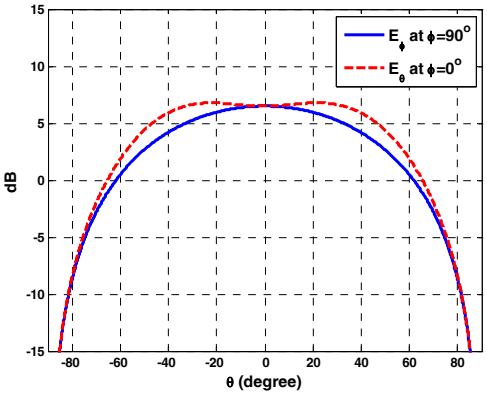

$P_{TE21}/P_{TE11}=0.5\angle 180^{o}$

Fig. 4.34. Radiation patterns of the feed defined by Eqs. 4.10-11 operating at the combined TE_{11} and TE_{21} modes ($\delta_{11}=90^{o}$ and $\delta_{21}=45^{o}$) with n=1 at f=10GHz.

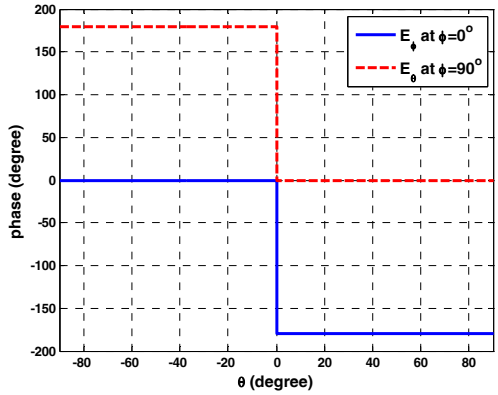

$P_{TE21}/P_{TE11}=0.5\angle +90^{o}$

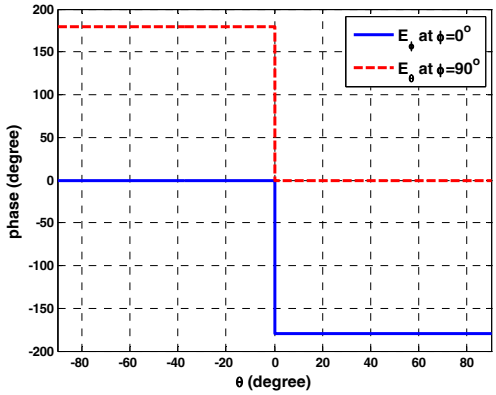

$P_{TE21}/P_{TE11}=0.5\angle -90^{o}$

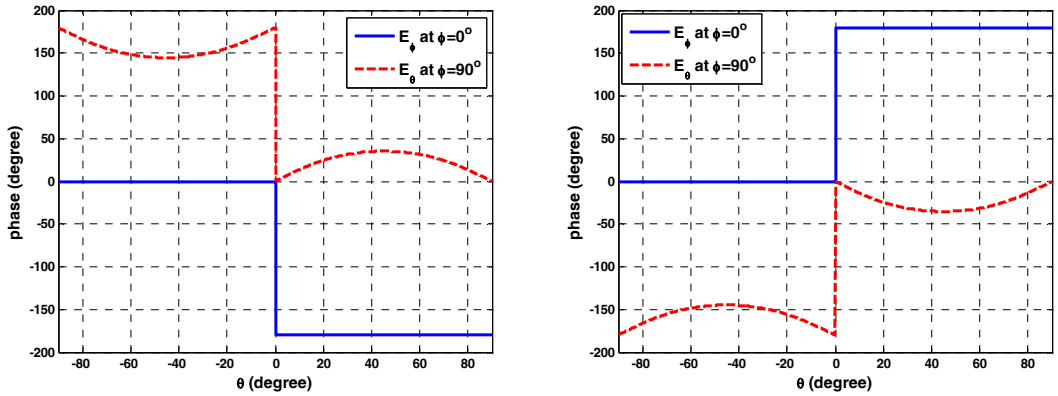

$P_{TE21}/P_{TE11}=0.5\angle 0^{o}$ $P_{TE21}/P_{TE11}=0.5\angle 180^{o}$

Fig. 4.35. Phase patterns of the feed defined by Eqs. 4.10-11 operating at the combined TE_{11} and TE_{21} modes ($\delta_{11}=90^{o}$ and $\delta_{21}=45^{o}$) with n=1 at f=10GHz.

Figs. 4.36 and 4.37 show the aperture amplitude and phase distributions for different phase excitations of the dual mode feed expressed by Eqs. 4.10 and 4.11, respectively. Similar to the case I, the phase centre location moves along the x-axis for the excitation phase of $\pm 90^{o}$. Again, the excitation phases of 0^{o} and 180^{o} do not displace the phase centre, even though the peak intensity has been shifted from the physical center. They generate non-uniform phase distributions over the aperture. The feed tilt angle is still 40.5^{o}. The aperture phase distributions are uniform for $\pm 90^{o}$ phase excitations, which confirm the phase centre location displaces from the aperture center.

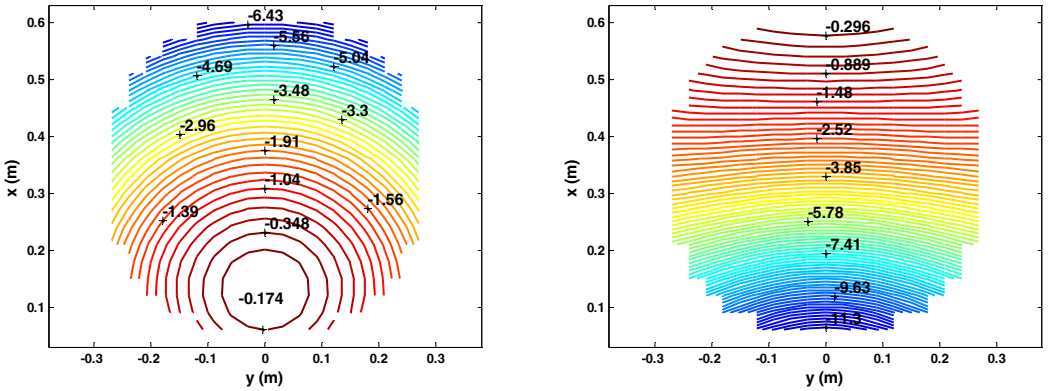

$P_{TE21}/P_{TE11}=0.5\angle +90^{o}$ $P_{TE21}/P_{TE11}=0.5\angle -90^{o}$

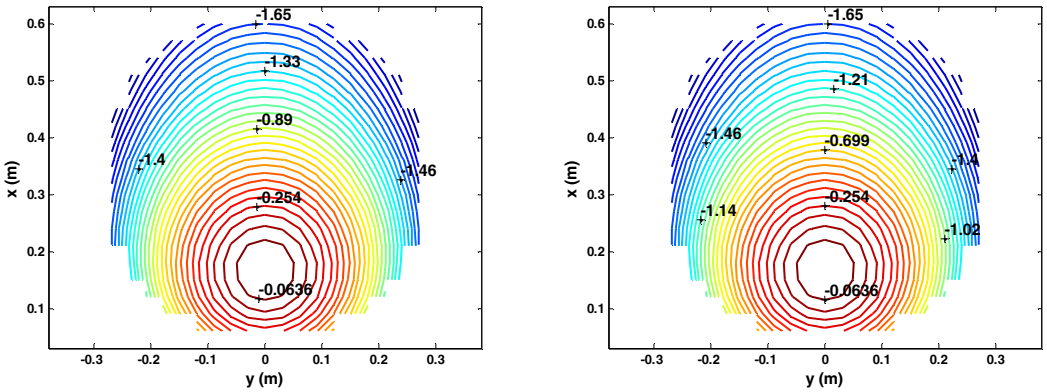

$P_{TE21}/P_{TE11}=0.5\angle 0^{o}$ $P_{TE21}/P_{TE11}=0.5\angle 180^{o}$

Fig. 4.36. Aperture distributions of the offset reflector fed by the feed model, defined by Eqs. 4.10-11 operating at the combined TE_{11} and TE_{21} modes ($\delta_{11}=90^{o}$ and $\delta_{21}=45^{o}$) with n=1, when F/D=1.1, $D=20\lambda$, $d_c=1\lambda$, and $\theta_f=40.5^{o}$ at f=10GHz.

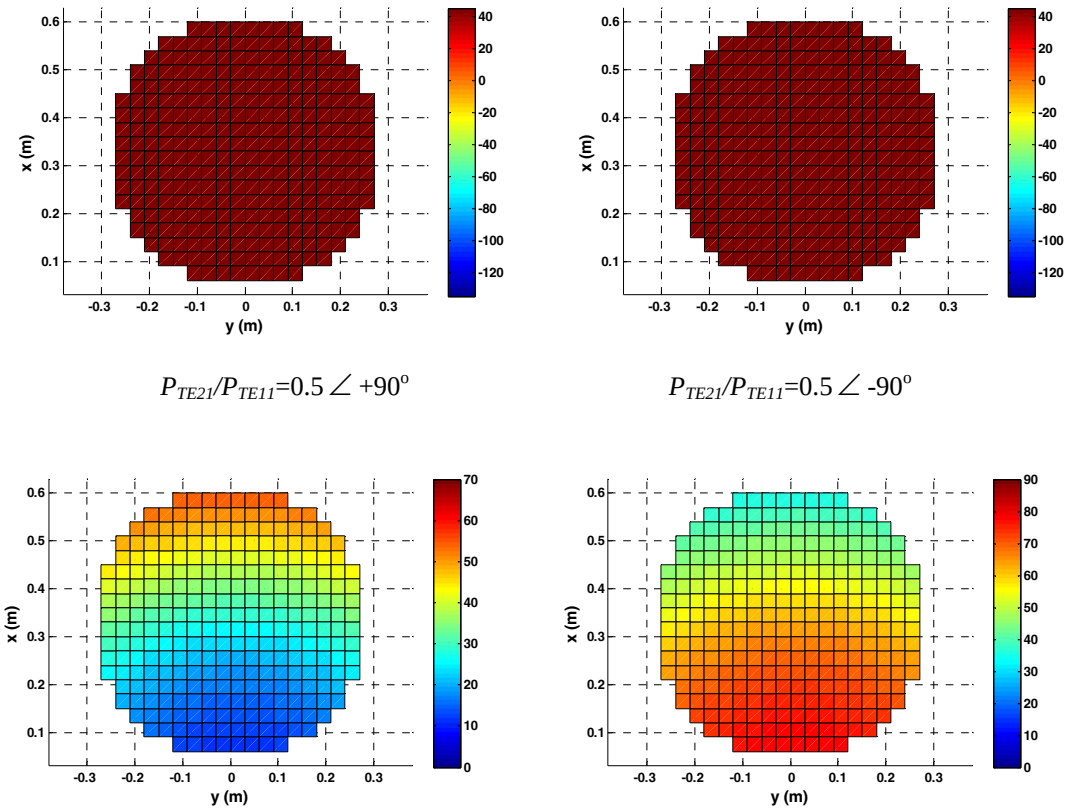

$P_{TE21}/P_{TE11}=0.5\angle +90^{o}$ $P_{TE21}/P_{TE11}=0.5\angle -90^{o}$

$P_{TE21}/P_{TE11}=0.5\angle 0^{o}$ $P_{TE21}/P_{TE11}=0.5\angle 180^{o}$

Fig. 4.37. Aperture phase distributions of the offset reflector fed by the feed model, defined by Eqs. 4.10-11 operating at the combined TE_{11} and TE_{21} modes ($\delta_{11}=90^{o}$ and $\delta_{21}=45^{o}$) with n=1, when F/D=1.1, $D=20\lambda$, $d_c=1\lambda$, and $\theta_f=40.5^{o}$ at f=10GHz.

The secondary far-field radiation patterns are shown in Fig. 4.38. As expected, the main beam is at the boresight angle for ±90° excitation phases, whereas it is tilted at ϕ=0° plane for in-phase, 0°, and out-of-phase, 180°, excitations. Similar to the case I, the main beam is tilted toward negative and positive θ for 0° and 180° phase excitations, respectively. Therefore, we have a virtual array antenna with identical main beams and displaced phase centre locations along the *x*-axis.

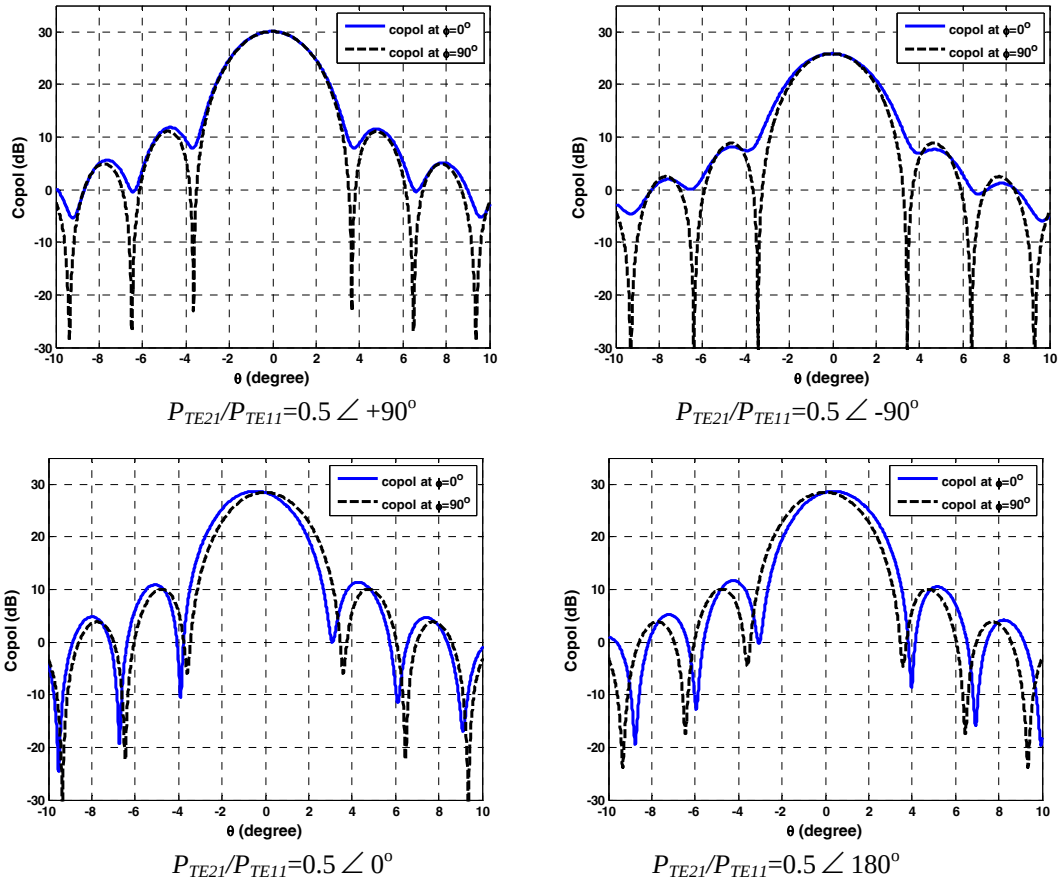

Fig. 4.38. Far-field radiation patterns of the offset reflector fed by the feed model, defined by Eqs. 4.10-11 operating at the combined TE_{11} and TE_{21} modes (δ_{11}=90° and δ_{21}=45°) with n=1, when F/D=1.1, D=20λ, d_c=1λ, and θ_f=40.5° at f=10GHz.

For the case IV, the exact phase centre locations, gain, SLL, and cross polarizations versus mode power ratios are the same as those of case I for each *F/D* ratios, shown in Figs. 4.11-15 and summarized in Tables 4.2 and 4.3. They are omitted here for brevity.

4.8 Virtual Array Antenna with a Tri-mode Feed

In all four cases studied in previous sections, the cross polarizations degraded as the mode power ratio increased and so moved the phase centre location. To reduce the unwanted cross polarization, the idea of a matched feed proposed in [10] can be used. Essentially, the primary feed should conjugately match the focal region of the reflector to reduce or cancel the cross polarization. In chapter three, a simplified analytical model was proposed, which included a tapered TE_{11} type mode along with the TE_{21} type mode. As shown in chapter three, the required mode content factor and tapering numbers were dependent on the offset geometry.

In this section, we use the tri-mode feed, with TE_{11}, TE_{21}, and TM_{11} modes, to reduce the cross polarization and investigate its effect on the phase centre location of the antenna studied above for F/D=0.6 and n=1. To do this, the case I is selected whose analytical model needs to be extended to accommodate the third TM_{11} mode as,

$$\begin{aligned} E_\theta &= [\sqrt{P_{TE\,11}}\cos^n\theta + \sqrt{P_{TM\,11}}\,\sin(2\theta)\cos\theta]\sin\phi + j\sqrt{P_{TE\,21}}\,\sin(2\theta)\cos\theta\,\sin(2\phi) \\ E_\phi &= \sqrt{P_{TE\,11}}\cos^n\theta\cos\phi + j\sqrt{P_{TE\,21}}\,\sin(2\theta)\cos\theta\,\cos(2\phi) \end{aligned} \qquad (4.12)$$

wherein P_{TM11}, equal to $35/4C_3^2$, is the mode power ratio of the TM_{11} mode and the remaining parameters are the same as defined in section 4.3. The TM_{11} mode, as expressed by Eqs. 2.36-37, has a split main beam with a null at the boresight and no E_ϕ component. Therefore, its radiation pattern function has been modeled similarly to the TE_{21} type mode pattern. As reported in [10], the TE_{21} and TM_{11} modes must have -90^o and 0^o phase shifts with the TE_{11} mode, respectively, in order to reduce the cross polarization.

We have selected three mode power ratios as P_{TE21}/P_{TE11}= 0.3, 0.4, and 0.5, with a -90^o phase shift to conduct the study. For each mode ratio, the optimized P_{TM11}/P_{TE11} is determined

such that it reduces the cross polarization at both 45^o and 90^o ϕ-cut planes. It is found that the extra TM_{11} mode does not change the phase centre location. The results are listed in Table 4.6. As can be seen, the cross polarization is decreased to less than -30dB at both planes, SLL improves at the ϕ=0^o plane and slightly increases at the ϕ=90^o plane. The gain is unchanged. Also, the required TM_{11} mode power ratio increases for the larger P_{TE21}/P_{TE11} to reduce the cross polarization.

Table 4.6. The impact of the extra TM_{11} mode of a tri-mode feed on the offset reflector studied in case I with n=1, F/D= 0.6, D=20λ and d_c=λ at f=10GHz.

	Gain (dB_i)	**SLL (dB)**		**XPOL (dB)**		**Phase centre (y=0)**
		ϕ=0^o	**ϕ=90^o**	**ϕ=45^o**	**ϕ=90^o**	
P_{TE21}/P_{TE11}= 0.3 $\angle$ -90^o P_{TM11}/P_{TE11}= 0	29.81	-18.76	-16.46	-22.71	-20.30	x=4.4cm
P_{TE21}/P_{TE11}= 0.3 $\angle$ -90^o P_{TM11}/P_{TE11}= 0.105 $\angle$ 0^o	**29.81**	**-19.31**	**-14.59**	**-34.34**	**-35.98**	**x=4.4cm**
P_{TE21}/P_{TE11}= 0.4 $\angle$ -90^o P_{TM11}/P_{TE11}= 0	29.28	-18.56	-15.82	-19.38	-16.82	x=5.2cm
P_{TE21}/P_{TE11}= 0.4 $\angle$ -90^o P_{TM11}/P_{TE11}= 0.19 $\angle$ 0^o	**29.28**	**-19.48**	**-13.53**	**-31.45**	**-32.73**	**x=5.2cm**
P_{TE21}/P_{TE11}= 0.5 $\angle$ -90^o P_{TM11}/P_{TE11}= 0	28.83	-17.89	-15.37	-17.01	-14.49	x=5.9cm
P_{TE21}/P_{TE11}= 0.5 $\angle$ -90^o P_{TM11}/P_{TE11}= 0.29 $\angle$ 0^o	**28.83**	**-19.10**	**-12.73**	**-29.41**	**-30.29**	**x=5.9cm**

4.9 Summary

A novel multi-phase centre antenna was studied using a single aperture antenna. A dual mode feed model, operating at the TE_{11} and TE_{21} type modes, was considered as a primary feed for the offset reflector antenna with a small clearance distance of 1λ at the frequency of 10GHz. Four cases of mode alignment or polarization were studied for different mode power ratios and excitation phases. The results of cases I and II were the same as those of cases IV and III,

respectively. Also, two *F/D* ratios with different edge tapers were considered. It was shown that, the phase centre location of the offset reflector antenna can be displaced from its physical center having identical main beams at the boresight angle, when there is a quadrature phase difference between the modes. The phase centre movement, along both orthogonal *x*- and *y*-axes, were obtained by appropriate mode polarization and could be easily extended to any direction as well. In general, the -10dB edge illumination provided better symmetry in terms of displacing the phase centre location particularly along the *x*-axis as well as pushing it further away from the aperture center. The resulting antenna is a virtual array antenna. The concept provides a simple and yet practical method for moving the antenna phase centre, without mechanically moving the antenna itself. Moreover, the in- and out-of-phase excitation cases can also be employed in beam scanning applications. It should be noted that secondary radiation patterns will have scanned main beams when the phase shift between the modes is different from $\pm 90^{o}$.

The antenna gain, SLL, and cross polarizations were investigated. It was shown that these properties were adversely affected as the phase centre moved further away from the aperture centre when the dual-mode feed illuminated the reflector antenna. Thus, the tri-mode matched feed was used to reduce the cross polarization. It was demonstrated that the extra TM_{11} mode improved the cross polarization performance at both asymmetry and inter-cardinal planes without affecting the phase centre location.

Chapter 5

Development of a Novel Dual-mode Feed for Displaced Phase Centre Virtual Reflectors

5.1 Introduction

In the previous chapter, multimode circular waveguides as primary feeds were used to investigate the virtual antenna concept in offset reflector antennas. Therefore, it is of great importance to design the primary feed itself to excite a specific higher order mode with appropriate mode alignments. For a dual-mode feed, the higher order TE_{21} mode was combined with the dominant TE_{11} mode in a circular waveguide antenna. To excite the higher order modes, either a sharp change in the cross-sectional dimension of a circular waveguide or an insertion of a piece of scatter such as a conductor or dielectric is required [1].

As shown in chapter 4, different mode polarizations were needed in order to displace the phase centre locations in two orthogonal directions. Of four cases studied in chapter 4, cases I and IV had identical results, so did cases II and III. The former cases moved the phase centre along the *x*-axis, whereas the latter ones displaced the phase centre location along the *y*-axis. Therefore, cases II and IV are selected to verify the multi-phase centre antenna along two orthogonal directions in practice. It is much preferred to electronically control the polarization and power of each mode instead of mechanically rotating the feed itself. The latter approach always adds mechanical complexity to the system. In this chapter, a novel dual-mode circular waveguide is proposed. The feed generates both TE_{11} and TE_{21} modes whose polarizations and mode power ratios can be controlled by a simple signal processing technique. The modes are

excited by two concentric shorted microstrip ring patches attached to a circular waveguide. It is shown that the proposed feed is capable of producing two perpendicular polarizations required for the primary feeds of cases II and IV discussed in chapter 4 within a single hardware. All simulations for the feed part were carried out using ANSOFT HFSS v.12 [19], which is based on the Finite Element method. A prototype antenna was fabricated and tested. The measured results satisfactorily validate the numerical ones.

To verify the multi-phase centre antenna concept, first the numerical results of the proposed feed will be used to illuminate the elliptical-rim offset reflector, available at the University of Manitoba's antenna lab, using TICRA's GRASP v.7 software [18], which is based on the physical optics, geometrical optics, and geometrical theory of diffraction. Finally, the results are verified experimentally exhibiting excellent agreement with the numerical results.

5.2 Dual-mode Circular Waveguide Feed

5.2.1 Geometry of the Proposed Dual-mode Circular Waveguide Feed

The geometry of the proposed dual-mode feed in shown in Fig. 5.1. It consists of a circular waveguide mounted on two concentrically shorted microstrip ring patches over a finite ground plane. The ring patches with their inner radius shorted to the ground plane were studied based on the cavity model in [55-57]. They have been selected to provide electromagnetic shielding to better isolate the excitation ports of each mode and reduce their mutual coupling. The inner and outer rings excite the fundamental TE_{11} and the higher order TE_{21} modes in the circular waveguide, respectively. To attain the corresponding mode polarizations in cases II and IV of chapter 4, expressed by Eqs. 4.6-7 and 4.10-11, the dominant TE_{11} mode should have two

perpendicular polarizations along the *x*- and *y*-axes, whereas the TE_{21} mode has a fixed alignment. To electronically alter the polarization of the TE_{11} mode without mechanically rotating the feed itself, the inner ring patch is designed such that it generates two orthogonally polarized TE_{11} modes, each of which is excited by two SMA probes with out-of-phase excitations, i.e. 0^o and 180^o. Then, the desired polarization will be selected by a simple signal processing technique to displace the phase centre of the offset reflector. The outer shorted ring also uses two out-of-phase probes to excite the TE_{21} mode. As shown in Fig. 5.1b, the inner ring patch, which excites the TM_{11} mode of the ring antenna and eventually the TE_{11} mode of the circular waveguide, has four SMA probes. The two probes located along the *x*-axis excite the *x*-polarized TE_{11} mode and the other two along the *y*-axis generate the *y*-polarized TE_{11} mode. The outer patch has two 90^o-apart probes to excite the TM_{21} mode of the ring and eventually the TE_{21} mode of the circular waveguide. The TM_{21} probes have a conductive cylindrical caps attached to their top ends to improve the impedance matching of the higher order TE_{21} mode.

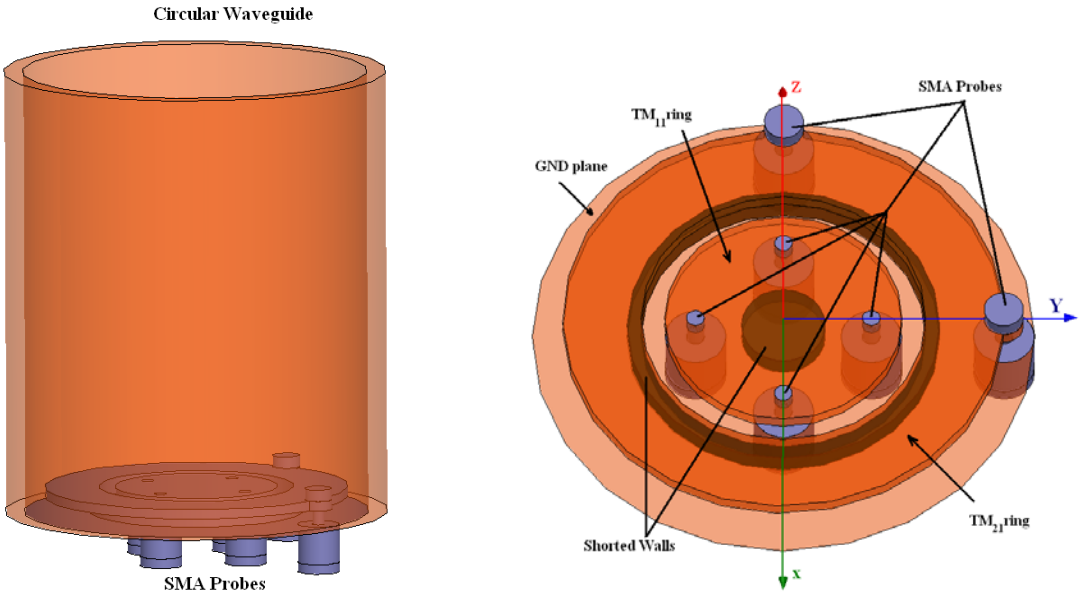

(a) (b)

Fig. 5.1. Geometry of the proposed dual-mode feed operating at the TE_{11} and TE_{21} modes (a) the circular waveguide and the shorted ring patches (b) shorted ring patches.

The radius of the waveguide is selected to dominantly support the TE_{11} and TE_{21} modes and effectively suppress all other higher order modes. It is equal to 18mm at the frequency of 10GHz. To specify the ring dimensions, the formulations based on the cavity model have been used assuming an infinite ground plane and no surrounding waveguide. To clarify this, the geometry of a single shorted ring patch is shown in Fig. 5.2, where the outer and inner radii are denoted by a and b, respectively. The resonant frequency of the mn^{th} mode are determined as,

$$f_{mn} = \frac{k_{mn}\, c}{2\pi\, a_{eff}\, \sqrt{\varepsilon_r}} \qquad (5.1)$$

where c is the light velocity, ε_r is the relative permittivity of the substrate, a_{eff} is the effective radius due to the fringing effect, and k_{mn} is the roots of the following equation, which satisfies the electric and magnetic wall boundary conditions at the inner and outer radii of the ring patch, respectively.

$$J'_m(k_{mn})\; N_m(k_{mn}\, g) - J_m(k_{mn}\, g)\; N'_m(k_{mn}) = 0 \qquad (5.2)$$

where g is the ratio of inner to outer radii, b/a, $J_m(x)$ and $N_m(x)$ are the first and second kind m^{th} order Bessel functions and the prime denotes the first derivative. Taking into account the fringing effect, the physical value of the outer radius is determined from $a = a_{eff} - 0.75t$ based on [58], where t is the thickness of the substrate.

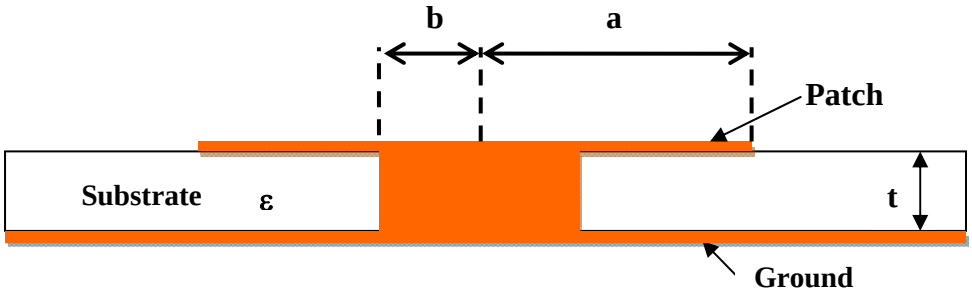

Fig. 5.2. Geometry of a shorted ring microstrip patch over an infinite ground plane.

There are some factors needed to be taken into consideration to design the proposed antenna at the frequency of 10GHz. First, the concentrically shorted ring patches must be fit to the waveguide size. Second, the ratio of the inner to outer radii of the TM_{11} shorted ring should be small enough to accommodate four SMA probes. Therefore, this ratio is selected as $g_{11}=b_{11}/a_{11}=0.35$ for the inner ring, which excites the TM_{11} mode of the ring. The corresponding eigenvalue, k_{11}, is then found from Eq. 5.2 and it is equal to 2.34. Thus, the outer and inner radii, a_{11} and b_{11}, are equal to 9.97mm and 3.52mm, respectively. Similarly, for the outer ring, which excites the TM_{21} mode of the ring, the above-mentioned ratio is chosen as $g_{21}=b_{21}/a_{21}=0.57$. The associated eigenvalue k_{21} is equal to 3.99 from Eq. 5.2. Then, the outer and inner radii, a_{21} and b_{21}, are equal to 17.8mm and 10.15mm, respectively. These values will be used as initial dimensions of the shorted ring patches shown in Fig. 5.1. After an extensive study to consider the effect of the waveguide, the above values are optimized to achieve best possible performance of the proposed feed to generate relatively pure circular waveguide TE_{11} and TE_{21} modes with reasonable impedance matching. These optimized values are listed in Table 5.1. The substrate thickness is 1.6mm. The thickness of the ring patches is 1mm. In order to omit the non-linearity effect of dielectric materials in the feed, the surrounding medium is air everywhere, i.e. $\varepsilon_r=1$. As for the circular waveguide mounted on the ring patches, its radius, height, and thickness are finalized to 18mm, 46.6mm, and 2mm, respectively.

Table 5.1. The optimized dimensions of the concentric shorted ring patches shown in Fig. 5.1b.

	Inner ring	**Outer ring**
a	**8.5mm**	**15.8mm**
b	**3.0mm**	**10.2mm**
Location of the probes	**6.3mm**	**15.8mm**
Substrate thickness	**1.6mm**	**1.6mm**
Ring thickness	**1.0mm**	**1.0mm**

5.2.2 Numerical Results of the Proposed Dual-mode Circular Waveguide Feed

The antenna shown in Fig. 5.1a is analyzed by the full-wave simulator HFSS v.12 [19]. As explained before, the antenna has six SMA probes in total. For the convenience of addressing these ports later on, the shorted ring patches are illustrated in Fig. 5.3a with numbered ports from 1 to 6. To obtain a good impedance matching with a 50Ω network, two conductive cylindrical caps are attached to ports #5 and #6. These caps act as inductive stubs to reduce the capacitive effects of these ports. The optimized radius and height of these caps are 1.4mm and 1.2mm, respectively. For mechanical stability, the outer ring patch is extended in a half-circle shape underneath these caps with the same radius. The resulting scattering parameters of all ports, S_{ii} with the index i changing from 1 to 6, are shown in Fig. 5.3b over the frequency range of 9.0-11GHz. As can be seen, the 10dB impedance bandwidth of the antenna is broader than 1.6GHz.

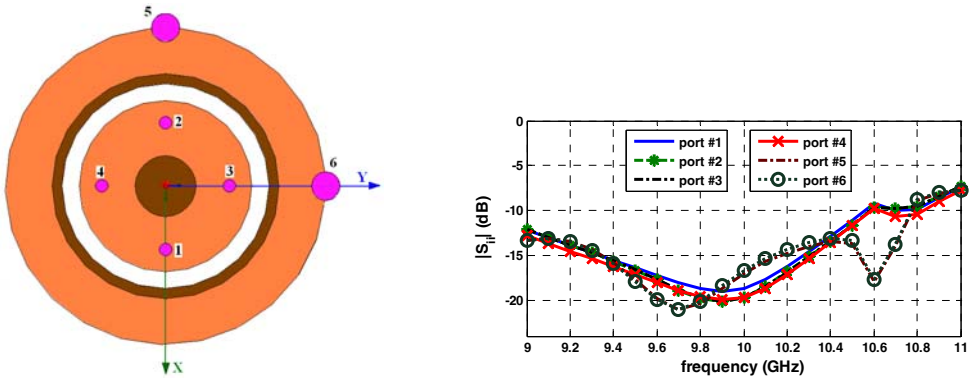

(a) (b)

Fig. 5.3. (a) Top view of the concentrically shorted ring patches with their numbered ports, (b) S_{ii} of the proposed antenna shown in Fig. 5.1a.

In order to examine the capability of the proposed antenna to generate pure TE_{11} and TE_{21} modes, the normalized radiation patterns of each mode are plotted in Fig. 5.4 at the frequency of 10GHz. Fig. 5.4a presents the x-polarized TE_{11} mode, when ports 1 and 2 are excited with equal powers and 0^{o} and 180^{o} phase excitations and the other ports are matched to a 50Ω load. The E_{θ}

component at the ϕ=90^o plane is 30dB below the *E*- and *H*-plane patterns, while it is theoretically zero. This is due to the coupling factor affecting ports 5 and 6, which excites the higher order TE_{21} mode. As shown in Fig. 5.4b, the same trend is observed, when the polarization of the TE_{11} mode is altered along the *y*-axis, ports 3 and 4 are excited with equal powers and out-of-phase excitations with the remaining ports matched. As for the TE_{21} mode, shown in Fig. 5.4c, the patterns have boresight-null shape instead of broadside beam, as expected. For this mode, the coupling factor is around -22dB.

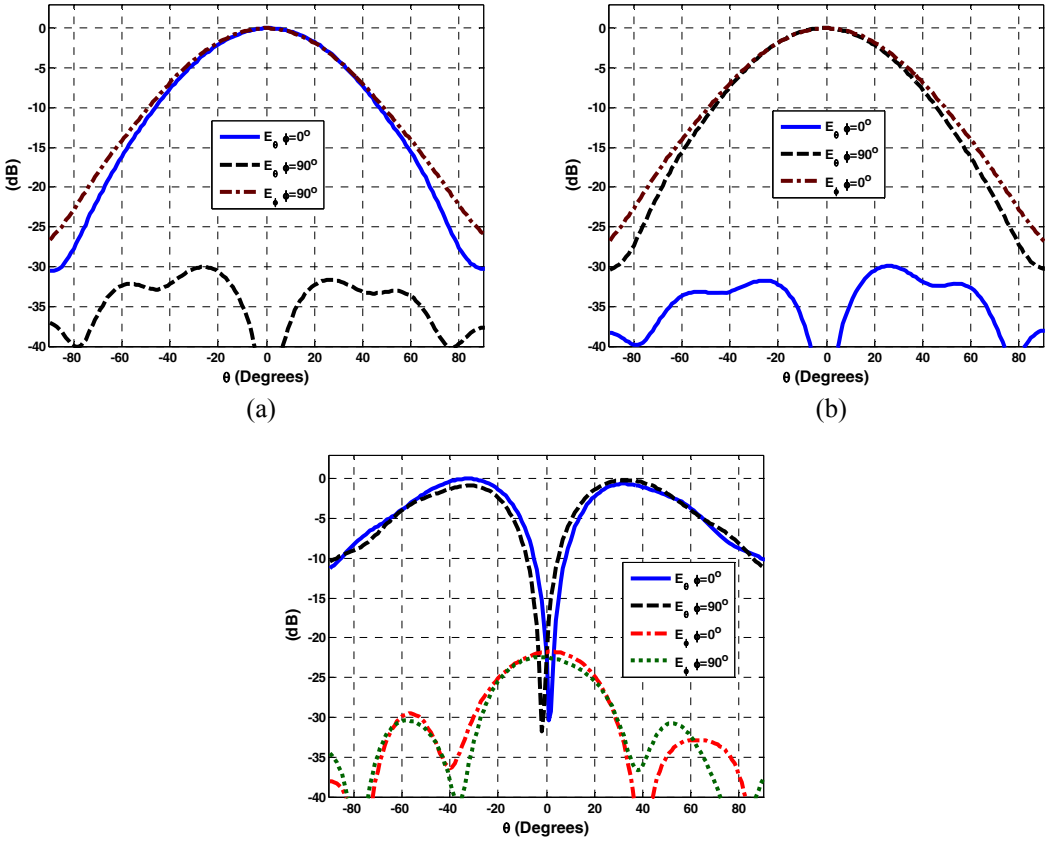

Fig. 5.4. Normalized radiation patterns of the proposed feed shown in Fig. 5.1a producing (a) the *x*-polarized TE_{11} mode, (b) the *y*-polarized TE_{11} mode, and (c) the TE_{21} mode at f=10GHz.

As for the dual-mode operation of the feed, the resulting radiation patterns (both amplitude and phase) of the combined TE_{11} and TE_{21} modes are illustrated in Figs. 5.5-6. As shown in chapter 4, the quadrature phase difference between the above modes displaced the

phase centre location of the offset reflector antenna. In order to have ±90° phase shift between the modes at the aperture of the proposed feed, the effect of the waveguide should be taken into account. That is, each mode has different phase velocity inside the waveguide and their difference is expressed by [5],

$$\Delta\phi = \frac{2\pi L}{a_{WG}}\left[\sqrt{\left(\frac{a_{WG}}{\lambda}\right)^2 - \left(\frac{K_{11}}{2\pi}\right)^2} - \sqrt{\left(\frac{a_{WG}}{\lambda}\right)^2 - \left(\frac{K_{21}}{2\pi}\right)^2}\right] \qquad (5.3)$$

where L is the distance between the ring patches and the aperture of the waveguide, a_{WG} is the radius of the waveguide, K_{11} and K_{21} are the eigenvalues of the TE_{11} and TE_{21} modes of circular waveguides, and λ is the wavelength, i.e. L=45mm, a_{WG}=18mm, K_{11}=1.841, K_{21}=3.054, and λ=30mm at f=10GHz. Therefore, $\Delta\phi$=155° at f=10GHz. Since, the ±90° phase shifts are required at the aperture, the actual phase shifts should be equal to $\Delta\phi$±90°, which are equal to +64° and -116°. Adding these to the original 0° and 180° values, the final phase excitations for the TE_{11} mode ports will be +64° and -116°. The theoretical and numerical values of these phase shifts are given in Table 5.2. They are very close to each other.

Table 5.2. The theoretical and numerical values of the phase excitations to generate quadrature phase shift between the TE_{11} and TE_{21} mode at the aperture of the proposed feed at f=10GHz.

Phase shifts	Port 1 or 3	Port 2 or 4	Port 5	Port 6
Theoretical	**+64°**	**-116°**	**0°**	**180°**
Numerical	**+57°**	**-123°**	**0°**	**180°**

With the above phase excitations and mode power ratio of 0.5, i.e. P_{TE21}/P_{TE11}=0.5, the resulting amplitude and phase patterns of the dual-mode feed are shown in Fig. 5.5, when the x-polarized TE_{11} mode is combined with the TE_{21} mode with -90° phase shift between them. This corresponds to the primary feed of case IV, shown on the top-right side of Fig. 4.34, where E_θ

component, at ϕ=0° plane, scans toward positive θ direction. Ports 3 and 4 are matched to a 50Ω load for this case. The other perpendicular polarization is achieved by matching ports 1 and 2 and applying the phase shifts according to Table 5.2. The results are shown in Fig. 5.6, which provides the primary feed patterns required for case II, as shown on the top-left side of Fig. 4.17. As can be seen, the E_θ component, at ϕ=90° plane, is scanned off the boresight direction. Also, the phase patterns are reasonably uniform around the main beam for both cases.

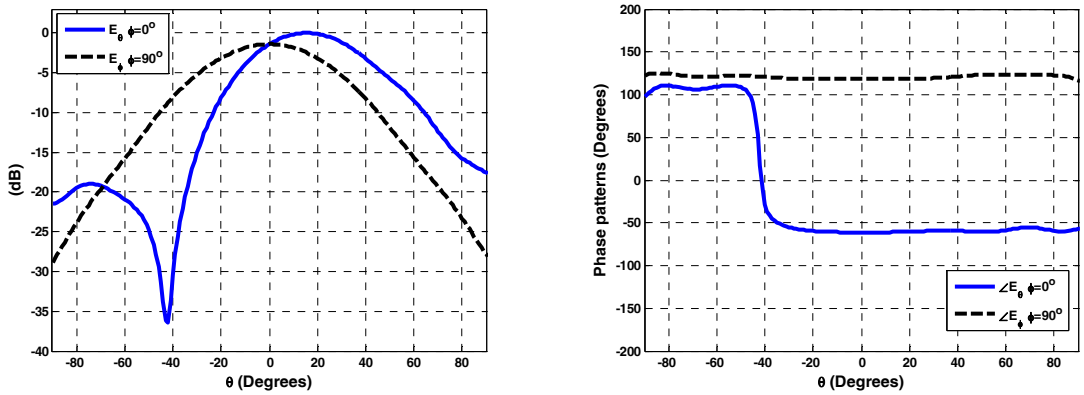

(a) (b)

Fig. 5.5. (a) Normalized radiation patterns (b) phase patterns of the proposed feed shown in Fig. 5.1a with the combined *x*-polarized TE_{11} mode and the TE_{21} mode with P_{TE21}/P_{TE11}=0.5/-90° at f=10GHz, when ports 3 and 4 are matched.

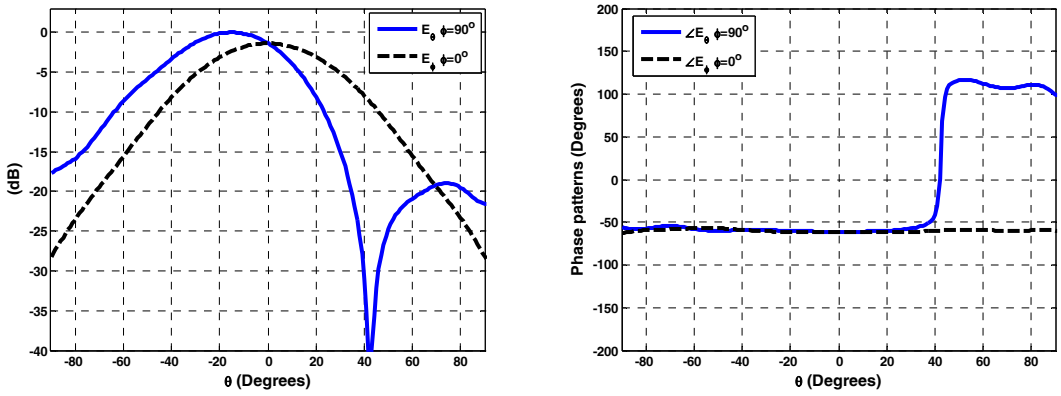

(a) (b)

Fig. 5.6. (a) Normalized radiation patterns (b) phase patterns of the proposed feed shown in Fig. 5.1a with the combined *y*-polarized TE_{11} mode and the TE_{21} mode with P_{TE21}/P_{TE11}=0.5/+90° at f=10GHz, when ports 1 and 2 are matched.

5.2.3 Measurement Results of the Proposed Dual-mode Circular Waveguide Feed

A prototype of the proposed dual-mode antenna was fabricated and tested at the University of Manitoba's Antenna Laboratory. Photograph of the prototype antenna is shown in Fig. 5.7. In this section, the measurement results are presented and compared with the numerical ones. It should be mentioned that the extended parts of the outer ring patch, underneath the caps, were missed during the fabrication. As a result, the new geometry is simulated and all numerical results are updated based on this geometry. This modification mainly degrades the impedance matching of the ports 5 and 6. The measured and simulated scattering parameters are shown in Fig. 5.8. Comparing to the original simulation results, shown in Fig. 5.3b, the simulated S_{55} or S_{66} degrades about 5dB, but they follow the same trend versus frequency. As can be seen, the measured and simulated S_{ii} are in good agreement with each other, except there are some discrepancies observed for S_{55} and S_{66}. The reason is that their corresponding ports, #5 and #6, are located in a close proximity to the waveguide wall, which made the fabrication process difficult. Thus, the connectivity of these ports was slightly deteriorated resulting in higher reflections at these ports in practice.

waveguide with the rings **shorted rings**

Fig. 5.7. Photograph of the prototype dual-mode waveguide feed excited by two concentric shorted ring patches.

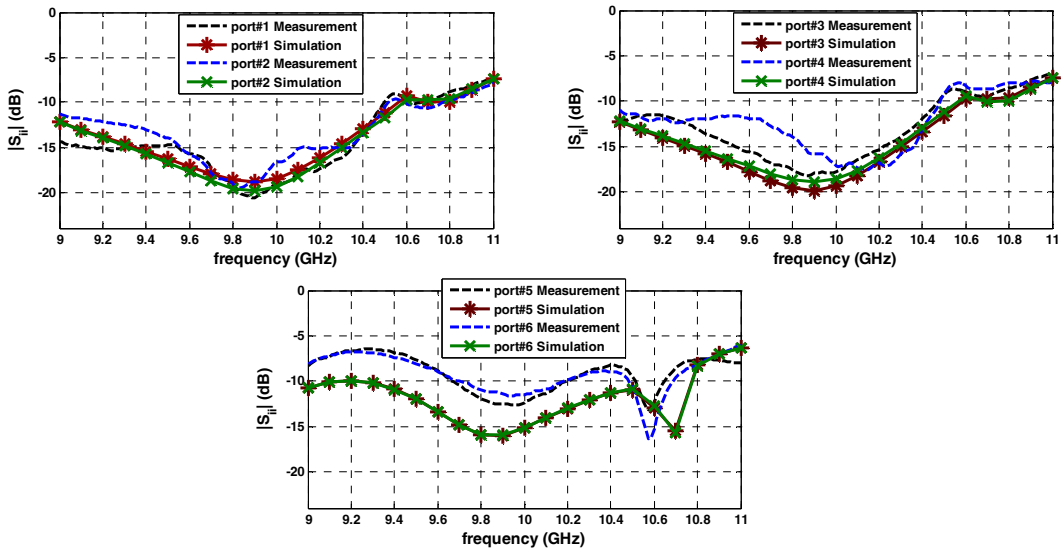

Fig. 5.8. Measured and simulated S_{ii} of the proposed antenna versus frequency.

To make sure the fabricated feed properly generates the desired modes, single mode operation was first tested. To excite each mode individually in practice, a 180° hybrid was used whose outputs provide equal amplitude with out-of-phase excitations. The measurement setup is illustrated in Fig. 5.9. For example, for the *x*-polarized TE_{11} mode, the hybrid outputs are connected to ports 1 and 2, whereas the remaining ports are matched to 50Ω loads.

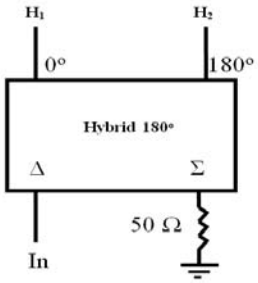

	x-polarized TE_{11}	y-polarized TE_{11}	TE_{21}
Port #1	H_1	50Ω	50Ω
Port #2	H_2	50Ω	50Ω
Port #3	50Ω	H_1	50Ω
Port #4	50Ω	H_2	50Ω
Port #5	50Ω	50Ω	H_1
Port #6	50Ω	50Ω	H_2

Fig. 5.9. Measurement setup for the single mode operation of the fabricated antenna.

The measured and simulated copolar and crosspolar radiation patterns of the proposed antenna, as a single-mode antenna, are compared in Fig. 5.10 at the frequency of 10GHz. As can be seen, the measured data satisfactorily validate the numerical ones. Moreover, the copolar patterns of the TE_{11} mode, both *x*- and *y*-polarized, produce broadside radiation patterns with nearly 10dB$_i$ gain at the θ=0° direction, whereas the TE_{21} mode has a split beam with 5dB$_i$ gain.

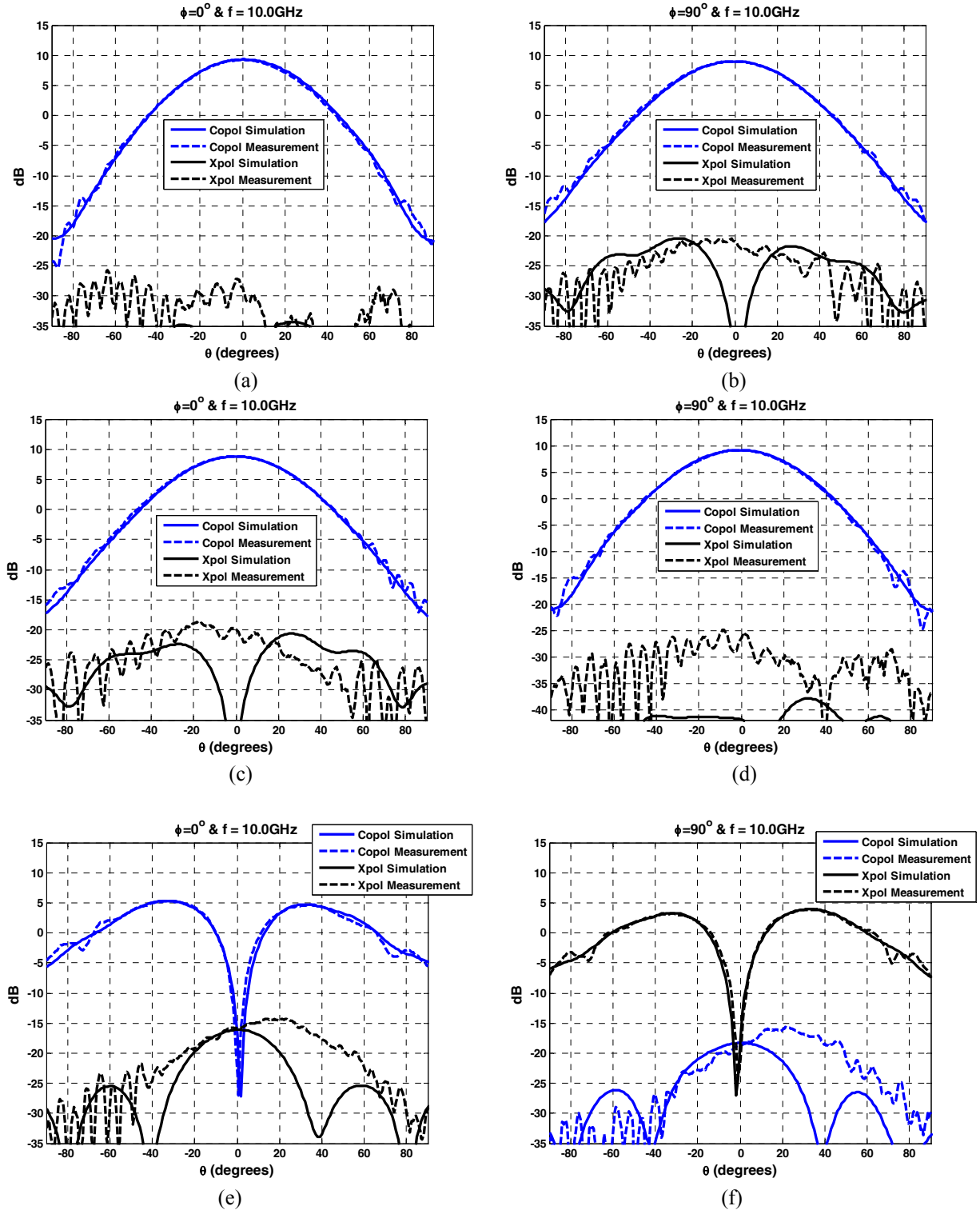

Fig. 5.10. Measured and simulated copolar and cross-polar radiation patterns of the proposed antenna at f=10GHz as a single mode feed operating at (a)-(b) *x*-polarized TE_{11} mode, (c)-(d) *y*-polarized TE_{11} mode, and (e)-(f) TE_{21} mode, with the measurement setup shown in Fig. 5.9.

The measurement setup for the dual-mode operation needs more complex feeding network as shown in Fig. 5.11. Three hybrids were used, two identical 180° and a 90°, along with two phase shifters to provide the desired phase excitations. With identical cables and no phase shifters, the hybrid outputs have equal amplitude and phase shifts of 0°, -90°, -180°, and -270° in their ideal performance. The two phase shifters were added to compensate the different phase velocity of the modes inside the waveguide, as discussed in previous section, as well as the phase difference due to the different lengths of the connecting cables.

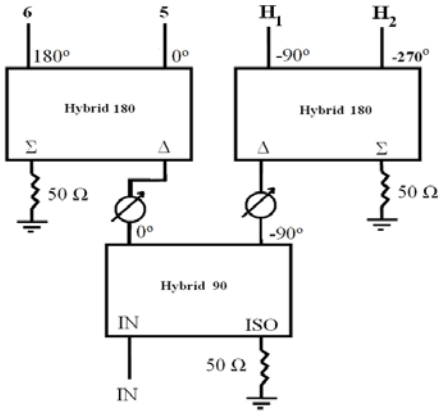

	x-polarized TE_{11} +TE_{21} modes	y-polarized TE_{11} +TE_{21} modes
Port #1	**H_1**	**50Ω**
Port #2	**H_2**	**50Ω**
Port #3	**50Ω**	**H_1**
Port #4	**50Ω**	**H_2**

Fig. 5.11. Measurement setup for the dual-mode operation of the fabricated antenna.

With the above measurement setup, the mode power ratio is ideally equal to unity. However, due to the insertion losses of the non-identical cables and the hybrids, nearly equal mode power ratio was obtained. The measured and simulated copolar and crosspolar radiation patterns of the proposed dual-mode feed are compared in Fig. 5.12 at the frequency of 10GHz. As can be observed, there is an excellent agreement between the computed and measured radiation patterns. Fig. 5.12a-b represents the *E*- and *H*-plane patterns of the combined *x*-polarized TE_{11} and the TE_{21} mode, which has the same mode alignments as the primary feed of case IV. The copolar component is scanned at the ϕ=0° plane. Similarly, the combined *y*-

polarized TE_{11} and the TE_{21} mode patterns, depicted in Fig. 5.12c-d, correspond to the primary feed of case II. For this case, the main beam is off the boresight direction at the ϕ=90^o plane. The patterns shown in Fig. 5.12 have nearly equal mode power ratio with quadrature phase shifts between the two modes.

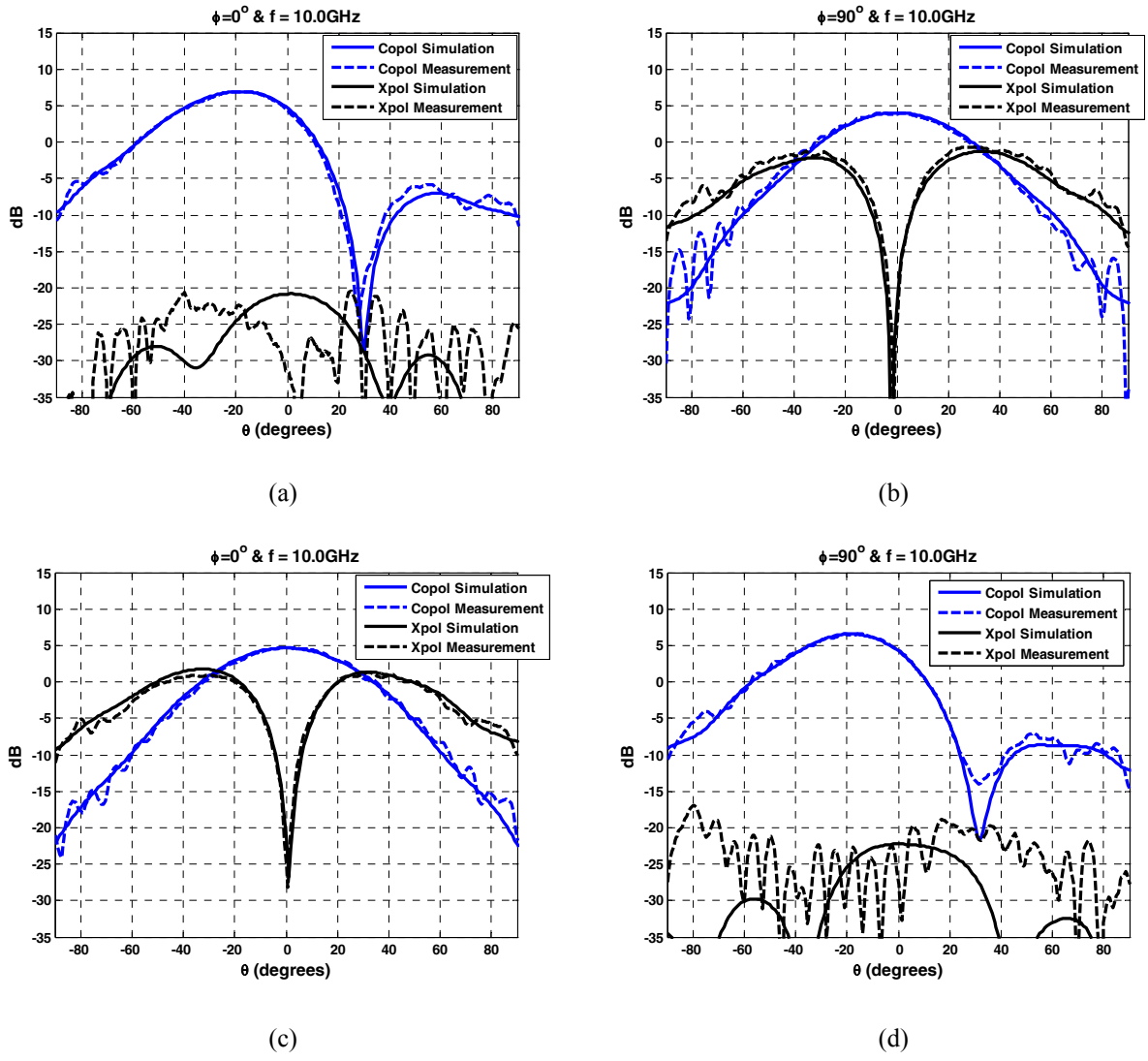

Fig. 5.12. Measured and simulated copolar and cross-polar radiation patterns of the proposed antenna at f=10GHz as a dual-mode feed operating at (a) and (b) combined *x*-polarized TE_{11} and the TE_{21} mode, (c) and (d) combined *y*-polarized TE_{11} and the TE_{21} mode, with the measurement setup shown in Fig. 5.11.

5.3 Elliptical-rim Offset Reflector with the Proposed Dual-mode Feed

In this section, an elliptical-rim offset reflector antenna, which is available as a commercial dish, is illuminated with the proposed feed to verify the multi-phase centre antenna concept both numerically and experimentally. First, the primary radiation patterns of the proposed feed, which is simulated by the full-wave 3-D HFSS v.12 [19], is exported to the TICRA's GRASP v.7 [18], to numerically calculate the secondary far-field radiation patterns and eventually find the phase centre location of the composite reflector and the feed. The geometry of the reflector antenna under study is shown in Fig. 5.13. Its rim is an ellipse with major and minor axes of 36"×27", i.e. D=91.44cm and D_H=68.58cm. The focal length is 45cm with an equivalent F/D of 0.6. The offset clearance distance and the feed tilt angle are -6.25cm, 34.61°, respectively.

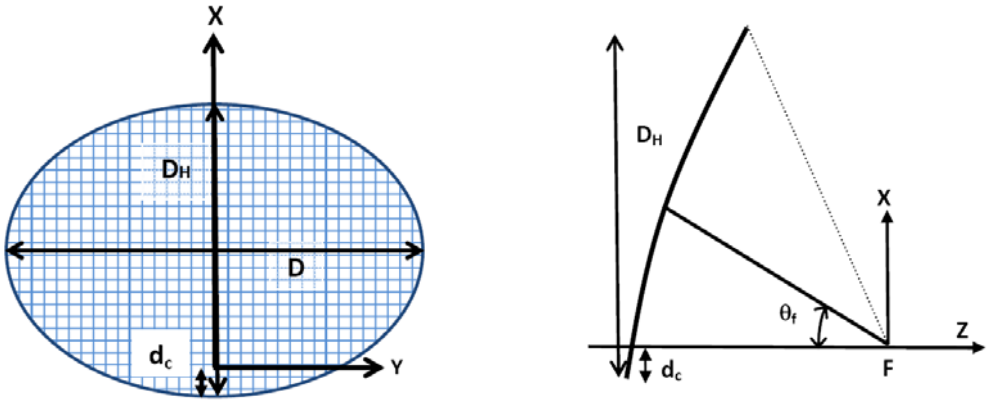

(a) (b)

Fig. 5.13. (a) Top view (b) side-view of the elliptical-rim offset reflector antenna with D=91.44cm, D_H=68.58cm, d_c=-6.25, θ_f = 34.61°, and F=45cm.

5.3.1 Numerical Results of the Compound Reflector and the Proposed Feed

First, the primary feed with the combined *y*-polarized TE_{11} and the TE_{21} modes are selected to numerically study the phase centre movements, gain, SLL, and cross polarizations in terms of different mode power ratios with the ±90^o quadrature phase excitation at the frequency of 10GHz. This corresponds to the primary feed of case II in section 4.5 with n=2.8, which is found by the curve-fitting method. The results of gain and phase centre location are shown in Fig. 5.14a. As can be seen, the antenna gain is the same for both +90^o and -90^o phase shifts and the antenna gain drops by about 3.0dB as the mode power ratio reaches to unity. For this case, the phase centre moves equally along the *y*-axis for the same mode power ratio with a maximum of 13.1cm displacement for P_{TE21}/P_{TE11}=1.0. The phase centre location normalized to the aperture radius, 0.5D_H, is also shown in Fig. 5.14b to show the ratio of the phase centre displacement with respect to the aperture radius of the reflector antenna. The corresponding sidelobe and cross polarization levels are plotted in Fig. 5.15. As can be seen, the sidelobe levels are below -20dB. As for the cross polarization, it is below -20dB when the phase shift between the modes is -90^o for mode power ratio less than 0.5, which displaces the phase centre location by about -9.5cm. The cross polarization keeps increasing when the phase shift is +90^o as the power ratio increases.

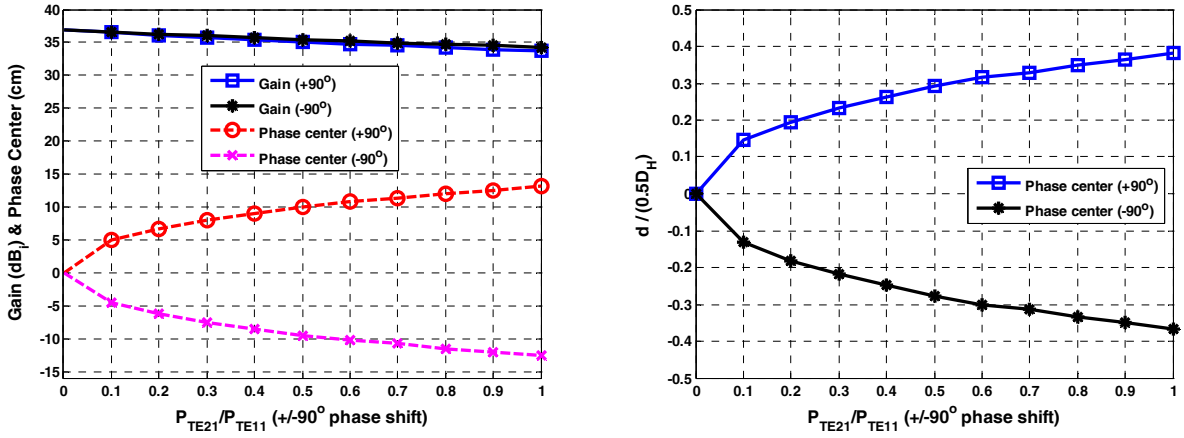

(a) (b)

Fig. 5.14. (a) Gain and phase centre location (b) normalized phase centre location of the elliptical-rim offset reflector fed by the proposed feed with the combined *y*-polarized TE_{11} and TE_{21} modes at f=10GHz. Phase centre moves along *y*-axis with reference to the center of the offset reflector aperture.

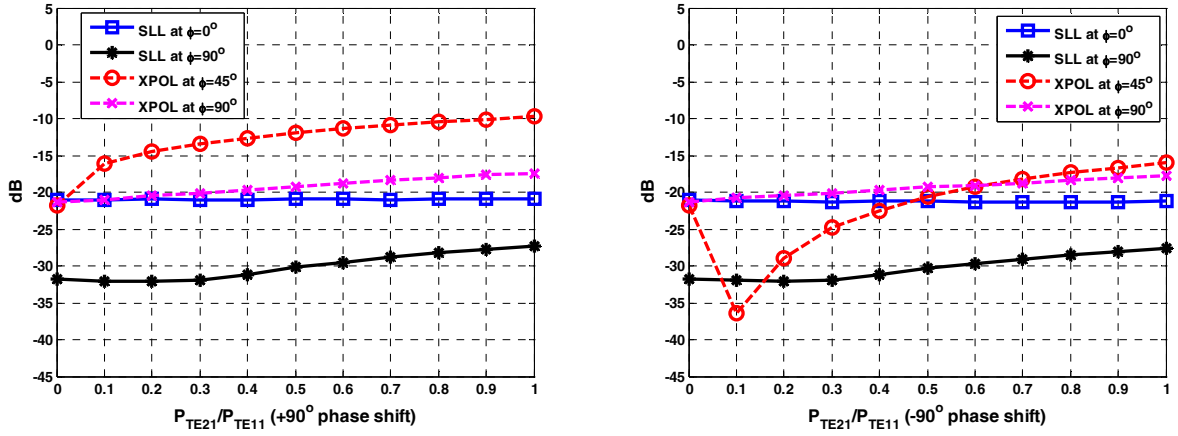

(a) (b)

Fig. 5.15. SLL and cross polarization of the elliptical-rim offset reflector fed by the proposed feed with the combined *y*-polarized TE_{11} and TE_{21} modes at f=10GHz, (a) +90° (b) -90° phase shifts.

Second, the primary feed with the combined *x*-polarized TE_{11} and the TE_{21} modes illuminate the reflector antenna shown in Fig. 5.13. This represents the feed of case IV investigated in section 4.7 with n=2.8. The numerical results of gain and phase centre locations are shown in Fig. 5.16a in terms of different mode power ratios with the ±90° quadrature phase excitation at the frequency of 10GHz. Similar to the above case, the antenna gain is the same for both +90° and -90° phase shifts and the antenna gain drops by about 3.0dB as the mode power ratio reaches to unity. For this case, the phase centre moves equally along the *x*-axis for the same

mode power ratio, with a maximum of 9.1cm displacement for P_{TE21}/P_{TE11}=1.0. The phase centre location normalized to the aperture radius, $0.5D_H$, is also shown in Fig. 5.16b. The corresponding sidelobe and cross polarization levels are plotted in Fig. 5.17. As can be seen, the sidelobe levels are below -20dB. As for the cross polarization, it is below -20dB when the phase shift of the modes is -90^o for mode power ratio less than 0.2, otherwise it considerably degrades. For this study, the feed tilt angle is adjusted to 37^o based on the discussion in section 4.3.

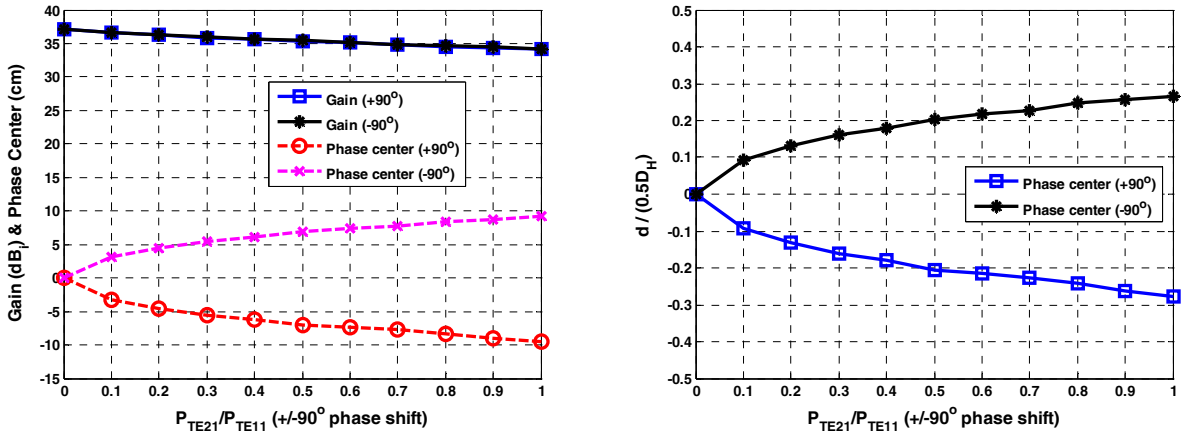

(a) (b)

Fig. 5.16. (a) Gain and phase centre location (b) normalized phase centre location of the elliptical-rim offset reflector fed by the proposed feed with the combined *x*-polarized TE_{11} and TE_{21} modes at f=10GHz. Phase centre moves along *x*-axis with reference to the center of the offset reflector aperture.

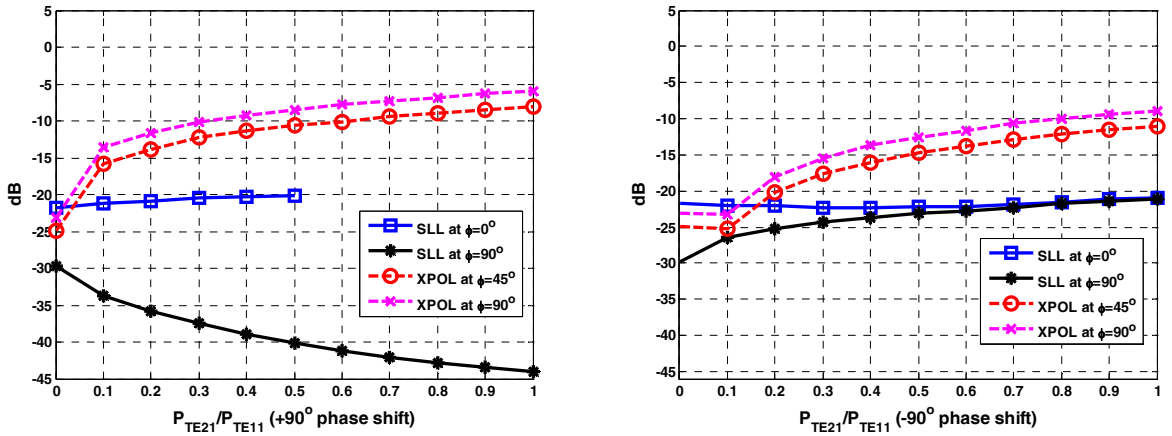

(a) (b)

Fig. 5.17. SLL and cross polarization of the elliptical-rim offset reflector fed by the proposed feed with the combined *x*-polarized TE_{11} and TE_{21} modes at f=10GHz, (a) +90^o (b) -90^o phase shifts.

5.3.2 Measurement Results of the Compound Reflector and the Proposed Feed

A photograph of the prototype antenna, including the reflector and the feed, is shown in Fig. 5.18. The whole hardware is mounted on the far-field antenna measurement tower in the Compact Range of the University of Manitoba's Antenna Laboratory. In order to find the phase centre location of the antenna, the antenna needs to be displaced to the point at which the far-field phase patterns become flat over the angular space covering the main beam of the antenna under test. Then, the amount of this displacement will be equal to the phase centre location of the antenna. To perform such a measurement, the antenna is attached to a sliding mount on the tower, which enables its lateral movement along the major axis of the ellipse.

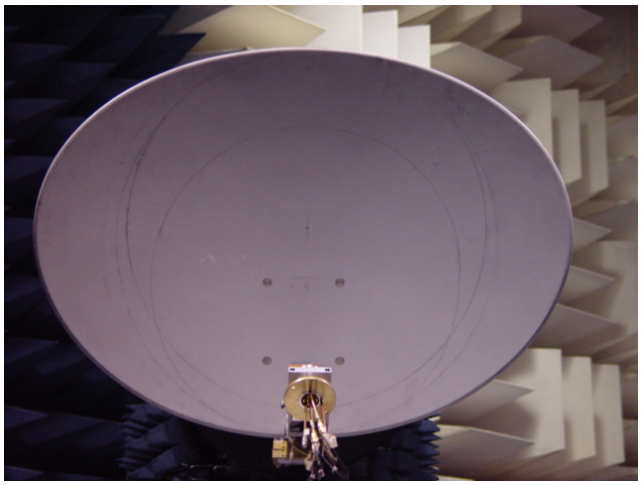

Fig. 5.18. Photograph of the prototype offset reflector antenna with the proposed feed.

Then, the reflector was illuminated with the dual-mode feed discussed in section 5.2 that corresponds to the primary feed of case II, which displaced the phase centre location along the *y*-axis. With the setup shown in Fig. 5.11, the mode power ratio is almost equal to unity. Since the phase centre is equally moved along the *y*-axis, as illustrated in Fig. 5.14, only positive

displacement is presented here. Fig. 5.19 shows the far-field phase patterns of the antenna under test when located at the coordinate origin of the tower at three frequencies of 9.5GHz, 10GHz, and 10.25GHz. As can be seen, the phase patterns have a negative slope at all frequencies indicating the phase centre location is expected to move along the positive y-axis. To confirm this, the reflector was slid toward the above direction and the flat phase patterns were achieved at each frequency, as illustrated in Fig. 5.20. As can be seen, the phase centre was displaced to y=12.5cm, y=13.0cm, and y=13.5cm at the frequencies of 9.5GHz, 10GHz, and 10.25GHz, respectively. At f=10GHz, the phase centre displacement of 13.0cm is what it has been numerically predicted before, as given in Fig. 5.14.

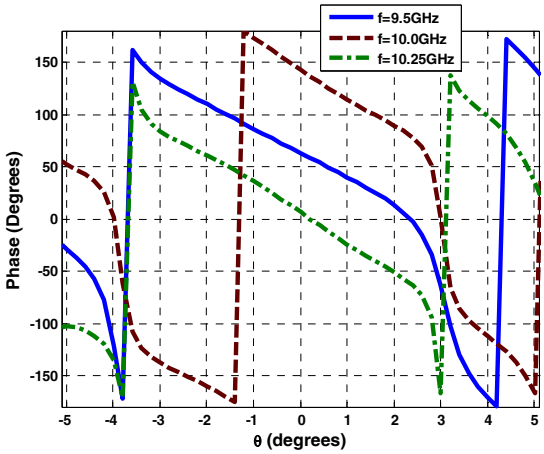

Fig. 5.19. Measured far-field phase patterns of the reflector antenna under test when it is located at x=y=0cm.

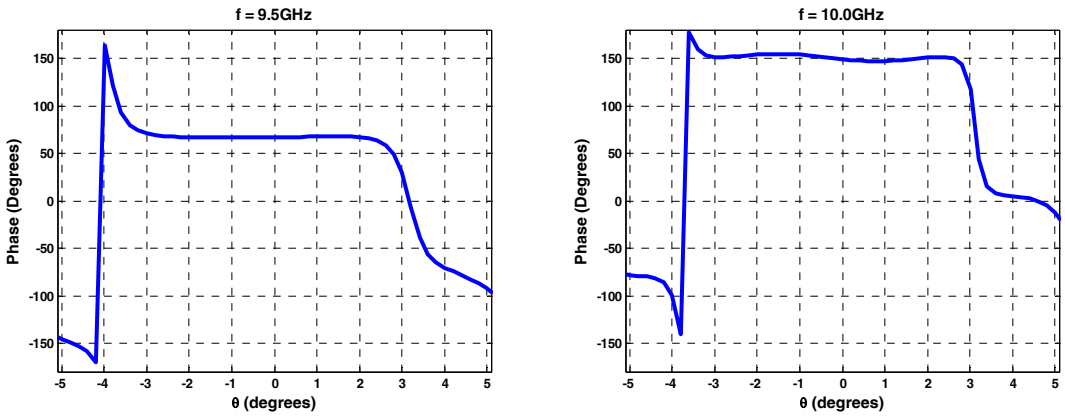

(a) (b)

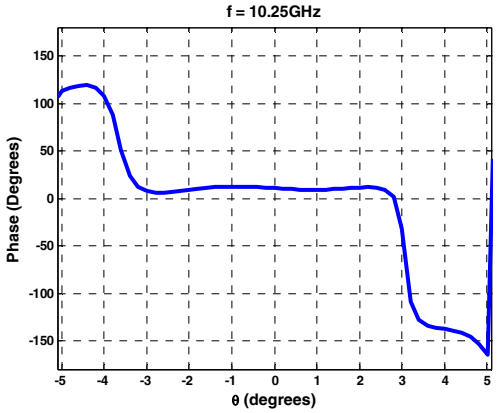

(c)

Fig. 5.20. Measured far-field phase patterns of the reflector under test when it was displaced laterally to (a) *y*=12.5cm at f=9.5GHz, (b) *y*=13.0cm at f=10GHz, and (c) *y*=13.5cm at f=10.25GHz.

To complete the study, the measured far-field radiation patterns of the antenna are plotted in Fig. 5.21 at the above-mentioned frequencies. As can be seen, the main beam is located at the boresight direction, while the phase centre was moved away from the physical center of the reflector aperture.

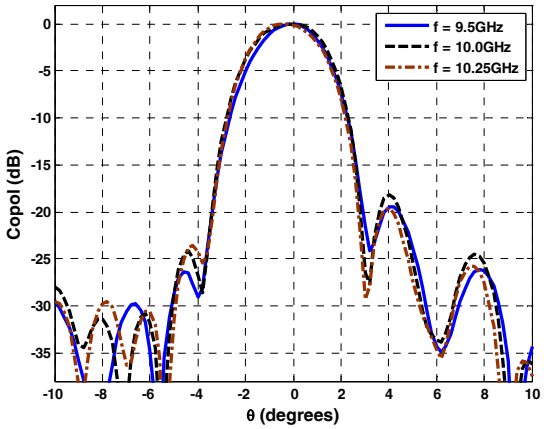

Fig. 5.21. Measured far-field radiation patterns of the reflector antenna at f = 9.5GHz, 10GHz, and 10.25GHz.

5.4 Summary

A novel dual-mode circular waveguide antenna was proposed as a primary feed for offset reflector antennas to verify the multi-phase centre antenna concept in practice. The modes included the fundamental TE_{11} mode and the higher order TE_{21} mode. These modes were independently excited by two concentrically shorted microstrip patches attached to the bottom of the waveguide. The proposed antenna was capable of generating two independent and orthogonal polarized TE_{11} modes along with the fixed aligned TE_{21} mode, similar to the primary feeds studied in cases II and IV of chapter 4. A prototype antenna was fabricated and tested. The measured and simulated results satisfactorily agreed with each other.

Then, the proposed feed was used to illuminate a commercial elliptical-rim offset reflector to move the phase centre location of the composite reflector and the feed. Base on the available hybrids and the mechanical slide, the phase centre was experimentally displaced along the *y*-axis for the mode power ratio of unity, which agreed well with the simulated results. Therefore, the concept developed in chapter 4 was successfully verified in practice resulting in virtual array antenna with multiple-phase centre locations. The antenna such developed can be used in GMTI applications, where the DPCA technique utilizes a simple signal processing technique to electronically control the phase centre movement within a single hardware, instead of employing mechanical DPCA with multi-aperture antennas.

Chapter 6

Conclusions

6.1 Summary

In this thesis, offset reflector antennas as single- and multi-phase centre antennas were thoroughly studied. First, properties of single-phase centre offset reflector antennas, such as sidelobe levels, and aperture efficiencies, and more importantly the cross polarization, were studied by proposing a simplified primary feed model representing the TE_{11} type and TE_{21} type modes of circular waveguides. The feed under study was modeled by appropriate trigonometric functions such that the TE_{11} type mode had asymmetric *E*- and *H*-plane patterns. Consequently, the secondary cross polarization was globally minimized by adjusting the amplitude ratio and phase difference of the two modes, and more importantly by selecting different tapering levels of the TE_{11} type mode in the principal planes. The concept provided a simple dual-mode primary feed model to reduce the unwanted cross polarization of offset reflector antennas, which is high in the plane of asymmetry when illuminated by a conventional linearly polarized feed. Moreover, the proposed dual-mode feed model improved the aperture efficiency of the reflector in comparison with a standard Gaussian feed of the same edge illumination. To verify the concept, two novel dual mode feeds were designed. Their radiation patterns were then used to illuminate an elliptical offset reflector antenna and determine its far field patterns. Feed #1 was a choke excited circular waveguide with a single slot. Feed #2 was a stepped circular waveguide with two tuning screws. They both exhibited wide impedance bandwidth as the higher order TE_{21} mode was isolated from the input port as opposed to the traditional multimode waveguides, whose

input impedance matching were adversely affected by exciting a higher order mode. Of these two feeds, feed #2 provided better frequency response to the cross polarization reduction technique, as the mode content factor and the tapering numbers of the dominant mode were easily adjusted by the tuning screws. To complete the study, the effect of asymmetric phase errors, applied to the proposed primary feed model, on the cross polarization of offset reflector antennas was also investigated. A broad range of *F/D* ratios were studied. Both linear and quadratic phase errors with asymmetric patterns were applied to the primary feed. Two cases were considered in terms of separate or coincident phase centre locations of the modes. It was shown that the cross polarization levels drastically increased at both inter-cardinal and asymmetry planes, whether the phase centre locations of the modes were coincident or not. More interestingly, the patterns of the cross polarization component had a broadside shape rather than a boresight-null, where the two modes had different phase centre locations. The corresponding results were the same as the radome effect on the cross polarization of monopulse systems.

Then, the concept of multi-phase centre virtual array antenna was thoroughly studied using a single aperture antenna, which was an offset reflector antenna illuminated by a dual-mode circular waveguide antenna as the primary feed. Again, the above-mentioned primary feed model was employed for simplicity. Four cases of different mode alignments or polarizations were investigated for different excitation phases and mode power ratios. It was shown that the phase centre location of the antenna can be displaced from the physical center of its aperture by changing the mode power ratios, as well as employing different mode orientations, when there is a quadrature phase difference between the modes. This resulted in a virtual array antenna, whose phase centre location can be displaced in two orthogonal directions, depending on the polarization of each mode, by a simple signal processing procedure using a single hardware

instead of mechanically moving the antenna itself. The antenna such developed has a potential application as a transceiver antenna in GMTI radar applications, as its phase centre movements were along two perpendicular directions. The phase centre motion along any direction can be easily done by proper polarization alignments of the two modes. Moreover, the in- and out-of-phase excitation cases can also be employed in beam scanning applications. The antenna gain, SLL, and cross polarizations were also investigated. It was shown that these properties were adversely affected as the phase centre moved further away from the aperture centre, when the dual-mode feed illuminated the reflector antenna. Thus, the tri-mode matched feed was used to reduce the cross polarization. It was shown that the extra TM_{11} mode improved the cross polarization performance at both asymmetry and inter-cardinal planes without affecting the phase centre location.

Finally, a novel dual-mode circular waveguide antenna was proposed as a primary feed for offset reflector antennas to experimentally verify the multi-phase centre antenna concept. The modes included the fundamental TE_{11} mode and the higher order TE_{21} mode. These modes were independently excited by two concentrically shorted microstrip patches attached to the bottom of a circular waveguide. The proposed antenna was capable of generating two independent and orthogonal polarized TE_{11} modes as well as the TE_{21} mode with a fixed polarization, similar to the primary feeds studied as cases II and IV of chapter 4. A prototype antenna was fabricated and tested. The measured and simulated results satisfactorily agreed with each other. The proposed feed was then used to illuminate a commercial elliptical-rim offset reflector to move the phase centre location of the composite reflector and the feed. Base on the available hybrids and the mechanical slide, the phase centre was experimentally displaced along the y-axis for the mode power ratio of unity, which agreed well with the simulated results. Therefore, the concept of

multi-phase centre antennas was successfully verified in practice resulting in a virtual array antenna. Such antennas can be used in GMTI applications, where the DPCA technique utilizes a proper signal processing technique to electronically control the phase centre movement within a single hardware, instead of employing mechanical DPCA with multi-aperture antennas. In addition, the concept finds useful applications in precise positioning systems such as GPS, by canceling the phase centre-related errors on the antenna part.

6.2 Future Work

While the basic concept of the single- and multi-phase centre antenna applications has been implemented using a dual-mode feed in an offset reflector antenna, there are some interesting areas which need further investigation, research, and development. They are listed below:

- Design a dual-mode feed for cross polarization reduction that closely fits to the analytical model proposed in chapter three for offset reflector antennas.
- Experimentally verify the cross polarization reduction of offset reflector antennas with the proposed feed #2 in chapter three, in low-crosspolarized chamber rooms.
- Increase the frequency bandwidth of the reduced crosspolarized single-phase centre offset reflector antennas.
- Investigate the effect of radome on the developed multi-phase centre antenna both numerically and experimentally.

- Simplify the proposed feed design in chapter five to lessen the complexity of the feeding network and modify it such that it will handle high powers in the transmit mode for radar applications.
- Compensate the SLL and cross polarization degradation in multi-phase centre antenna without adding complexity to the system.
- Study the frequency response of the proposed multi-phase centre virtual array.

REFERENCES

[1] A.D. Olver, P.J.B. Clarricoats, A.A. Kishk and L. Shafai, *Microwave horns and feeds.* IEE Electromagnetic Waves Series 39, 1994.

[2] A. W. Rudge, K. Milne, A.D. Olver and P. Knight, *The Handbook of Antenna Design.* London, UK: Peter Peregrinus Ltd, 1982.

[3] P.J. Wood, *Reflector antenna analysis and design.* IEE Electromagnetic Waves Series 7, London, UK: Peter Peregrinus Ltd,1986.

[4] C.A. Balanis, *Antenna theory and design.* Second edition, John Wiley, 1997.

[5] S. Silver, *Microwave Antenna Theory and Design.* New York: McGraw-Hill, 1949.

[6] M. I. Skolnik, *Radar Handbook,* McGraw-Hill, 1990.

[7] D. C. Schleher, *MTI and Pulsed Doppler Radar with MATLAB,* MA: Artech House, 2010.

[8] J. Jacobson, "On the cross polarization of asymmetric reflector antennas for satellite applications", *IEEE Trans. on Antenna Propagat.*, vol. AP-25, pp. 276-283, Mar. 1977.

[9]T. Chu, and R. H. Turrin, "Depolarization properties of offset reflector antennas", *IEEE Trans. on Antennas and Propagation*, vol. 21, Issue 3, pp. 339 – 345, May 1973.

[10] A. W. Rudge and N. A. Adatia, "New class of primary-feed antennas for use with offset parabolic-reflector antennas", *Electron. Lett.*, vol. 11, pp. 597-599, Nov. 27, 1975.

[11] K.M. Prasad and L. Shafai, "Performance of offset prime focus reflectors as a function of feed orientation", *IEEE Tran. On Antennas and propagation*, Vol. AP-35, No. 6, June 1987

[12] L. Shafai, and S. K. Sharma, "A Virtual Array Concept for Reflector Antenna Aperture", *2004 Inter. Symposium on Antennas Propaga.*, Japan, August 17-21, 2004.

[13] D. Carter, "Phase centers of microwave antennas", *IRE Trans. Antennas Propagat*., Vol. AP-4, pp. 597-600, Oct. 1956.

[14] L. Shafai, S.K. Sharma, B. Balaji, A. Damini, and G. Haslam, "Multiple Phase Center Performance of Reflector Antennas Using a Dual Mode Horn", *IEEE Trans. Antennas Propagat.*, vol. 54, Issue 11, Part 2, pp. 3407-3417, 2006.

[15] S. K. Sharma, L. Shafai, B. Balaji, A. Damini, and G. Haslam, "Multimode feed horn providing multiphase centres with offset reflector antenna", 2005 *Antennas and Propagation Society International Symposium*, vol. 3A, pp. 355 – 358.

[16] A. Damini, B. Balaji, L. Shafai, and G. Haslam, "Novel multiple phase centre reflector antenna for GMTI radar", *IEE Proc. Microw. Antennas Propagat*. Vol. 151, No.3, pp. 199-204, June 2004.

[17] S. K. Sharma, L. Shafai, B. Balaji, A. Damini, and G. Haslam, "Performance of Multimode (TE11+TE21) feed horn for offset reflector antenna providing multiphase centres", *Proc. 10th International Symposium on Antenna Technology and Applied Electromagnetics and URSI Conference*, Ottawa, Canada, pp. 155-158, July 20-23 2004.

[18] TICRA's GRASP 7.0 Software, TICRA Engineering Consultants Læderstræde 34 DK-1201 Copenhagen K Denmark.

[19] High Frequency Structure Simulator (HFSS 12.0). Canonsburg, PA Boston, MA: ANSYS.

[20] W. V. T. Rusch and P. D. Potter, *Analysis of reflector antennas*, New York: Academic Press Inc., 1970.

[21] K. F. Lee, *Principles of antenna theory*, John Wiley & Sons Ltd, 1984.

[22] A.W. Rudge and N. A. Adatia," Offset-Parabolic-Reflector Antennas: A Review", *Proc. of IEEE*, vol. 66, No. 12, Dec. 1978.

[23] GRASP9 Technical Description Manual.

[24] A.C. Ludwig, "The definition of cross-polarization", *IEEE Trans. On Antennas and Propagation*, vol. 21, pp. 116-119, 1973.

[25] R. E. Collin and F. J. Zucker, *Antenna Theory*, Parts I and II. New York: McGraw-Hill, 1969.

[26] R. Collin, *Antennas and radiowave propagation*. New York: McGraw-Hill, 1985.

[27] M. J. Pagones, "Gain factor of an offset-fed paraboloidal reflector", *IEEE Trans. On Antennas and Propagation*, vol. AP-16, no. 5, pp. 536-541, 1968.

[28] L. Shafai and Z. Allahgholi Pour, "Displacement of phase center location in circular microstrip antennas", *Microwave and Optical Technology letters*, Vol. 50, No. 10, pp.2531-2535, October 2008.

[29] Z. Allahgholi Pour and L. Shafai, ”Control of Phase Centre Location in Circular Microstrip Antennas operating at TM_{11} and TM_{02} modes”, *Microwave and Optical Technology letters*, Vol. 51, No. 1, pp.166-169, January 2009.

[30] J. L. Volakis, *Antenna Engineering Handbook*. Fourth Edition, New York: McGraw-Hill, 2007.

[31] G. C. Southworth and A. P. King, “Metal horns as directive receivers of ultra-short waves”, *IRE Proc*., vol. 27, pp.95-102, Feb. 1939.

[32] N. M. Rust, “*Lectures* on Aerials and wave guides: The phase correction of horn radiators”, *Journal Inst. Elec. Eng*., vol. 93, pt. IIIA, pp. 50-51, 1946.

[33] W. E. Koch, “Metal lens antennas”, *IRE Proc*., vol. 34, pp. 828-836, Nov. 1946.

[34] W. L. Barrow and L. J. Chu, “Theory of the electromagnetic horn”, *IRE Proc*., vol. 27, pp. 51-64, Jan. 1939.

[35] A. P. King, “ The radiation characteristics of conical horn antennas”, *IRE Proc*., vol. 38, pp. 249-251, Mar. 1950.

[36] P.D. Potter, “A new horn antenna with suppressed sidelobes and equal beamwidths”, *Microwave J.*, pp. 71-78, 1963.

[37] K. Bahadori and Y. Rahmat-Samii, “Back-to-back reflector antennas with reduce moment of inertia for spacecraft spinning platforms”, *IEEE Trans. on Antennas and Propagation*, vol. 55, No. 10, Oct. 2007.

[38] K. Bahadori and Y. Rahmat-Samii, “Tri-mode Horn Feeds Revisited: Cross-Pol Reduction in Compact Offset Reflector Antennas”, *IEEE Trans. on Antenna Propagat.*, vol. 57, No. 9, pp. 2771-2775, Sept. 2009.

[39] Z. Allahgholi Pour and L. Shafai, ”A Simplified Feed Model for Investigating the Cross Polarization Reduction in Circular- and Elliptical-Rim Offset Reflector Antennas”, *IEEE Transactions on Antennas and Propagation,* Accepted on August 2011.

[40] Z. Allahgholi Pour and L. Shafai, “Offset Reflector Antennas: Crosspolarization Reduction Using Tapered Dual-Mode Primary Feeds”, Technical Report, Engineering Library, Department of Electrical and Computer Engineering, University of Manitoba, Winnipeg, Canada, October 2010.

[41] Z. Allahgholi Pour and L. Shafai, ”A Novel Dual Mode Circular Waveguide Horn Antenna”, *2010 ANTEM*, Ottawa, Canada, July 5-9 2010.

[42] Z. Allahgholi Pour and L. Shafai," A Ring Choke Excited Compact Dual-mode Circular Waveguide for Offset Reflector Antennas", *IEEE Transactions on Antennas and Propagation,* Accepted on November 2011.

[43] Z. Allahgholi Pour and L. Shafai, " A Novel Impedance Matched Mode Generator for Excitation of the TE_{21} Mode in Compact Dual-mode Circular Waveguide Feeds", *IEEE Antenna and Wireless Propagation Letters,* Vol. 10, pp. 427-430, May 2011.

[44] E. R. Nagelberg and J. Shefer, "Mode Conversion in Circular Waveguides", *The Bell System Technical Journal*, pp. 1321-1338, Sept. 1965.

[45] Z. Allahgholi Pour and L. Shafai, " Investigation of Asymmetric Phase Errors of an Optimized Dual-Mode Primary Feed on the Cross Polarization of Offset Reflector Antennas", *IEEE Antennas and Wireless Propagation Letters,* Vol. 9, pp. 872-875, Sept. 2010.

[46] K. Miyata, "Center-fed Parabolic Antenna Crosspolarization due to Slightly Right-left Asymmetric Feed Patterns", *IEEE Trans. On Antennas and Propagation,* vol. AP-28, No. 2, pp. 203-209, 1980.

[47] Z. Allahgholi Pour and L. Shafai, "Effect of Feed Phase Errors on the Crosspolarization of Offset Reflector Antennas", *Microwave and Optical Technology letters*, Vol. 53, No. 1, pp. 231-235, January 2011.

[48] F. Arpin and T. Ollevier, "Cross-polarization Tracking Errors of a Radome Covered Monopulse Radar", *Microwave and Optical Technology Lett.*, Vol. 49, No. 10, October 2007.

[49] C. E. Muehe and M. Labitt, "Displaced-Phase-Center Antenna Technique", *LINCOLN LABORATORY JOURNAL*, Vol. 12, No. 2, pp. 281-296, 2000

[50] Z. Wang, E.P. Blasch, K. Pham, and G. Chen, " A GMTI method via comparing two consecutive phase difference maps of the same target area for small UAVs", *Proceeding of the IEEE 2010 National Aerospace and Electronics Conference*, pp. 369-373, July 2010.

[51] Z. Allahgholi Pour, L. Shafai, and A. M. Mehrabani, " Virtual Array Antenna with Displaced Phase Centers for GMTI Applications", *2011 IEEE Radar Conference,* Kansas City, Missouri, USA, May 23-27 2011.

[52] Y. T. Lo, "On the beam deviation factor of a parabolic reflector", *IRE Trans. Antennas Propagat.*, vol. AP-8, pp. 347-349, May 1960.

[53] J. Ruze, "Lateral-feed displacement in a paraboloid", *IEEE Trans. On Antennas and Propagation*, vol. AP-13, pp. 660-665, Sep. 1965.

[54] W. A. Imbriale, P. G. Ingerson, and W. C. Wong, “Large lateral feed displacement in a parabolic reflector”, *IEEE Trans. On Antennas and Propagation*, vol. AP-22, pp. 742-745, Nov. 1974.

[55] Y. Lin and L. Shafai, “Properties of centrally shorted circular patch microstrip antennas,” *IEEE Antennas and Propagation Symp.*, Syracuse, NY, 1988, pp. 700–703.

[56] Y. Lin and L. Shafai, “Characteristics of concentrically shorted circular patch microstrip antennas,” *IEE Proc., Microwaves, Antennas Propagat.*, vol. 137, pp. 18–24, Feb. 1990.

[57] V. González-Posadas, D. Segovia-Vargas, E. Rajo-Iglesias, J. Vázquez-Roy, and C. Martín-Pascual, “Approximate analysis of short circuited ring patch antenna working at TM_{01} mode,” *IEEE Trans. Antennas Propagat.*, vol. 54, pp. 1875–1879, Jun. 2006.

[58] I. J. Bahl and P. Bhartia, *Microstrip Antennas*. Norwood, MA: Artech House, 1980.